
Landing Gear Design Integration for the TU Delft Initiator

Master of Science Thesis

by

Nick van Oene



Landing Gear Design Integration for the TU Delft Initiator

Master of Science Thesis

by

Nick van Oene

in partial fulfillment of the requirement for the degree of

Master of Science

in Aerospace Engineering

at the Delft University of Technology

to be defended publicly on 07-03-2019, at 13:00

Supervisor: Dr.ir. R. Vos
Thesis Committee: Prof.dr.ir. L.L.M. Veldhuis
Ir. V.P. Brügemann
Student number: 1521802
Cover image: <http://www.airliners.net/photo/Airbus/Airbus-A340-642/1086962>



Preface

*N. van Oene
Delft, February 2019*

Slightly over a year ago, the final chapter of my life as a student started: working on my master thesis. After my internship at DLR Hamburg where I worked on the landing gear design for VAMPzero, deepening my knowledge on landing gear design seemed a great topic for my thesis. Creating a method to integrate the landing gear design into the conceptual design process of the Initiator was a perfect fit. I learned how to incorporate the optimization of the landing gear while also interacting with different design disciplines such as aerodynamics and structures. It truly showed me how difficult placing the gear on an aircraft may be, while it sounds so easy.

I like to thank Dr. ir. R. Vos for his guidance to solve the puzzle which is the undercarriage design. His insights showed me aspects of the design process which I had not thought of and I'm grateful to have learned from him. Furthermore, I like to thank ir. M.T.H. Brown and Dr.ir. M.F.M. Hoogreef for their help with debugging and integrating my module into the Initiator. Having the freedom to work with and adjust such a large MDO program is a valuable experience, although a bit intimidating at first. Last, but certainly not least, I like to thank my girlfriend, parents, brother and sisters and of course my friends for their support. Without them and their humor (and a lot of coffee), I would not be where I am today.

While writing the last words, I can proudly say that the final chapter of my life as MSc student is closed. Now it's time to take off to the next challenge!

Abstract

Multidisciplinary Design Optimization (MDO) software allows to generate reliable concepts quickly and with great ease. The benefits of MDO drive companies and research facilities to put great effort in creating these design programs. The Delft University of Technology is developing an MDO tool for the conceptual design of transport aircraft, called the Initiator. The current program is not able to investigate the influence of the landing gear design on the weight, drag and geometry of transport aircraft. To create a landing gear, one needs to work with different disciplines including structures, weights, aerodynamics and runway design. The MDO environment of the Initiator makes this collaboration of disciplines much easier. The general landing gear design methodology is described in many sources such as Torenbeek[31] and Roskam[25], but the integration of the landing gear design into an MDO tool has had little focus thus far. In this thesis, a new design method for the landing gear is proposed for which a new design module is created and integrated into the Initiator architecture. This new method will allow the user to investigate the influence of the undercarriage design on the weight, drag and geometry transport aircraft concept.

The landing gear design is limited by several requirements, such as: nacelle clearance and/or wing tip during a roll with pitch-up attitude, take-off stability, good steering and stability during ground operations, and airport compatibility. First, a list of possible bogie types is obtained which satisfy the flotation requirements of the concept and can be retracted without interfering with the floor. For each valid bogie, the brakes are sized. The module will evaluate the design space based on the set design requirements, by trying to design a landing gear for the concept. This will give a first gear design estimation on which a first shock absorber estimation is based. Next, the main wing is shifted at a fixed interval and each position is evaluated if a valid gear design is possible. This will give a forward and aft limit on the main wing position at which an undercarriage can be designed. These limits are passed on to the horizontal stability estimation module, which will move the main wing to optimize the size of the empennage. The wing is then placed on the forward limit. Next, the design requirements are evaluated using an optimization routine, which designs the shortest gear for each bogie type. From the list of valid gear designs, the lightest design is chosen as the optimal design. For the optimal design, the shock absorber is redesigned. With the gear layout fixed, the auxiliary spar is designed and the kink location of the wing planform is added to the geometry or updated. If the landing gear design is of the fuselage, podded or nacelle stowed type, a fairing is estimated. This fairing estimation and the undercarriage layout are passed on to the parasitic drag estimation module.

The method is validated by designing the undercarriage for six aircraft, including the B737-800 and ATR 72-600. The module was able to match the track width of low wing transport aircraft with a maximum 9.3% difference, and 14.9% difference for the ATR 72. Due to the incorrect cg estimation of the Initiator, the module was unable to match the wheelbase correctly. The difference in wheelbase ranged from a 4% underestimation for small aircraft up to 38% underestimation for B777-300. The main gear length is estimated well, with two exceptions. For the ATR 72 the set tire clearance forced the gear to be longer. For the B737-800, the nacelle clearance forced the module to design a longer gear. For all other cases, the difference in length was less than 10%.

To demonstrate that the new design strategy allows the user to evaluate the impact of the gear design on the characteristics of the concept, two cases are used: the design of a podded and traditional wing mounted gear for a low-wing aircraft and the design of a fuselage mounted gear and a nacelle stowed gear for a high-wing aircraft. These cases demonstrate that the new strategy allows the user to investigate the impact on drag, weight and geometry of the concept. Hence, the new landing gear design module is able to reliably and consistently design an undercarriage for a given transport aircraft concept. Also it allows the user to evaluate the impact of the undercarriage on the drag, weight and geometry of the concept.

Contents

1	Introduction	1
I	Research paper	3
2	Introduction	5
3	Methodology	6
3.1	Aircraft component design order	6
3.2	Module flowchart	9
3.3	Limits on the design space	10
3.4	Design bogies	18
3.5	Design landing gear struts	20
3.6	Evaluate wing position	22
3.7	Designing the auxiliary spar	22
3.8	Estimation of the gear fairing dimensions	23
3.9	Landing gear drag	25
3.10	Fairing drag estimation	26
3.11	Supported aircraft configurations	27
4	Verification	27
4.1	Weight Estimation	29
4.2	Pod design	31
4.3	Effect of wing sweep on design	32
4.4	Effect of lateral tip over requirement	34
5	Validation	35
5.1	B727-200	37
5.2	B737-800	39
5.3	B777-300	41
5.4	Fokker 100	43
5.5	ATR 72-600	45
5.6	A320-200	47
5.7	Wrapping it up	49
6	Test cases	49
6.1	Case 1: landing gear design for a low wing aircraft	50
6.2	Case 2: landing gear design for a high wing turboprop	54
7	Conclusion	58
II	Supportive chapters	61
8	Literature Research	62
8.1	The Initiator	62
8.2	Current design methods	63
8.3	Design challenges	68
8.4	Conclusion	71

9	Module Integration and program structure	73
9.1	Optimization routine	75
9.2	Design bogies	78
9.3	Design landing gear struts	80
9.4	Evaluate wing position	82
9.5	Design optimal landing gear	84
9.6	Design auxiliary spar	84
9.7	Estimation of the gear fairing and drag calculation	86
10	Conclusion	88

List of Tables

3.1	Landing gear design requirements	11
3.2	Aircraft Design Group	15
3.3	Aircraft Approach Category	15
3.4	FAA taxiway design parameters	16
3.5	FAA runway widths	17
3.6	Riemann step size verification	25
3.7	Landing gear component drag	25
4.1	Module features	27
4.2	Fuselage aft shape correction factors	28
4.3	Center of gravity verification	29
4.4	Effect of sweep on gear design	33
4.5	Effect of lateral tip over on gear design	34
5.1	Gear design validation	35
5.2	Scaled constraint values final gear design	36
5.3	Relative difference in weight estimations	36
5.4	B727-200 relative difference	37
5.5	B737-800 relative difference	39
5.6	B777-300 relative difference	41
5.7	Fokker 100 relative difference	43
5.8	ATR 72-600 relative difference	45
5.9	A320-200 relative difference	47
6.1	Skin friction and parasitic drag coefficients of the pods	53
6.2	Gear design comparison	57
7.1	Module features	59
8.1	Gudmundsson's conceptual design strategy	68
9.1	Design vector of the optimization routines	76
9.2	Optimization bounds	76
9.3	Constraints of the optimization	78
10.1	Module features	89

List of Figures

3.1	N2 chart of the Initiator	8
3.2	N2 chart of gear module	9
3.3	Module design steps	10
3.4	Side view design space limits	12
3.5	Front view design space limits	13
3.6	Top view design space limits	14
3.7	Lateral tip over definition	15
3.8	FAA runway design	16
3.9	Aircraft turn radius	17
3.10	Implemented bogie types	18
3.11	Brake assembly weight estimation by Currey[11]	19
3.12	Folded and canted gear example	21
3.13	Fairing shape example	23
4.1	Fuselage shape correction factor	28
4.2	Comparison of weight estimation methods[9]	30
4.3	Top view pod estimation comparison	31
4.4	Front view pod estimation comparison	32
4.5	Effect of cruise Mach on aircraft concept	33
4.6	Lateral tip over effect comparison	35
5.1	B727-200 top overlay	38
5.2	B727-200 front overlay	38
5.3	B727-200 side overlay	39
5.4	B737-800 top overlay	40
5.5	B737-800 front overlay	40
5.6	B737-800 side overlay	41
5.7	B777-300 top overlay	42
5.8	B777-300 front overlay	43
5.9	B777-300 side overlay	43
5.10	Fokker 100 top overlay	44
5.11	Fokker 100 front overlay	44
5.12	Fokker 100 side overlay	45
5.13	ATR 72-600 top overlay	46
5.14	ATR 72-600 front overlay	46
5.15	ATR 72-600 side overlay	47
5.16	A320-200 top overlay	48
5.17	A320-200 front overlay	48
5.18	A320-200 side overlay	49
6.1	Side-by-side gear layout comparison	50
6.2	Wing dihedral vs gear length	51
6.3	Wing dihedral vs mass ratio	52
6.4	Wing dihedral vs total C_{D_0}	52
6.5	Side view pod design	53
6.6	Wing dihedral vs L/D	54
6.7	side-by-side, top comparison of gear design	55
6.8	Side comparison of gear design	56
6.9	side-by-side, front comparison of gear design	57
8.1	N2 chart of the Initiator	62

8.2	KEACDE flowchart (Hoacheng et al p. 712)	64
8.3	VAMPzero flowchart	65
8.4	Roskam's preliminary design process (Roskam part I, p. 4)	66
8.5	Sadraey's preliminary design process (Sadraey p. 50)	67
8.6	Flow around a two-wheeled landing gear(Imamura et al p. 301)	69
8.7	Source strength comparison at 875 Hz: a) fully configured gear and b) gear with hydraulic hoses removed (
8.8	Tip over angles for undercarriage design	71
9.1	N2 chart of the Initiator	73
9.2	N2 chart of the integrated landing gear module	74
9.3	Module design steps	75
9.4	Flowchart of the optimization routine	77
9.5	Flowchart of the bogie design script	79
9.6	MTOM vs total number of main gear tires	79
9.7	Implemented bogie types	80
9.8	Flowchart of the strut design script	81
9.9	Folded and canted gear example	82
9.10	Flowchart of the wing position evaluation script	83
9.11	Flowchart of the optimal design script	84
9.12	Flowchart of the auxiliary spar design script	85
9.13	Wing planform definition	86
9.14	Fairing shape example	86
9.15	Flowchart of the fairing estimation script	87

List of Symbols

Symbol	Units	Description
α_{wb}	[deg]	Angle between nose and main gear location
Γ	[deg]	Dihedral
γ_{strut}	[deg]	Strut cant angle
θ_{TO}	[deg]	Pitch angle at takeoff
Λ	[deg]	Sweep
λ	[—]	Taper ratio
ϕ	[deg]	Roll angle
ϕ_{strut}	[deg]	Strut fold angle
ψ	[deg]	Lateral tip over angle
A	[m ²]	Area
b	[m]	Span
B_{gear}	[m]	Base of the landing gear
c	[m]	Chord
g_0	[$\frac{m}{s^2}$]	Gravitational acceleration
l_m	[m]	Distance between main gear location and the center of gravity
L_m	inch	Length of main gear
l_n	[m]	Distance between nose gear location and the center of gravity
$l_{n,aft}$	[m]	Distance between nose gear location and the most aft location of the center of gravity
$l_{n,fwd}$	[m]	Distance between nose gear location and the most forward location of the center of gravity
N_{mss}	-	Number of main gear shock struts
N_{mw}	-	Number of main gear wheels
S	[inch]	Shock stroke
V_{st}	knot	Stall speed
W_l	lbs	Landing design gross weight
W_{mlg}	lbs	Weight of main landing gear

List of Abbreviations

AAC	Aircraft Approach Category
ACAP	Aircraft Characteristics Airport and maintenance Planning.
ACN	Aircraft Classification Number.
ADG	Airplane Design Group
AoA	Angle of Attack.
B	Wheelbase
CPACS	Common Parametric Aircraft Configuration Schema.
Cg	Center of gravity.
FBD	Free Body Diagram.
g	gravitational constant.
N	Landing load factor.
n_s	Shock absorber efficiency.
n_t	Tire absorbing efficiency.
MAC	Mean Aerodynamic Chord.
MDO	Multidisciplinary design optimization
MTOW	Maximum Takeoff Weight.
MTOM	Maximum Takeoff Mass.
OEW	Operational Empty Weight.
PCN	Pavement Classification Number.
SQP	Sequential Quadratic Programming
T	Track width
TO	Takeoff
XML	Extensible Markup Language.

1 Introduction

Nowadays, a growing part of the conceptual design phase of aircraft is done with the help of computer software. The use of software allows for a faster way of generating concepts and even creating multiple concepts at once. The digital environment also allows an easy implementation of the concurrent engineering principle, as information and data are easily exchanged between different disciplines. The TU Delft is continuously developing its own aircraft design tool: the Aircraft Design Initiator. The goal of this tool is to quickly conceive a realistic aircraft design to investigate the effect of new technologies and different aircraft configurations. The current focus is on turbofan-powered civil aircraft. The current program is not able to investigate the influence of the landing gear design on the weight, drag and geometry of transport aircraft. The landing gear design strategy implemented by N.C. Heerens[19] designs the landing gear after all other parts of the aircraft are designed. Often, this means that there is no feasible landing gear design possible. To remedy this, the landing gear design should be more integrated into the design process of the Initiator, with increased interaction between the different design disciplines. By doing so, the landing gear is no longer added 'as an afterthought' and a feasible design is always realized. This means that, the Initiator can be used to investigate the influence of the undercarriage design on the weight, drag and geometry of transport aircraft as well.

A lot of research has been done on how to create a knowledge-based design flow using computers for the conceptual design phase of aircraft. Examples of this are DLR's Technology Integration for the Virtual Aircraft (TIVA), followup project Virtual Aircraft Multidisciplinary Analysis and Design Process (VAMP) and current project VAMPzero[10] and the Knowledge-based and Extensible Aircraft Conceptual Design Environment (KEACDE) created by F. Haocheng et al [13]. The author of this thesis had the privilege of doing his internship at DLR to help improve VAMPzero by creating a module which would design the undercarriage for the aircraft concept. However, undercarriage design in VAMPzero would still be done when the rest of the design was more or less finished. Therefore, the landing gear design had no influence on other components which would have to be adapted in the next iteration cycle. This shows that there is still improvement possible by doing research on the influence of the landing gear design and create a new design strategy.

The general landing gear design methodology is described in many sources such as Torenbeek[32], Currey[11] and Roskam[25], but the integration of the landing gear design into an MDO tool has had little focus thus far. As the design of the landing gear involves many different disciplines, there are several challenges to overcome when designing the gear. First, the wake of the landing gear can disrupt the flow around the wing and empennage and cause an increase in the drag of the aircraft when extended[29]. This should be kept in mind when designing the aircraft. Second, the structural impact of the landing gear[27] should be taken into account at an earlier stage of the design so large changes in wing planform are no longer needed at a later stage of the design. This may reduce the waste of precious time and resources. So it seems there is a gap in the literature, as the design strategies do not pay attention to the consequences of adding the landing gear at the end of the design cycle. This often means that the entire design cycle will have to be reiterated losing precious time. This leads to the hypothesis that *careful integration of the design of the undercarriage into the conceptual design routine of the Initiator, results in a design method capable of assessing the impact on weight, drag and geometry of transport aircraft*. This hypothesis is tested by answering the following question: *What is the impact of the undercarriage design on the performance parameters of a transport aircraft?*

If the hypothesis is validated, the Initiator program can be used to investigate the impact of the undercarriage design on the performance characteristics of transport aircraft which was not possible thus far. This allows engineers to make a more accurate trade-off between the different undercarriage layouts for aircraft concepts.

This thesis is split up into two parts. Part I is written as a standalone research paper. It covers the methodology of the landing gear design module in section 3 and the verification of the new method in section 4. Validation of the new design method is given in section 5. The validation is done by redesigning existing aircraft types, such as the A320-200 and B737-800, and comparing the new concepts with the current aircraft. To demonstrate the capability of the new method to be used to investigate the influence of the gear design on a concept, two study cases are presented in section 6. Each case consists of a fixed aircraft concept for which different gear types are designed. The case study is followed by the conclusion in 7. Part II consist of the literature study in section 8, supporting the thesis subject and methodology. Section 9 discusses the integration of the landing gear module in the Initiator. Finally, a general conclusion is given in section 10.

Part I
Research paper

Landing gear design integration for TU Delft Initiator

Delft University of Technology, Delft, 2600 AA, The Netherlands

Nick van Oene

SUPERVISOR: R. Vos

February 19, 2019

Abstract

The Delft University of Technology is developing an MDO tool for the conceptual design of transport aircraft. However, the current program is not able to investigate the influence of the undercarriage design on the weight, drag and geometry of transport aircraft. This research proposes a new design method for the undercarriage, for which a new design module is created and integrated into the Initiator architecture. This new method will allow the user to investigate the influence of the undercarriage design on the weight, drag and geometry transport aircraft concept.

By designing the undercarriage for six existing aircraft, it is shown that the updated Initiator is able to reliably and consistently design an undercarriage for a given transport aircraft concept. Also, two test cases demonstrate that the new method allows the user to evaluate the impact of the undercarriage on the drag, weight and geometry of the concept.

List of Symbols

Symbol	Units	Description
α_{wb}	[deg]	Angle between nose and main gear location
Γ	[deg]	Dihedral
γ_{strut}	[deg]	Strut cant angle
θ_{TO}	[deg]	Pitch angle at takeoff
Λ	[deg]	Sweep
λ	[—]	Taper ratio
ϕ	[deg]	Roll angle
ϕ_{strut}	[deg]	Strut fold angle
ψ	[deg]	Lateral tip over angle
A	[m ²]	Area
b	[m]	Span
B_{gear}	[m]	Base of the landing gear
c	[m]	Chord
g_0	[$\frac{m}{s^2}$]	Gravitational acceleration
l_m	[m]	Distance between main gear location and the center of gravity
L_m	inch	Length of main gear
l_n	[m]	Distance between nose gear location and the center of gravity

$l_{n,aft}$	[m]	Distance between nose gear location and the most aft location of the center of gravity
$l_{n,fwd}$	[m]	Distance between nose gear location and the most forward location of the center of gravity
N_{mss}	-	Number of main gear shock struts
N_{mw}	-	Number of main gear wheels
S	[inch]	Shock stroke
V_{st}	knot	Stall speed
W_l	lbs	Landing design gross weight
W_{mlg}	lbs	Weight of main landing gear

List of Abbreviations

AAC	Aircraft Approach Category
ACAP	Aircraft Characteristics Airport and maintenance Planning.
ACN	Aircraft Classification Number.
ADG	Airplane Design Group
AoA	Angle of Attack.
B	Wheelbase
CPACS	Common Parametric Aircraft Configuration Schema.
Cg	Center of gravity.
FBD	Free Body Diagram.
g	gravitational constant.
N	Landing load factor.
n_s	Shock absorber efficiency.
n_t	Tire absorbing efficiency.
MAC	Mean Aerodynamic Chord.
MDO	Multidisciplinary design optimization
MTOW	Maximum Takeoff Weight.
MTOM	Maximum Takeoff Mass.
OEW	Operational Empty Weight.
PCN	Pavement Classification Number.
T	Track width
TO	Takeoff
XML	Extensible Markup Language.

2 Introduction

Nowadays, a growing part of the conceptual design phase of aircraft is done with the help of computer software. The use of software allows for a faster way of generating concepts and even creating multiple concepts at once. The digital environment also allows an easy implementation of the concurrent engineering principle, as information and data are easily exchanged between different disciplines. The TU Delft is continuously developing its own aircraft design tool: the Aircraft Design Initiator. The goal of this tool is quickly conceiving a realistic aircraft design to investigate the effect of new technologies and different aircraft configurations. The focus of the Initiator is on the design of turbofan-powered civil aircraft. The current program is not able to investigate the influence of the landing gear design on the weight, drag and geometry of transport aircraft. The landing gear design strategy implemented by N.C. Heerens[19] designs the landing gear after all other parts are designed. Often, this means that there is no feasible landing gear

design possible. To remedy this, the landing gear design should be more integrated into the design process of the Initiator, with increased interaction between the different design disciplines. By doing so, the landing gear is no longer added 'as an afterthought' and a feasible design is always realized. This means that, the Initiator can be used to investigate the influence of the undercarriage design on the weight, drag and geometry of transport aircraft as well.

A lot of research has been done on how to create a knowledge-based design flow using computers for the conceptual design phase of aircraft. Examples of this are DLR's Technology Integration for the Virtual Aircraft (TIVA), followup project Virtual Aircraft Multidisciplinary Analysis and Design Process (VAMP) and current project VAMPzero[10] and the Knowledge-based and Extensible Aircraft Conceptual Design Environment (KEACDE) created by F. Haocheng et al [13]. The author of this thesis had the privilege of doing his internship at DLR to help improve VAMPzero by creating a module which would design the undercarriage for the aircraft concept. However, undercarriage design in VAMPzero would still be done when the rest of the design was more or less finished. Therefore, the landing gear design had no influence on other components which would have to be adapted in the next iteration cycle. This shows that there is still improvement possible by doing research on the influence of the landing gear design and create a new design strategy.

The general landing gear design methodology is described in many sources such as Torenbeek[32], Currey[11] and Roskam[25], but the integration of the landing gear design into an MDO tool has had little focus thus far. As the design of the landing gear involves many different disciplines, there are several challenges to overcome when designing the gear. First, the wake of the landing gear can disrupt the flow around the wing and empennage and cause an increase in the drag of the aircraft when extended[29]. This should be kept in mind when designing the aircraft. Second, the structural impact of the landing gear[27] should be taken into account at an earlier stage of the design such that large changes in wing planform are no longer needed at a later stage of the design. This may reduce the waste of precious time and resources. So it seems there is a gap in the literature, as the design strategies do not pay attention to the consequences of adding the landing gear at the end of the design cycle. This often means that the entire design cycle will have to be reiterated losing precious time. This leads to the hypothesis that *careful integration of the design of the undercarriage into the conceptual design routine of the Initiator, results in a design method capable of assessing the impact on weight, drag and geometry of transport aircraft*. This hypothesis is tested by answering the following question: *What is the impact of the undercarriage design on the performance parameters of a transport aircraft?*

If the hypothesis is validated, the Initiator program can be used to investigate the impact of the undercarriage design on the performance characteristics of transport aircraft which was not possible thus far. This allows engineers to make a more accurate trade-off between the different undercarriage layouts for aircraft concepts.

3 Methodology

Before the research question can be answered, a new design method for the undercarriage has to be developed. This section will discuss the process of creating the design method and the methodology of it.

3.1 Aircraft component design order

As the current literature does not provide a clear answer to how the undercarriage design should be iterated in a design loop, the following question will have to be answered first: *"In what order should the various aircraft components be designed and integrated?"* First, the problem of the current undercarriage design module had to be investigated. It was discovered that the combination

of aft center of gravity (c.g.) position and wing position lead to a gear design which was located behind the wing. This meant that the wing would have to be repositioned to fit the gear but, as the gear was only designed at the very last instant, this was not possible. Thus no valid gear design could be obtained and only the basic gear estimation created during the Class 2 weight estimation was available. To deal with this issue, the landing gear needed to be able to move the wing. However, this would influence the outcome of multiple other modules. Another module which moves the wing is the horizontal stability estimation module. This module optimizes the empennage/wing position combination with upper and lower bounds on the wing position. The landing gear design is dependant on, including but not limited to, the following geometrical characteristics of the aircraft and landing gear design options:

- Wing planform
- Fuselage aft shape
- Aft and forward location center of gravity
- Engine type and location
- Landing gear attachment position
- Landing gear stowage type (Nacelle, pod, fuselage, wing root)
- takeoff angle of attack

As the design is dependant on the center of gravity, at the very least an initial estimation of the aircraft geometry should be available. If the gear is attached to the wing, it may be required to adjust the wing planform or move the entire wing to a better position. As this will influence the empennage design, the gear should be designed before the empennage conceptual design is made. Changes on the other aircraft components due to the change in wing planform and/or position will be evaluated in the next design iteration. Also, the lift-curve slope should be available to estimate the angle of attack at takeoff. Thus the following design order of components is required: a first estimation of the aircraft geometry and center of gravity should be available, but the landing gear should be designed before the empennage design is finalized. Also, the takeoff performance of the initial concept should be available.

With the design order set, the methodology of the landing gear design module can be created. As the horizontal stability estimation module moves the main wing within bounds, the best option for the landing gear design integration is to evaluate at what wing positions a valid gear design can be obtained and give the upper and lower limits as bounds for the horizontal stability estimation module. Figure 3.1 shows the N2 chart of the Initiator.

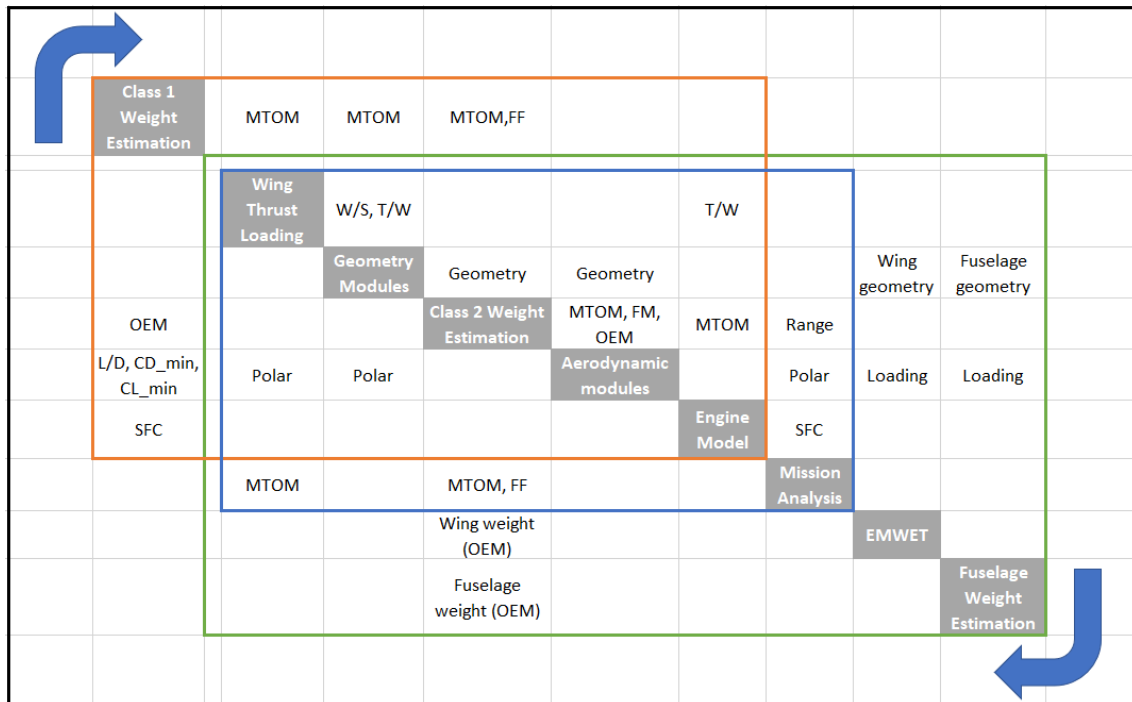


Figure 3.1: N2 chart of the Initiator

The initiator uses three design loops: a Class 2, a Mission Analysis and a Class 2.5 design loop, indicated by the red, blue and green squares respectively. The design is said to be converged when the results of all three design loops are within a specified range. To ensure the correct information is available for the landing gear design, the design module will have to be run after the aerodynamics modules. Hence, the position of the new module in the N2 chart of figure 3.1 will be after the Aerodynamics Modules. The N2 chart of the landing gear module interaction with the Initiator is shown in figure 3.2.

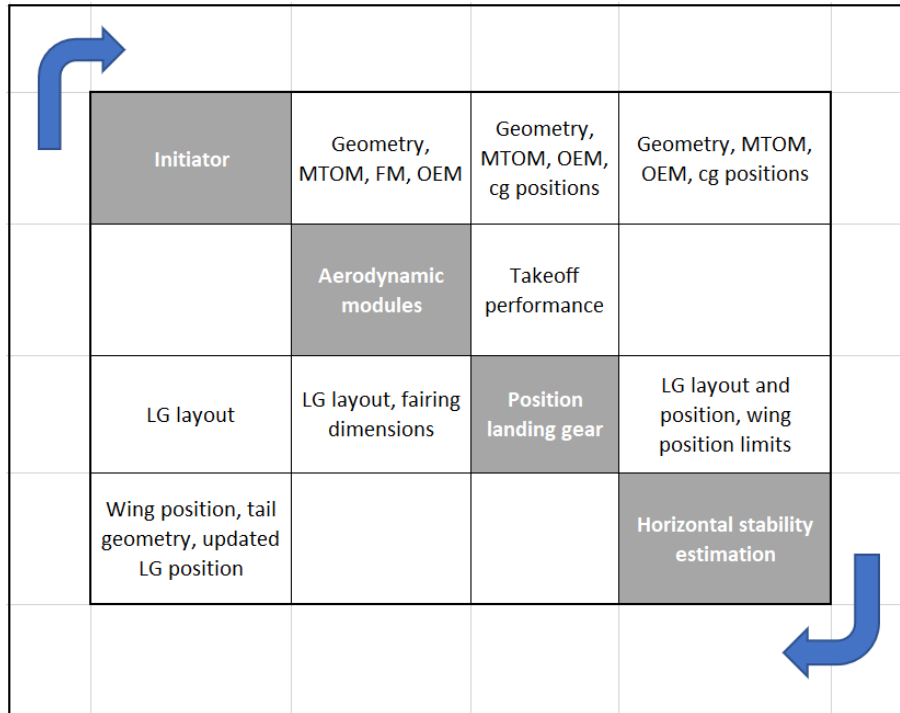


Figure 3.2: N2 chart of gear module

With the required information obtained from the other modules, as shown in figure 3.2, the landing gear module can create a landing gear layout and main wing positions. The new layout is passed on to the aerodynamic modules, which can then evaluate the parasitic drag of the gear type in the following iteration.

3.2 Module flowchart

The module itself consists of multiple scripts, each with its own specific goal. The flowchart of the landing gear design module is shown in figure 3.3.

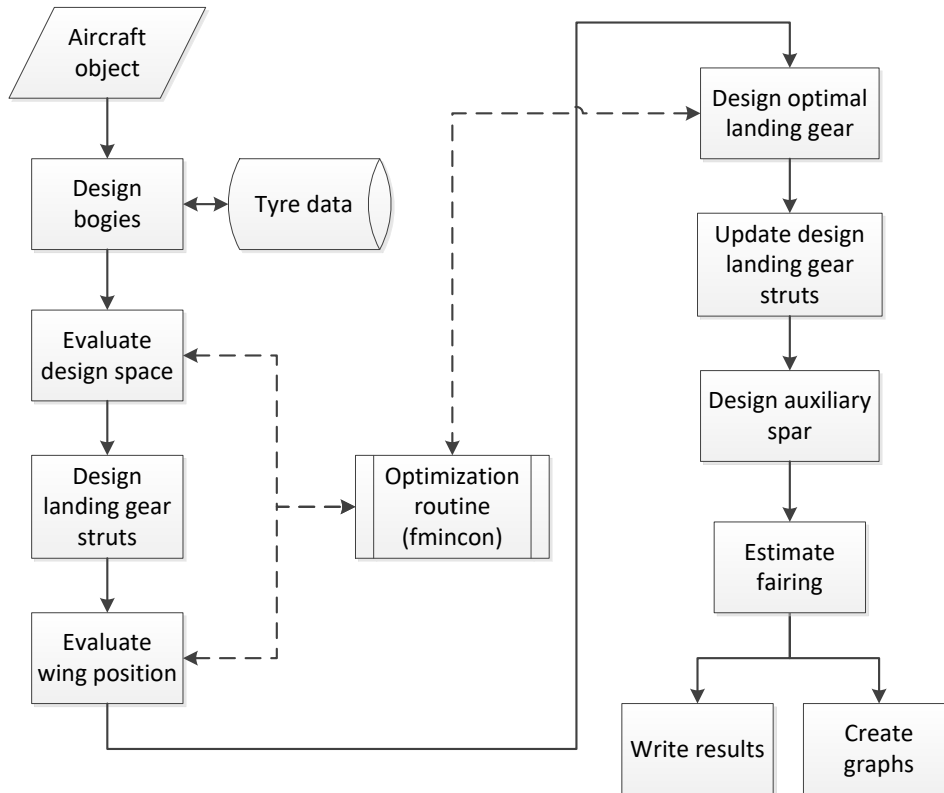


Figure 3.3: Module design steps

In the first step, the bogie designs which could be used for the aircraft concept are selected. Using the valid bogie designs, the design space is evaluated. This is done with the bogie with the smallest wheelbase, to ensure that the wing is placed on a proper location. This gives a first estimation of the gear design and notifies the user if a design is possible for the initial concept. The next step is to evaluate the wing positions at which a valid design is possible, which is discussed in detail in subsection 3.6. This will give the forward and aft bounds used in the horizontal stability estimation module. After the main wing is set on the forward bound, a landing gear will be designed for each valid bogie type. From all these concepts the lightest option is selected as the optimal design. With this design, the landing gear struts are redesigned. The last step is to update (or create, if not present) the kick spar in the wing planform.

3.3 Limits on the design space

Before the gear can be designed, several design requirements will have to be imposed on the landing gear. The tool currently supports five gear designs: fuselage mounted, wing mounted, a combination of the two for 3 and 4 struts, podded gear and nacelle stowed gear. First, table 3.1 gives an overview of all the design requirements and for which design case they are used. Next a mathematical representation is given of these requirements, supported by a side, front and top view of a gear design case.

Table 3.1: Landing gear design requirements

Constraint	Active during case	Description
Scrape angle	All	Scrape angle used for takeoff scrape.
Roll angle limit	All	Minimum allowed roll angle to avoid wingtip and/or engine strike.
Lateral tip over angle	All	Tip over angle to avoid tip over during a taxi turn.
Longitudinal tip over angle	All	Tip over angle to avoid auto-rotation.
Minimum nose load	All	Ensure minimum nose load to ensure good steering quality.
Maximum nose load	All	Ensure nose load to be below maximum load to ensure good steering quality.
Nose stowage	All	Ensure nose gear can be stowed.
FAA track limit	All	Ensure track is within FAA specified limit.
FAA wheelbase limit	All	Ensure wheelbase is within FAA specified limit.
180 turn limit	All	Ensure aircraft can make 180 turn on runway.
Wheel clearance	All	Ensure clearance between wheels and fuselage.
Attachment fwd limit	Wing, Both, Engine and Pod	Ensure main gear attachment is within range of rear spar.
Attachment aft limit	Wing, Both, Engine and Pod	Ensure main gear attachment is within range of rear spar.
Main gear longitudinal stowage	Wing and Both	Ensure main gear is retracted behind rear spar.
Main gear lateral stowage limits	Wing and Both	Ensure main gear bogie is within fuselage when retracted, but is not overlapping.
Strut/nacelle interference	Wing and Both, (if engine is on wing)	Ensure main gear strut is not placed within the engine nacelle.

First, the takeoff angle of attack is determined. From the aerodynamic analysis, the lift-curve slope is obtained. The lift curve slope is determined using the aerodynamic solver AVL¹. For the takeoff run, the following input is used:

- Altitude of 0[m]
- $V_{TO} = 1.1 \cdot V_{stall}$
- $C_L = 0.75 \cdot C_{L_{TO,max}}$ (point used to determine slope, before stall affects the slope)

The stall speed is based on the max C_L during takeoff using equation 3.1.

$$V_{stall} = \sqrt{\frac{2 \cdot MTOM \cdot g}{\rho \cdot S_{ref} \cdot C_{L_{TO,max}}}} \quad (3.1)$$

To determine the C_L increase for flaps and slat in TO configuration, the set aircraft performance parameters are used in equation 3.2.

$$dC_{L,TO} = C_{L_{TO,max}} - C_{L_{clean,max}} \quad (3.2)$$

¹<http://web.mit.edu/drela/Public/web/avl/>

Then, the required CL for takeoff is calculated using equation 3.3.

$$C_{L_{TO,req}} = \frac{2 \cdot MTOM \cdot g}{\rho \cdot S_{ref} \cdot V_{TO}^2} \quad (3.3)$$

The C_L during takeoff at 0 AoA is determined using the DATCOM method. And last, the angle of attack during takeoff is calculated with equation 3.4.

$$\alpha_{TO} = \frac{C_{L_{TO,req}} - dC_{L,TO} - C_{L_{TO,\alpha=0}}}{\frac{dC_L}{d\alpha}} \quad (3.4)$$

The longitudinal tip over angle, θ_{TO} , is set to be $\alpha_{TO} + 5$ degrees[26] to ensure no auto-rotation occurs. Figure 3.4 shows a side view of the A320[1] with gear design limits. For readability, not every limit is shown in every figure.

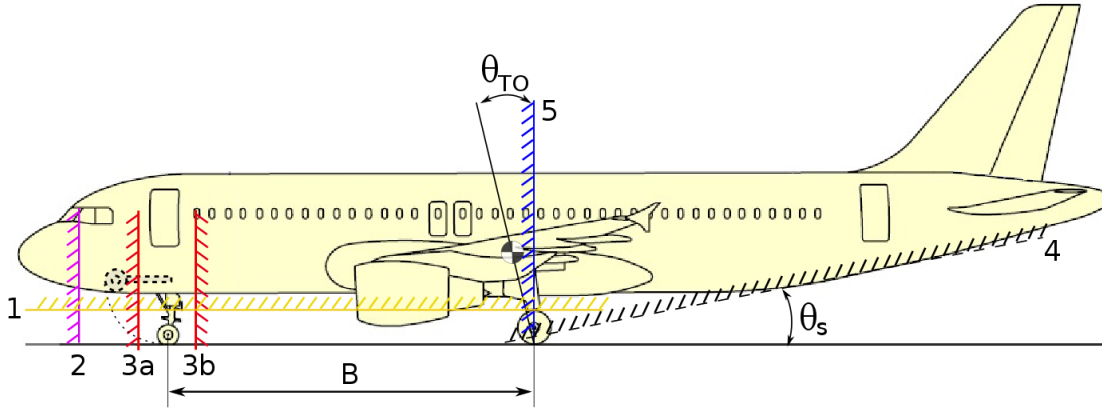


Figure 3.4: Side view design space limits

Limit 1 in figure 3.4 represents the tire clearance limit given by equation 3.5.

$$z_{fus} - z_{tire,top} - 0.1524 \leq 0 \quad (3.5)$$

Equation 3.6 is used to impose limit 2, which ensure the nose gear can be stowed when retracted.

$$L_{NG,stowed} - x_{NG} + 0.2 \leq 0 \quad (3.6)$$

Limit 3a and 3b limit the longitudinal position of the nose gear. 3a, the minimum nose load, is set by equation 3.7.

$$0.08 - F_{NG,min} \leq 0 \quad (3.7)$$

in which the minimum nose load is calculated with equation 3.8, assuming the main gear carries 92% of the load

$$F_{n,min} = \frac{x_{cg,aft} - x_{MG}}{x_{NG} - x_{cg,aft}} \cdot F_{m,max} \quad (3.8)$$

The maximum nose load limit, indicated by 3b, is set by equation 3.9.

$$F_{n,max} - 0.15 \leq 0 \quad (3.9)$$

in which the minimum nose load is calculated with equation 3.10, assuming the main gear carries 85% of the load.

$$F_{n,max} = \frac{x_{cg,fwd} - x_{MG}}{x_{NG} - x_{cg,fwd}} \cdot F_{m,min} \quad (3.10)$$

The scrape limit, number 4 in figure 3.4, is determined with equation 3.11. The fully compressed gear with flat tire must still be below this line to ensure no structure hits the ground during rotation.

$$\theta_s - \tan^{-1} \left(\frac{z_{MG} - z_{fus}}{x_{fus} - x_{gear}} \right) \leq 0 \quad (3.11)$$

The longitudinal tip over limit is set by equation 3.12.

$$\theta_{TO} - \tan^{-1} \left(\frac{x_{cg,aft} - x_{MG}}{z_{MG} - z_{cg}} \right) \leq 0 \quad (3.12)$$

Figure 3.5 shows the limits in the front view of the aircraft.

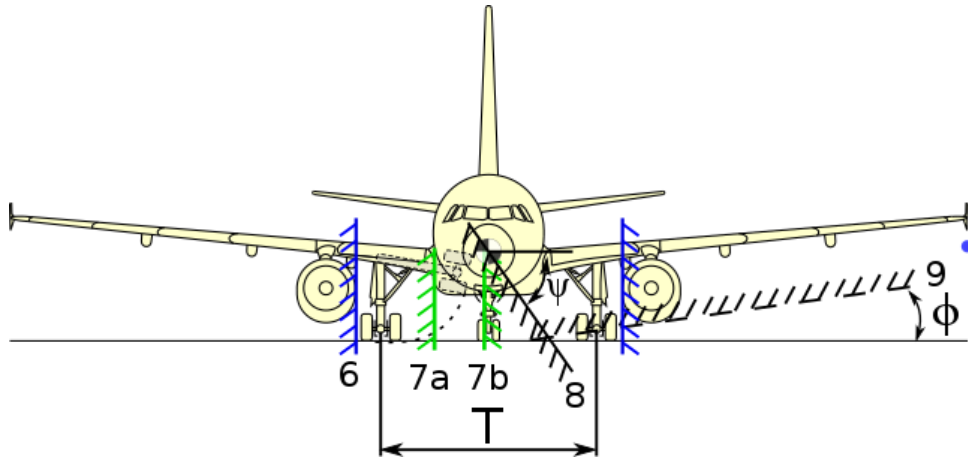


Figure 3.5: Front view design space limits

The nacelle-strut interference, indicated with number 6, is set by equation 3.13.

$$y_{MG} - \left(y_{eng} - \frac{D_{eng}}{2} \right) \leq 0 \quad (3.13)$$

For the lateral main gear stowage, two limits are imposed: 7a and 7b. 7a ensures that the bogie is inside the wing box when retracted. The limit is calculated with equation 3.14.

$$y_{wheel,top} - y_{wingbox} \leq 0 \quad (3.14)$$

Limit 7b ensures that there is still clearance (no overlap) between the bogies when retracted. It is set with equation 3.15.

$$0.05 - y_{wheel,bot} \leq 0 \quad (3.15)$$

Limit 8 represents the lateral tip over limit. The derivation of this limit is based on Torenbeek[32] and is shown in figure 3.7. The roll limit is indicated with number 9. When the aircraft is rolled by 8° [32], the lowest part of the aircraft should not hit the ground. This is either the nacelle (3.16a) or the pitched up wing tip (3.16b) indicated by the blue dot in figure 3.5.

$$\phi - \tan^{-1} \left(\frac{z_{eng} - z_{MG}}{y_{eng} - y_{MG}} \right) \leq 0 \quad (3.16a)$$

$$\phi - \tan^{-1} \left(\frac{z_{tip,pitched} - z_{tip,pitched}}{y_{eng} - y_{MG}} \right) \leq 0 \quad (3.16b)$$

Figure 3.6 gives a top view of the imposed limits on the design space.

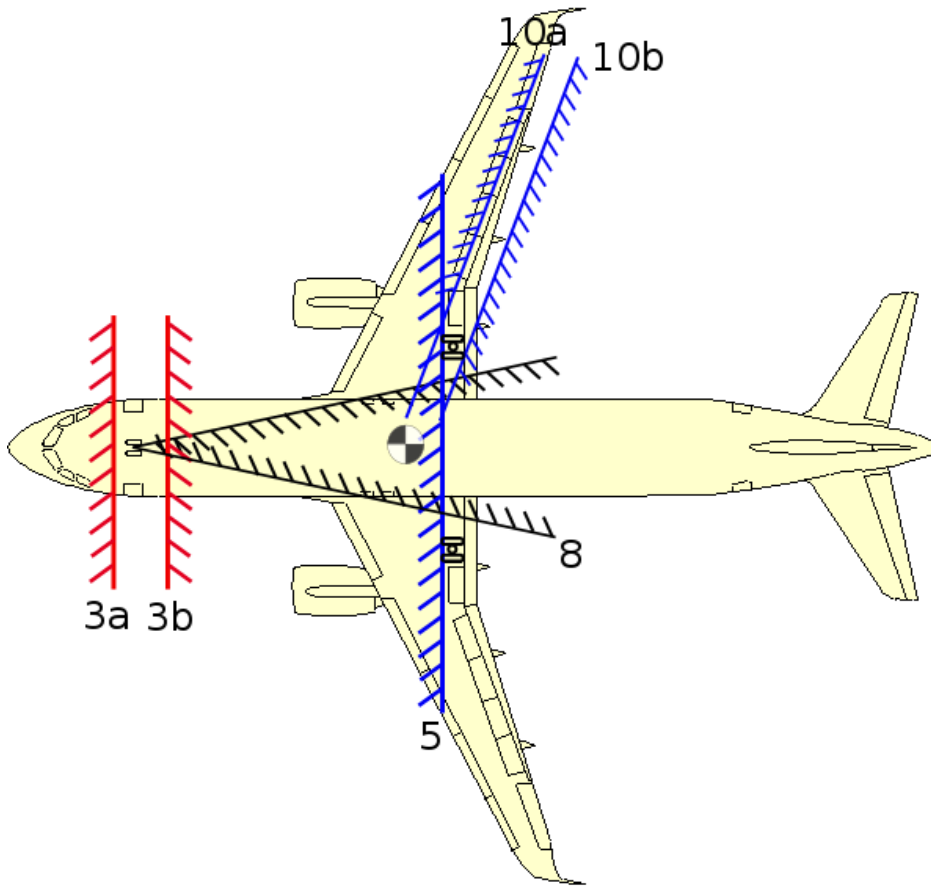


Figure 3.6: Top view design space limits

Lines 3a and 3b are again the nose load limits set by equations 3.7 and 3.9 respectively. Limits 10a and 10b ensure that the main gear (if attached to the wing) will be close enough to the rear spar. 10a ensures that the gear is located behind the rear spar, set by equation 3.17.

$$x_{spar} + D_{strut} - x_{MG} \leq 0 \quad (3.17)$$

Equation 3.18 ensures that the main gear is not too far aft of the rear spar. This is done to avoid extremely large yehudi's. The 2.5% fuselage length is estimated based on the main gear location of five transport aircraft. The main bogie is allowed to have a positive trailing, as this relaxes the requirement and also improves shimmy stability[4]. An example of increasing the mechanical trail to increase shimmy stability is the design of the DASH 8[23].

$$x_{MG} - (x_{spar} + 0.025 \cdot L_{fus}) \leq 0 \quad (3.18)$$

The derivation of the lateral tip over limit, line 8, will be discussed next. The definition of the lateral tip over angle ψ is shown in figure 3.7.

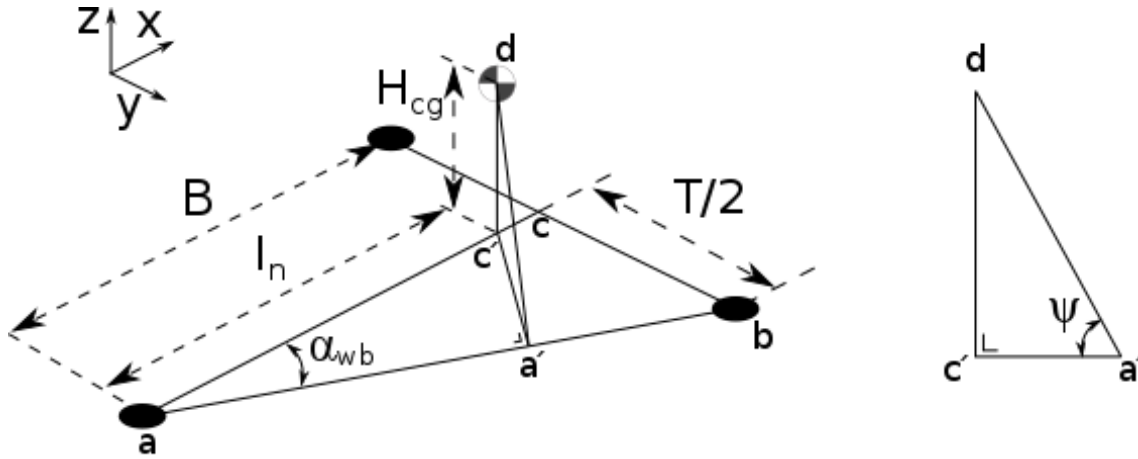


Figure 3.7: Lateral tip over definition

As can be seen in figure 3.7, ψ is a function of gear location and cg location. First, the angle α_{wb} is calculated with equation 3.19.

$$\alpha_{wb} = \tan^{-1} \left(\frac{0.5 \cdot T}{B} \right) \quad (3.19)$$

Next, ψ is calculated with equation 3.20.

$$\psi = \tan^{-1} \left(\frac{H_{cg}}{I_n \cdot \sin(\alpha_{wb})} \right) \quad (3.20)$$

The angle ψ of the gear design is limited by a minimum of 55° , as suggested by Torenbeek[31] and Heslehurst[20]. This results in the design requirement 3.21.

$$\psi - 55 \leq 0 \quad (3.21)$$

In addition to these constraints, the following requirements due to airport operations are implemented. First, the Aircraft Design Group (ADG) and Aircraft Approach Category (AAC) of the aircraft concept are determined. This is done based on table 3.2[14] and table 3.3[14].

Table 3.2: Aircraft Design Group

Group	Tail Height [m]	Wingspan [m]
I	< 6	< 15
II	6 - 9	15 - 24
III	9 - 13.5	24 - 36
IV	13.5 - 18.5	36 - 52
V	18.5 - 20	52 - 65
VI	20 - 24.5	65 - 80

The ADG for both the tail and the span are determined and the highest value of the two gives the aircraft ADG. The AAC of the aircraft is based on the approach speed, as shown in table 3.3[14]

Table 3.3: Aircraft Approach Category

V_{ap} [kt]	< 91	91 - 121	121 - 141	141 - 166	> 166
AAC	A	B	C	D	E

Figure 3.8 shows the design guideline for taxiways as set up by the FAA[14], with the design requirements per ADG given in table 3.4[9].

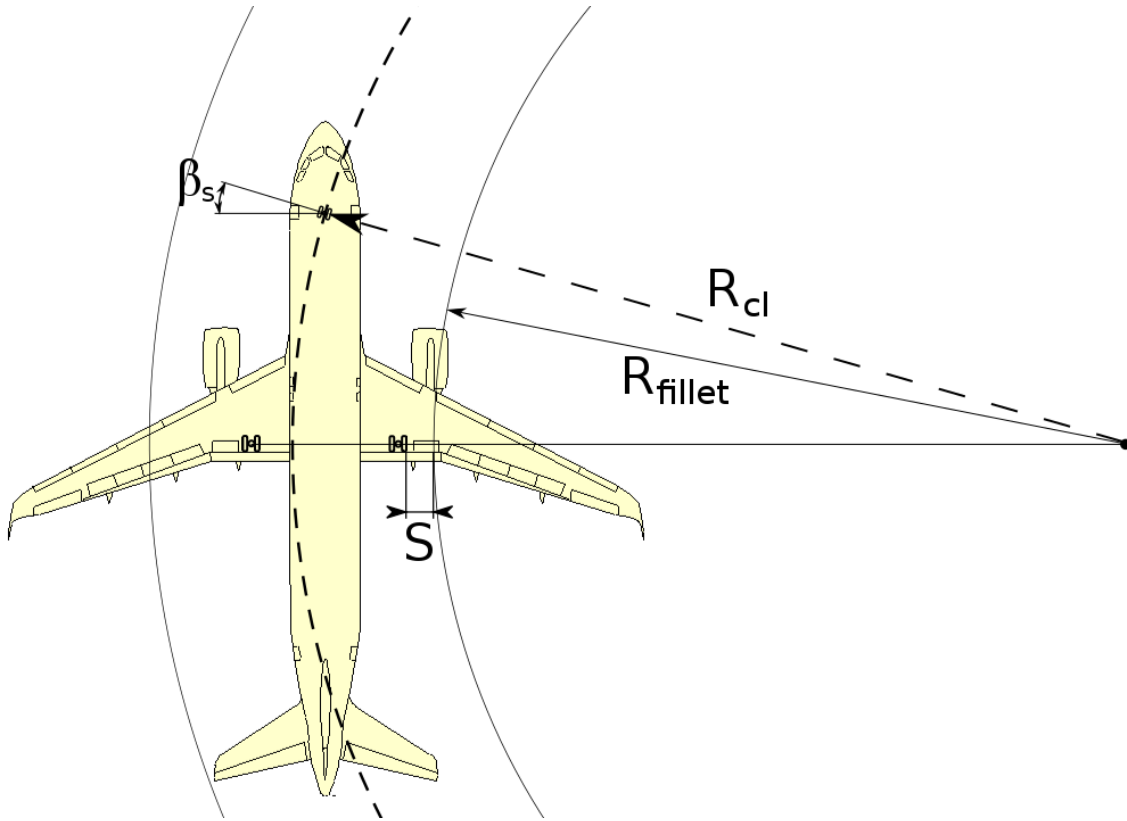


Figure 3.8: FAA runway design

Table 3.4: FAA taxiway design parameters

ADG	III	IV	V	VI
Centerline radius (R_{cl}) [ft]	100	150	150	170
Fillet radius (R_{fillet}) [ft]	55	80	85	85
Distance MG to runway edge (S) [ft]	10	15	15	20

To avoid the main gear running off the pavement during the turn, a safety distance S is taken into account. The values in table 3.4[9] are used to compute the maximum allowable track width in equation 3.23 and wheelbase in equation 3.22 for the ADG.

$$B_{FAA,max} = R_{cl} \cdot \sin(\beta_s) \quad (3.22)$$

$$T_{FAA,max} = \sqrt{\left(R_{cl}^2 + B_{FAA,max}^2\right)} - R_{fillet} - S \quad (3.23)$$

A maximum steering angle of $\pm 60^\circ$ is assumed, which is common for transport aircraft[11]. The maximum track and wheelbase are used in equations 3.24 and 3.25 to evaluate if the aircraft can use a runway designed for its ADG. If an aircraft has an ADG smaller than 3, the runway parameters of ADG 3 are used.

$$(x_{MG} - x_{NG}) - B_{FAA,max} \leq 0 \quad (3.24)$$

$$(2 \cdot y_{MG}) - T_{FAA,max} \leq 0 \tag{3.25}$$

Next, the runway design requirements set by the FAA[14] are checked to see if the aircraft can make a 180° turn on a runway designed for its AAC and ADG. The 180° turn is shown in figure 3.8.

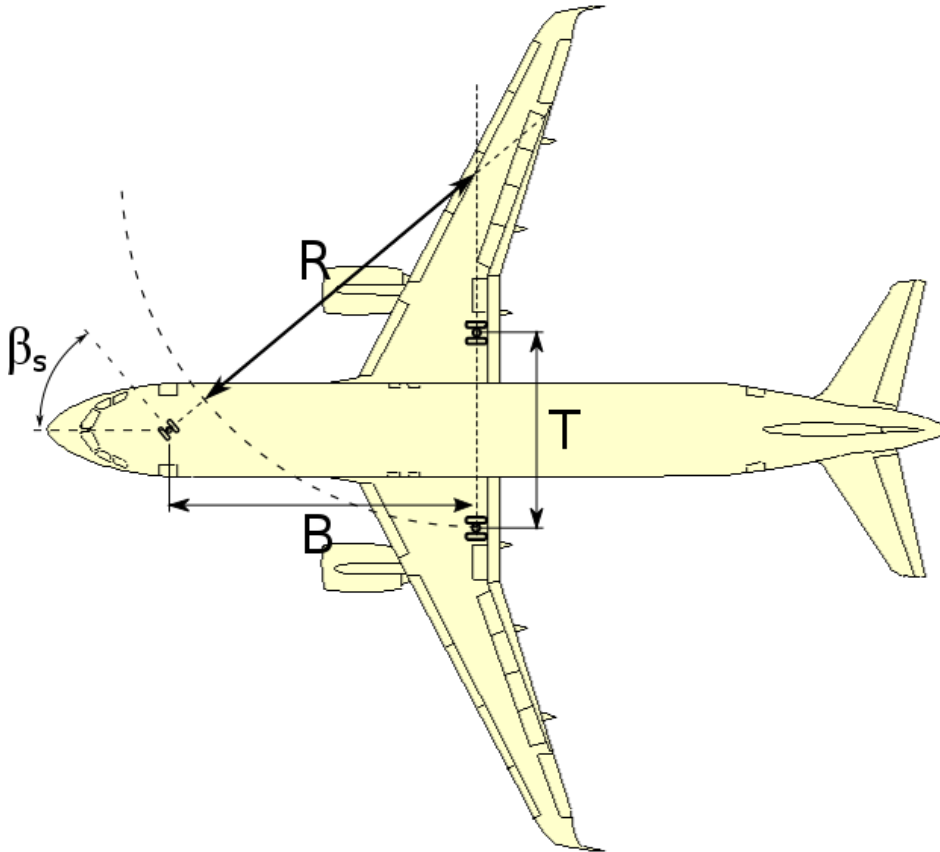


Figure 3.9: Aircraft turn radius

The turn radius of the aircraft is calculated using 3.26.

$$R_{180} = B \cdot \tan(90 - \beta_s) + 0.5 \cdot T \tag{3.26}$$

For each ACC/ADG combination the design runway width is shown in table 3.5[14].

Table 3.5: FAA runway widths

AAC \ ADG		I	II	III	IV	V	VI
		A	60 ft	75 ft	100 ft	150 ft	
B	60 ft	75 ft	100 ft	150 ft			
C	100 ft	100 ft	150 ft	150 ft	150 ft	200 ft	
D	100 ft	100 ft	150 ft	150 ft	150 ft	200 ft	
E	100 ft	100 ft	150 ft	150 ft	150 ft	200 ft	

The constraint on the track width and wheelbase is then given by 3.27.

$$2 \cdot R_{180} - W_{runway} \leq 0 \quad (3.27)$$

3.4 Design bogies

The first step is to check whether or not the MTOM of the aircraft is close to the so-called switch limit. The MTOM is checked to be within 10% of 100, 200 or 300 tons, based on an observation made when investigating the MTOM vs the total number of main gear tires of 67 transport aircraft. If this is the case, the bogie wheelbase of a larger bogie is used for the design. This is done to allow the aircraft to be fitted with a larger bogie if required when the design is already finished, avoiding the need to redesign the aircraft. The supported bogie types are shown in figure 3.10.

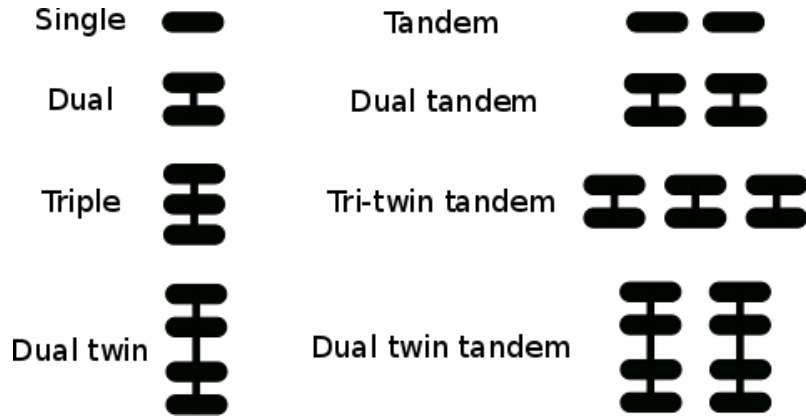


Figure 3.10: Implemented bogie types

For each bogie configuration, the load per tire is computed. From a database the information of the tires is loaded, based on the Goodyear tire databook[17]. From the database the tire closest to the computed tire load times 1.25 is selected. With this tire, the dimensions of the bogie is calculated, including a grown tire ratio of 4% for width and 10% for diameter and tire clearances for each bogie type as specified by Torenbeek[31]. Each bogie is then checked on the following points:

- Interference with floor when retracted
- Fuselage width to stow fuselage bogies in case of 3 or 4 struts
- Flotation requirements

For the floor interference, a boundary box is calculated around the bogie. For wing mounted gear, the box is rotated around the main gear attachment point with equation 3.28a. In case of 3 or more struts, the fuselage bogie is rotated with equation 3.28b. All other cases assume $\alpha_{rot} = 90$.

$$\alpha_{rot} = 90 - \tan^{-1} \left(\frac{z_{kink,min} - z_{root,min}}{y_{kink}} \right) \quad (3.28a)$$

$$\alpha_{rot} = 90 - \sin^{-1} \left(\frac{z_{floor} + 0.5 \cdot D_{tire} + C_{rad}}{L_{gear} - 0.5 \cdot D_{tire}} \right) \quad (3.28b)$$

C_{rad} is the radial tire clearance as specified by Torenbeek[32]. The minimum and maximum outer points are checked with equations 3.29, 3.30 and 3.31.

$$x_{box,min} > x_{stowspace,fwd} \quad (3.29)$$

$$x_{box,max} < x_{stowspace,aft} \quad (3.30)$$

$$z_{box,max} < z_{floor} \quad (3.31)$$

The limits on the stowage space can be set by the user. The flotation requirement is set by the worst flexible and rigid Pavement Classification Numbers (PCN's) of the airfields the aircraft is set to operate on. The bogie design will have to satisfy equation 3.32 for both pavement types.

$$ACN \leq PCN_{min} \quad (3.32)$$

After the valid bogie(s) is/are selected, the brakes are sized for each bogie based on the methods of N. S. Currey[11]. First, the stall speed at takeoff and landing are computed using equation 3.33 with $C_{LTO,max}$ and $C_{LLand,max}$.

$$V_{stall} = \sqrt{\frac{2 \cdot M \cdot g}{\rho \cdot S \cdot C_L}} \quad (3.33)$$

M is the mass of the aircraft during takeoff and landing. The power off speed V_{PO} is assumed to be 20% higher than the stall speed. For aborted takeoff the kinematic energy (in $10^6 \text{ lbf} \cdot \text{ft}$) absorbed by the brakes is determined with equation 3.34, assuming a 6 ft/s^2 deceleration and MTOM.

$$E_{kin,TO} = \frac{M \cdot V_{PO}^2}{2 \cdot 10^6 \cdot N_{brakes}} \quad (3.34)$$

Using figure 3.11 from Currey[11] the weight of the brakes is determined.

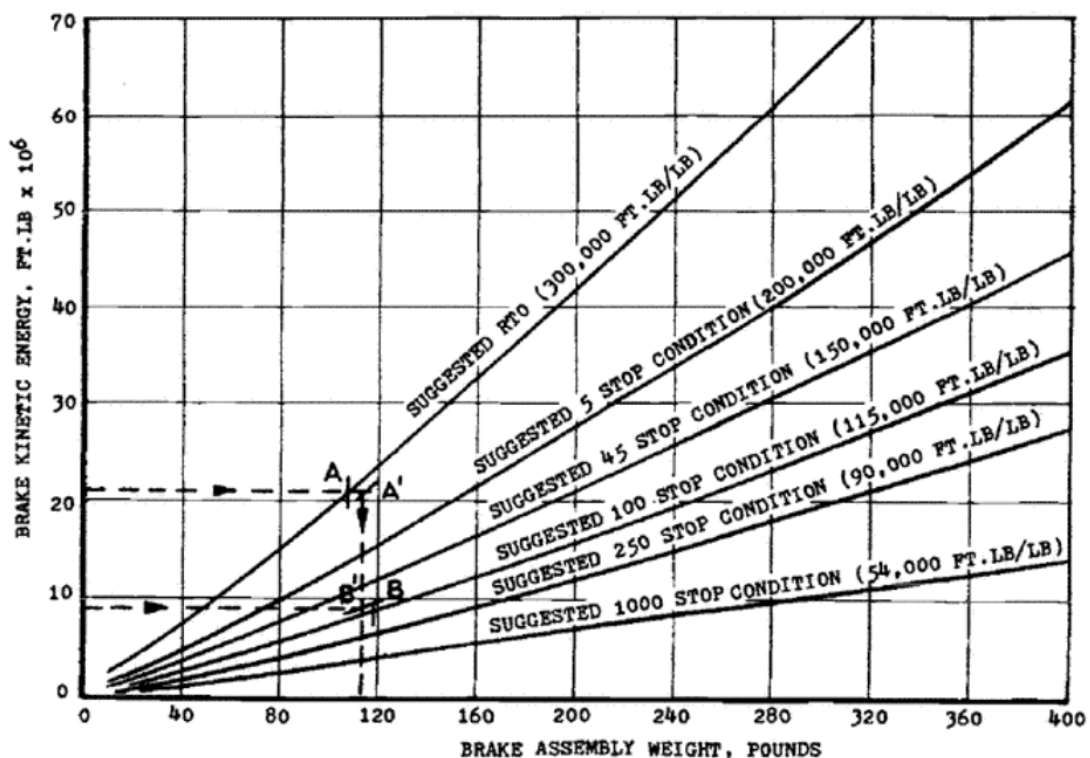


Figure 3.11: Brake assembly weight estimation by Currey[11]

Next, the weight of the brakes is calculated for 5 and 250 stops with 10 ft/s^2 deceleration at maximum landing weight. Equation 3.34 is used to determine the kinetic energy and figure

3.11 to determine the assembly weight. The weight of the brakes is determined by taking the average of the three cases. The volume of the brake is estimated using figure 7.7 from chapter 7 of Currey[11]. If carbon brakes are used instead of steel, the weight is reduced by 60% and the volume increased by 28%.

3.5 Design landing gear struts

For the shock absorber design, the design book of Currey[11] was used. The following assumptions[11] are made:

- The absorber is of the oleo-pneumatic type.
- The static pressure inside the strut is assumed to be 1500 psi. This is assumed to have easier maintenance of the shock absorber.
- The sink speed V_{sink} of the aircraft during landing is 10 ft/s.
- The landing load factor is 1.2. This factor should be between 0.7 and 1.5, so a slightly worse than average factor is assumed.
- The tire efficiency n_t is 0.472.
- The absorber efficiency n_s is 0.9. It is assumed that the most state of the art absorbers are used for the aircraft design.
- The pressure ratio between static and unloaded is 4/1. This ratio is typical for transport aircraft.
- The pressure ratio between fully compressed and static is 3/1. This ratio is typical for transport aircraft.

To determine the required stroke, equation 3.35 given by Currey is used. It is assumed that the absorber and the tire will have to absorb the energy of a zero lift landing.

$$S = \frac{V_{sink}^2}{2g \cdot N} - \left(\frac{S_t \cdot n_t}{n_s} \right) \quad (3.35)$$

An additional inch is added to the stroke for safety. The user is also free to specify an amount of stroke. Stroke S is then set to this value. For each phase of the shock absorber (fully compressed, static load and unloaded) the pressure and volume are computed using Boyle's law 3.36. The piston area is calculated by dividing the static load of the strut by the assumed static pressure. The displacement volume is then calculated by multiplying this area with the stroke.

$$P_1 \cdot V_1 = P_2 \cdot V_2 \quad (3.36)$$

The strut diameter is estimated using equation 3.37 from Torenbeek[31].

$$D_{strut} = 0.5 + 0.03 \cdot \sqrt{F_{strut}} \quad (3.37)$$

in which F_{strut} is the static load on the strut. The orifice area is determined using equation 3.38.

$$A_{or} = \frac{0.3 \cdot A_{piston}}{G_{comp}} \cdot \sqrt{\frac{A_{piston} \cdot S}{F_{strut,stat}}} \quad (3.38)$$

With the shock absorber designed, the rest of the strut can be sized. Three different design cases are distinguished: engine or pod stowed gear, fuselage mounted gear and wing/wing and fuselage mounted gear. If the gear is stowed within the engine nacelle or within a wing mounted pod, the gear would have to be folded to have a small fairing. The main strut is divided into two parts: The top part A and the lower part B containing the shock absorber. First, an 'ideal fold length' is calculated for each strut. For the lower part, this is determined with equation 3.39.

$$L_{B,ideal} = \frac{L_{comp,gear} + 1.1 \cdot D_{tire}}{2} \quad (3.39)$$

This value is compared to the required minimum length, equation 3.40

$$L_{min} = L_{pist,min} + 0.55 \cdot D_{tire} \quad (3.40)$$

in which the minimum piston length is calculated with 3.41[11].

$$L_{pist,min} = S + 2.75 \cdot 2 \cdot \sqrt{\frac{A_{piston}}{\pi}} \quad (3.41)$$

The largest of the two values is used as the length for B. The remaining length of the main gear is set as the length of strut A. It is assumed that when retracted, part B is rotated such that it is horizontal. A distance between the tire center and the main gear attachment point of at least $0.55 \cdot D_{tire} + 0.025$ [m] is required for save stowage. Fold angle ϕ_{strut} of A is determined with equation 3.42.

$$\phi_{strut} = \sin^{-1} \left(\frac{0.55 \cdot D_{tire} + 0.025}{L_A} \right) \quad (3.42)$$

If part A is smaller than the minimum stowage distance, part A does not rotate and the fold angle is set to 90 degrees. An example of the folded gear is given in figure 3.12a.

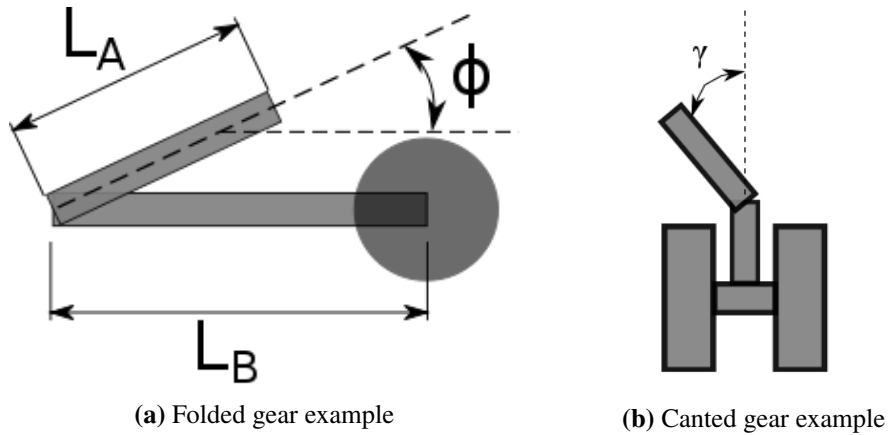


Figure 3.12: Folded and canted gear example

For the fuselage mounted gear, the gear's main strut might consist of two parts, of which the top part A is canted inward. This is done to keep a larger track width while having a smaller fairing to house the undercarriage. For this case a cant angle γ_{strut} of the top strut is calculated, for the other cases this angle is set to 0. A maximum of 40 degrees canting is assumed. The shock absorber is assumed to be in the upper part of the strut. An example is shown in figure 3.12b As strut part A is canted inward, it is elongated to ensure the same overall landing gear height. For all strut designs, the attachment point coordinates of the gear to the aircraft are also computed.

3.6 Evaluate wing position

With the initial strut design available, a better design can be generated with the optimization routine discussed in 3.3. This allows to make a better estimation of the wing position limits and for the initial wing position. If the main gear is attached to the wing, the script selects the bogie which should be used for the evaluation based on the smallest wheelbase. If multiple bogie design fit the description, the first one is used. The wing is set at 90% of it's initial value and moved aft up to 1.1 times the initial wing position, with a step size of 10cm. For each position, the optimization routine is run to see if a landing gear design is possible. The change in cg is estimated using a Class I estimation[33]. For the Class I cg estimation, the following assumptions were made:

- The cg of the fuselage is at 40% fuselage length.
- The weights of systems, furniture are assumed to be spread out evenly among the fuselage length.
- The cg of the main wing is located at 40% MAC.
- The cg of the empennage is located at 90% fuselage length.
- The cg of the engines is located at 40% engine length.

By calculating the arm l_{cg} of each individual cg w.r.t. the aircraft nose and using equation 3.43 the cg position is estimated.

$$cg_{AC} = \frac{l_{cg,fus} \cdot M_{fus,tot} + l_{cg,wing} \cdot M_{wing} + l_{cg,emp} \cdot M_{emp} + l_{cg,eng} \cdot M_{eng,tot} + l_{cg,gear} \cdot M_{gear,tot}}{M_{tot}} \quad (3.43)$$

If a design is possible, the wing position is saved. The most forward position and most aft position are passed on to the horizontal stability estimation module as bounds for the wing position. The wing is then set to the most forward wing bound. The user can relax this forward limit by a percentage of the fuselage length in the settings file. This can help with the Initiator converging to a feasible design. If no solution exists or if the gear is not attached to the wing, the bounds are also set to the initial wing position $\pm 5\%$ fuselage length and the wing is not moved.

3.7 Designing the auxiliary spar

With the landing gear design finalized, the auxiliary (or kick) spar can be designed if the gear is attached to the wing. If not, the auxiliary spar does not have to be (re)designed. The script loads the spar data and checks if the number of spar fractions is correct. This is done by checking if a kink is already present in the wing or not. If a kink is present, the number of spar sections should be one more than the number of wing sections. If a kink is not present, the difference should be two. If neither is the case, additional spar fractions and the section chords will be added for the auxiliary spar to the existing spar data. From the given gear location, a straight spar is generated going from the fuselage towards the rear spar. Of this new spar, the coordinates of the intersection locations with the fuselage and the rear spar are calculated. Then, the chord lengths at these locations are calculated. For the new kink location, the chord is calculated using extrapolation of the most outer and the second most outer spar sections. If a kink was already present, the semi-spanwise location of the kink is updated to the new value. If not, the new value will be added to the wing structure. The spar coordinates are then converted into chord fractions and saved into the spar structure. The updated values are then written as input for the geometry estimation module.

3.8 Estimation of the gear fairing dimensions

For the gear fairing dimensions a rough estimation of the fairing was made. It was decided that the fairing would consist of elliptical shapes, as they are easy to implement and give a fairly good approximation. The fairing is not created when the undercarriage is of the wing mounted type. There are three types of fairing which can be created: a fuselage fairing, an extended engine fairing and a wing mounted pod. An example of the fairing is shown in figure 3.13. **a** indicates the major axis and **b** the minor axis.

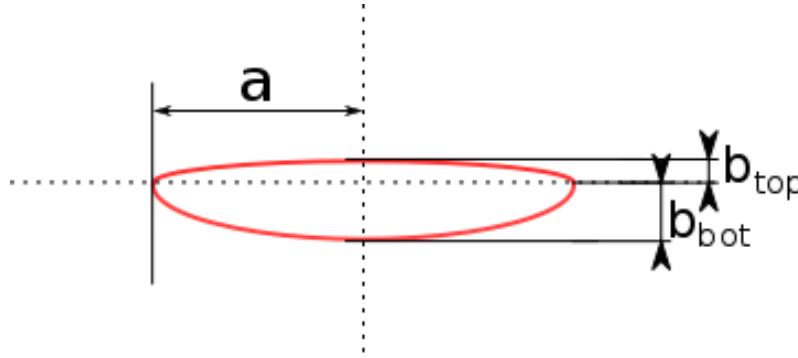


Figure 3.13: Fairing shape example

For the fuselage fairing, equation 3.44a, 3.44b and 3.44c are used for the frontal shape. Equations 3.45a, 3.45b and 3.45c are used for the longitudinal shape.

$$a_{front} = y_{attach,gear} \quad (3.44a)$$

$$b_{front,bot} = z_{attach,gear} - z_{bogie,stowed} \quad (3.44b)$$

$$b_{front,top} = 0.2 \cdot b_{front,bot} \quad (3.44c)$$

$$a_{long} = B_{bogie} + 1.1 \cdot D_{tire} + 0.1 \quad (3.45a)$$

$$b_{long,bot} = z_{bogie,stowed} \quad (3.45b)$$

$$b_{long,top} = 0.2 \cdot b_{long,bot} \quad (3.45c)$$

The side profile of the fairing is checked to have at least a slenderness ratio of 2. If this is not the case, the major axis is adjusted to satisfy the slenderness ratio. For the nacelle fairing, equation 3.46a, 3.46b and 3.46c are used for the frontal shape. Equations 3.47a, 3.47b and 3.47c are used for the longitudinal shape.

$$a_{front} = \max([R_{eng}, y_{bogie,stowed} - y_{attach,gear}]) \quad (3.46a)$$

$$b_{front,top} = R_{eng} + (z_{eng} - z_{attach,gear}) \quad (3.46b)$$

$$b_{front,bot} = \max([b_{front,top}, z_{attach,gear} - z_{bogie,stowed}]) \quad (3.46c)$$

$$a_{long} = 0.5 \cdot (x_{aft,bogie,stowed} - x_{eng,front}) \quad (3.47a)$$

$$b_{long,top} = R_{eng} + (z_{eng} - z_{attach,gear}) \quad (3.47b)$$

$$b_{long,bot} = \max([b_{long,top}, z_{attach,gear} - z_{bogie,stowed}]) \quad (3.47c)$$

For the pod stowed gear, the design is based on the Tu-154. The center point of the pod is shifted aft by 33% of the major axis. This is done to cover the gear correctly, while still being able to

properly mount the pod to the wing. Equations 3.48a, 3.48b and 3.48c are used for the frontal shape. Equations 3.49a, 3.49b, 3.49c and 3.49d are used for the longitudinal shape.

$$a_{front} = y_{bogie, stowed} - y_{attach, gear} + 0.05 \quad (3.48a)$$

$$b_{front, top} = z_{attach, gear} - z_{bogie, stowed} \quad (3.48b)$$

$$b_{front, bot} = z_{attach, gear} - z_{bogie, stowed} \quad (3.48c)$$

In case of a single row bogie, equation 3.49a is used. In case of a multi-row bogie, equation 3.49b is used.

$$a_{long} = (x_{aft, bogie, stowed} - x_{attach, gear}) + 0.5 \cdot 1.1 \cdot D_{tire} \quad (3.49a)$$

$$a_{long} = (x_{aft, bogie, stowed} - x_{attach, gear}) + 1.1 \cdot D_{tire} \quad (3.49b)$$

$$b_{long, top} = z_{attach, gear} - z_{bogie, stowed} \quad (3.49c)$$

$$b_{long, bot} = z_{attach, gear} - z_{bogie, stowed} \quad (3.49d)$$

For the frontal area, equation 3.50 is used in which **a** is the major axis and **b** the minor axis.

$$A_{ellipse} = \left[\int_0^\pi (a \cdot b \cdot \cos^2(t) dt) \right]_{top} + \left[\int_0^\pi (a \cdot b \cdot \cos^2(t) dt) \right]_{bot} \quad (3.50)$$

For the fuselage case however, this includes the area of the fairing which is actually inside the fuselage. The area covered by the fuselage is calculated using the coordinates of the fuselage section at which the center point of the fairing is located, taking the difference with the curve of the upper ellipse and estimate the area by making a Riemann sum. The center point is set to be in the middle of the main gears. The number of steps is determined by the available data points which describe the fuselage shape.

The wetted area is calculated by a combination of integrals and a Riemann sum, as the length of the minor and major axis of the cross-section depend on the longitudinal position due to the double elliptical shape. The integral for the circumference of an ellipse is given by equation 3.51, in which **e** is the eccentricity of the ellipse and **a** the major axis.

$$L_{ellipse} = a \cdot \int_{t_{low}}^{t_{up}} \sqrt{1 - e^2 \cdot \sin^2(t)} dt \quad (3.51)$$

The lower and upper limits of the integral depend on which ellipse is to be integrated. The assumption is made that the fairing is always wider than the fuselage itself. Therefore, the lower ellipse the limits are 0 and π respectively. For the upper ellipse, the limits depend on the intersection location with the fuselage. The length of each segment is the total fairing length divided by the number of steps of the sum. The number of steps for the sum is set to 80 to have sufficient accuracy but with minimal computational time, as table 3.6 shows. The base value of steps for the check is taken as 100 steps. One should take into account that the computational time is only around a couple of hundredth of a second (for example, 0.22 seconds for 100 steps). So even if the percentual gain is large, the actual gain in seconds is small. Therefore, the change in area is determined to be more important.

Table 3.6: Riemann step size verification

Number of steps	Change in area	Change in computational time
10	-3.2%	-76%
30	-0.5%	-62%
50	-0.2%	-45%
80	-0.04%	-19%
100 (base)	0%	0%
120	+0.03%	+12%
150	+0.05%	+34%
300	+0.09%	+154%

At each step, the average of the frontal minor and major axis for both the upper and lower ellipse at $(N - 1) \cdot dx$ and $N \cdot dx$ are taken. Of both ellipses the circumference is calculated and summed. Also the covered area is calculated to account for the reduction in fuselage wetted area. The equivalent diameter of the ellipse, used to calculate C_{D_0} of the fairing, is calculated using equation 3.52[24]

$$D_{eq} = \sqrt{\left(\frac{\pi}{4}\right) A_{max}} \quad (3.52)$$

For the nacelle stowed gear, the frontal area is calculated using equation 3.50 and the wetted area in a similar fashion as for the fuselage fairing. The covered wing skin area per fairing is assumed to be twice the area of the airfoil located in the center of the fairing. The equivalent diameter is set to be the propeller diameter for the drag calculation.

For the pod design, the frontal area is calculated with 3.50. The wetted area is calculated in the same way as for the nacelle fairing. The equivalent diameter is determined with equation 3.52.

3.9 Landing gear drag

The landing gear drag is calculated by the Parasite drag estimation module and is determined with the method suggested by Raymer[24]. If the landing gear design module has not been run yet, it returns the default parasitic drag, which is given as input. If the gear module has been run, the drag is computed using Raymer's method. The drag for each gear is calculated using equation 3.53.

$$C_{D_0, gear} = \frac{\sum_{n=1}^{N_{components}} (D/q)_{component}}{S_{ref}} \quad (3.53)$$

The ratio $(D/q)_{component}$ for each component is calculated with equation 3.54.

$$(D/q)_{component} = \left(\frac{(D/q)}{A_{frontal}} \right)_{component} \cdot A_{component} \quad (3.54)$$

The frontal area of each component is calculated and converted to ft^2 . The $\frac{D}{A}$ suggested by Raymer for each component is given in table 3.7.

Table 3.7: Landing gear component drag

Component	$\frac{D}{A_{frontal}} [ft^2]$
Regular wheel and tire	0.25
Second wheel and tire in tandem	0.15
Round strut or wire	0.30
Fork, bogey, irregular fitting	1.0 - 1.4

The total parasitic drag is then calculated by summing the individual gear drags and multiplying the total by 1.2 to account for mutual interference. The fact that the landing gear drag is a function of lift (at higher lift coefficients the drag of the gear actually reduces due to a reduction in airflow velocity underneath the wing) is currently ignored.

3.10 Fairing drag estimation

The fairing drag is also estimated by the parasitic drag estimation module. If the landing gear design module has been run, the designed fairing will be evaluated. If not, the default value for the fairing drag will be used. The drag is estimated by making use of the estimation by Raymer[24]. Like Torenbeek, Raymer states that the drag of a blister fairing or pod can be estimated using the same method as used for the fuselage drag. The parasitic drag is estimated using equation 3.55.

$$C_{D_0} = C_f \cdot FF \cdot Q \cdot \frac{S_{wet}}{S_{ref}} \quad (3.55)$$

In equation 3.55, C_f is the skin friction coefficient, FF the form factor and Q the interference factor. The skin friction coefficient is a function of the object's length, Reynolds number, Reynolds transition number and Mach number.

For the skin friction coefficient, in case of turbulent flow, the curves of Roskam part 6[25], p. 25 are used. The value obtained from the curves is compared to the calculated skin friction coefficient using equivalent sand grain roughness. First the equivalent Reynolds number is determined with equation 3.56.

$$Re_{sg} = \left(\frac{39.5 \cdot c}{k_{sg}} \right)^{\frac{1}{0.94}} \quad (3.56)$$

C is the length of the shape and k_{sg} the equivalent sand grain roughness, which is set to $2.54 \cdot 10^{-5}$. The skin friction drag obtained using the equivalent sand grain roughness method is then determined with 3.57.

$$C_{f,sg,turb} = \frac{0.074}{Re_{sg}^{0.2}} \quad (3.57)$$

The largest of $C_{f,Rosk,turb}$ and $C_{f,sg,turb}$ is used for the turbulent skin friction coefficient. For laminar flow, equation 3.58 given by Anderson[2] is used.

$$C_{f,lam} = \frac{1.328}{\sqrt{Re}} \quad (3.58)$$

The friction coefficient for turbulent flow is scaled with the transition Reynolds number, based on fairing length, with equation 3.59.

$$C_f = \frac{Re_{tr} \cdot C_{f,lam} + (Re - Re_{tr}) \cdot C_{f,turb}}{Re} \quad (3.59)$$

The form factor is calculated with equation 3.60. It must be noted that this equation could under predict the form factor if the shape has a high slenderness, but performs better for shapes with a low slenderness ratio than the other equation suggested by Raymer. As the fairing often has a low slenderness ratio, it was decided to use this equation.

$$FF = 1 + \frac{0.35}{f} \quad (3.60)$$

The slenderness ratio is calculated using equation 3.61.

$$f = \frac{l}{D_{eq}} \quad (3.61)$$

The equivalent diameter is already calculated by the fairing estimation using equation 3.52. With all information loaded from the object, the drag for the fairing is computed. If the fairing is located on the fuselage, the wetted area covered by the fairing is subtracted from the wetted area of the fuselage. If the gear is stowed in pods, the drag is calculated for a single pod and then multiplied by the number of main gear struts. In case of engine mounted gear, the script does not calculate the fairing drag, but uses the engine drag script to determine the increased drag. The wetted area of the engine is replaced by that of the fairing after which the drag is calculated in a similar fashion as described for the fuselage fairing or pods.

3.11 Supported aircraft configurations

The current module supports aircraft with a maximum of four main gear struts, with a maximum total of 26 tires. Main gear placement is possible on the wing, on the fuselage, on both wing and fuselage, stowed in the engine nacelle and in wing mounted pods. Only the wing/fuselage combination supports three and four main gear struts. The author is aware of possible turbofan nacelle stowed gear, as a patent[16] by Boeing shows, and the module will give a result if that combination is chosen. However, this option is intended for propeller aircraft and any other attempt to use it most likely will result in an invalid gear design. The module has not been verified to support the blended wing body (BWB) configuration, as no input model was available.

4 Verification

To ensure a valid gear design is created, several changes had to be made to the existing landing gear design module. The difference between the old and new module are shown in table 4.1.

Table 4.1: Module features

	Old Initiator	New Initiator
Wing mounted gear	✓	✓
Fuselage mounted gear	✓	✓
Nacelle mounted gear	X	✓
Pod mounted gear	X	✓
Optimization routine	X	✓
Can adjust wing planform	X	✓
Wingbox sizing	X	✓
Fairing sizing	X	✓
Fairing drag estimation	X	✓
Landing gear drag estimation	X	✓

The old method only allowed for wing mounted and fuselage mounted gears. This meant that a design such as the Fokker 50 or Tu - 134 like aircraft were not possible. To make the tool more versatile, the options for nacelle and pod stowed gears were implemented. The old method would try to fit the lowest gear as possible by evaluating a matrix of gear height and takeoff angles. This objective of designing the lowest gear is still kept, as the lowest gear will also yield the lightest design, but the matrix is replaced with an optimization routine. This gives more accurate results

and reduces the computation time of the method. The new method is also allowed to change the wing position and adjust the kink location. The kink location is based on the attachment point of the auxiliary spar at the rear spar. To position the landing gear correctly behind the rear spar, a simple wingbox was added as well. To evaluate the difference and benefits of a certain design, the fairing of podded, fuselage mounted and nacelle stowed gears is also estimated. With this estimation the increase in drag added by the fairing can be added to the Initiator. A basic gear parasitic drag estimation was also added to have the gear dimensions also have an effect on C_{D_0} .

The base of obtaining a good concept is having a model which is an accurate representation of the reality. Hence, the wing and fuselage models used should be as accurate as possible or the inaccuracies should be dealt with. First, the fuselage shapes of the models used are investigated. The following aircraft were used for calculations with the landing gear design module: A320-200[1], B727-200[6], B737-800[7], B777-300[5], ATR 72-600[3] and the Fokker 100[15]. The comparison of the fuselage shape and definition of the correction factor is shown in figure 4.1.

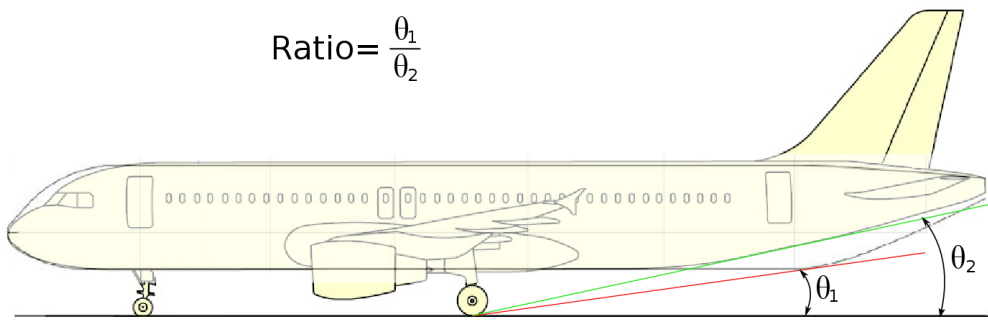


Figure 4.1: Fuselage shape correction factor

θ_1 is the angle of the actual gear with the model fuselage and θ_2 the angle of the actual aircraft. Using this method, the correction factors for the scrape angle shown in table 4.2 were obtained. Applying the correction factor to the scrape angle will help obtaining more accurate results, as gear height and longitudinal position are often driven by the minimal scrape angle requirement.

Table 4.2: Fuselage aft shape correction factors

Aircraft type	Correction factor
A320-200	0.685
B727-200	0.926
B737-800	1.0
B777-300	1.0
ATR 72-600	0.843
Fokker 100	0.882

Another factor which determines the longitudinal landing gear position, is the most forward and aft location of the center of gravity. To verify if the center of gravity estimation is done correctly, the OEM cg of the A320-200, B727-200, ATR 72-600 and Fokker 100 were computed with a Class I estimation[33], as described in section 3.6, and compared to the value computed by the Initiator. To verify the cg position, the results of the weight estimation done by the Initiator were used. The result is shown in table 4.3.

Table 4.3: Center of gravity verification

Aircraft	A320-200	B737-800	ATR 72-600	Fokker 100
Fuselage group mass [kg]	22516	24107	8605	13477
Wing group mass [kg]	6960	7577	2630	4530
Empennage group mass [kg]	2253	3355	426	1437
Engine group mass [kg]	5562	5614	2012	3016
Landing gear group mass [kg]	2353	2375	731	1332
Initiator cg long. position [m]	18.75	20.62	12.76	17.70
Class I cg long. position [m]	17.15	18.93	11.70	16.26
Difference in cg position [%]	-8.53	-8.20	-8.25	-8.13

As can be seen in table 4.3 the estimation done by the initiator is quite in agreement with the Class I estimation, as the difference between the cg values is always around 8%. The initiator computes the aircraft cg by taking more component groups and calculating their individual cg's instead of the five groups used for the Class I estimation, hence the difference between the outcomes. One thing that must be noticed however, is that the cg estimation used by the Initiator overestimates the most forward and aft location of the cg[22]. For example, when the cg estimation of the Initiator was validated using the B707, the calculated cg range according to the cg is 12% to 38% MAC. According to the B707 manual, the operational range for the cg is 14% to 23% MAC. As no adjustments to the cg range are currently implemented, this will affect the result of the landing gear design module. Hence the Initiator is consistent in giving the cg location when compared to a Class I method, but still has an error in the location when compared to the actual data of the aircraft.

4.1 Weight Estimation

A critical part of the new method is the weight estimation, as the gear with the least weight is selected as the most optimal solution. A common issue with the statistical weight estimation methods is that only a limited number of weight-affecting parameters are considered. As it is also based on designs of the past, gears for unconventional aircraft configurations might end up with different weights than predicted with these methods. Figure 4.2[9] shows the difference in statistical weight estimation methods.

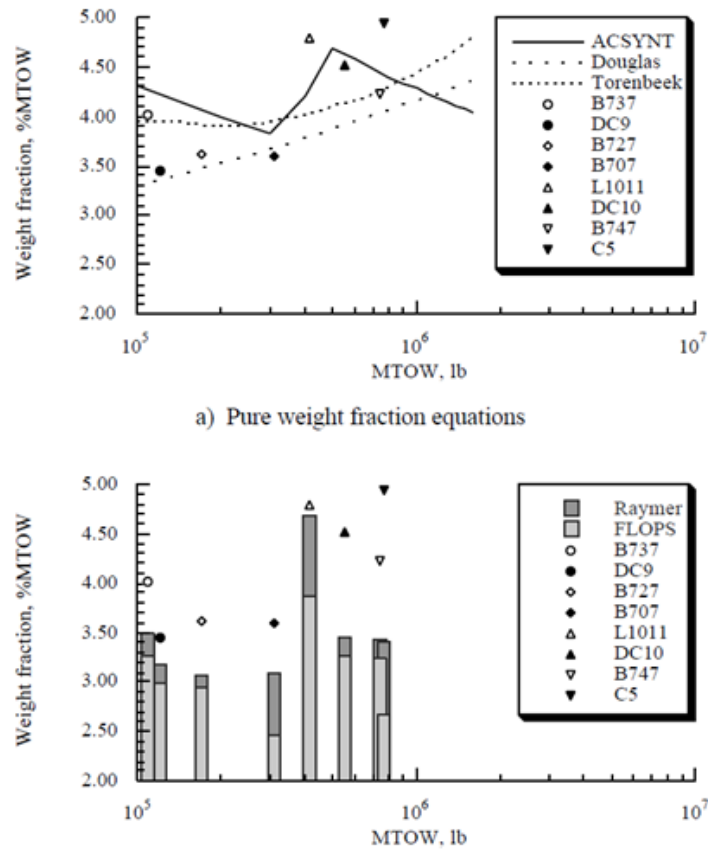


Figure 4.2: Comparison of weight estimation methods[9]

For the weight estimation, the method created by Raymer[24] is used. This weight estimation method has, among others, the gear length as a variable. The weight estimation of Torenbeek lacks this variable, making it less suitable for the optimization routine. Figure 4.2 shows that for larger MTOWs, the estimation of all methods is off by a large margin. This is most likely due to the fact that less gear weight data is available for aircraft in the 500000+ lbs weight category and the readily available data for lighter aircraft. However, even where a lot of data is present there is still a lot of scatter in the estimation results. The figure does show that the weight estimation of Raymer yields the best results. An improvement suggested by Chai and Mason[9] is to use an analytical weight estimation method to improve the accuracy. To do so, a more detailed design of the landing gear should be available. As a detailed design of the gear is not generated during the conceptual design stage, this improvement should be implemented after the conceptual design phase is completed. The detailed gear design can then also be used for the design of the kinematics of the gear.

The weight equation used during the optimization is shown in equation 4.1.

$$W_{mlg} = 0.0106 \cdot k_{mp} \cdot k_x \cdot W_l^{0.888} \cdot N_l^{0.25} \cdot L_m^{0.4} \cdot N_{mw}^{0.321} \cdot N_{mss}^{-0.5} \cdot V_{st}^{0.1} \quad (4.1)$$

in which k_{mp} is 1.126 for kneeling main gears and 1.0 otherwise, k_x is 0.536 for XC-142 type (experimental VTOL aircraft) and 1.0 otherwise. One must note that for the case of an equal total number of main gear wheels, an increase in main gear shock struts will lead to a reduction of total main gear weight. E.g. assuming all other parameters to be equal, an aircraft with a total of twelve wheels and two main gear struts will have a heavier gear than an aircraft with twelve wheels and three main gear struts. After consulting the derivation of the equation[12], it might

be a small numbers problem. The verification given in the report shows that the equation has a correlation coefficient of 0.999 for the eleven aircraft used. However, as the number of main gear struts will only be increased if no feasible bogie design exists and not after the bogie designs are set, this situation will not occur during the optimization process. The weight based selection thus remains valid, but the weight estimation of cases such as described above can result in an incorrect gear weight estimation at the end of the conceptual design phase. Again, an analytical weight estimation method will remedy this problem in the detailed design phase.

4.2 Pod design

To verify the fairing design of podded landing gear, the Fokker 100 model is used to fit a podded gear on the wing. The 2.5° dihedral of the Fokker is changed to -2° to match the Tu-134. The Fokker 100 is comparable to the Tu-134, which is fitted with this type of gear. The resulting fairing on the Fokker 100 is compared to the fairing of the Tu-134 to if an acceptable result is obtained. Figures 4.3² and 4.4² show the resulting top and front view, respectively.

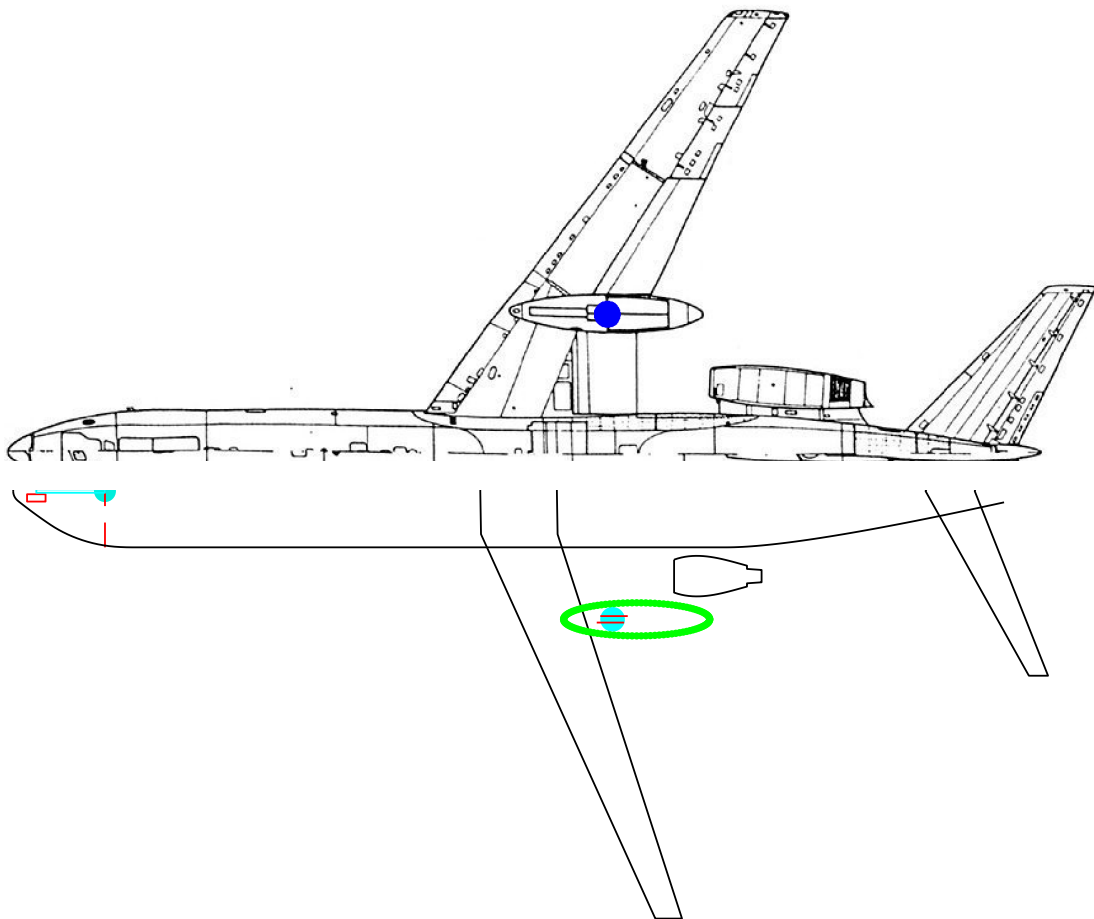


Figure 4.3: Top view pod estimation comparison

Compared to the Tu-134, the pods generated by the Initiator are shorter and have a more blunt nose. The pods of the Tu-134 also run up to the front spar, while the initiator result has the pods further to the back. The pods of the Fokker are shorter as they only require to house the gear. The pod design of the Tu-134 includes the drag struts, which runs up to the front spar. The top of the

²Image Tu-134 from <https://www.aviationsmilitaires.net/v2/base/view/Model/1097.html>

Tu-134 pod is in agreement with the pod designed on the Fokker. This difference is due to the fact that the pod estimation assumes symmetrical pods.

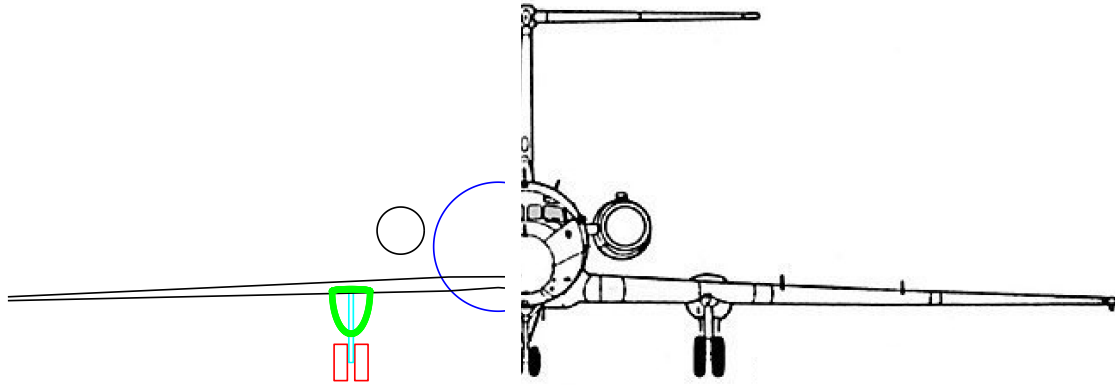


Figure 4.4: Front view pod estimation comparison

The front view shows a slight difference in pod design. The pods of the Fokker house a folded gear, which causes the upper part of the pod to be more flattened, while the bottom part is lower. The width of both designs is similar. Overall the pod estimation is in agreement with a comparable actual pod design.

4.3 Effect of wing sweep on design

To test the effect of wing sweep on gear design, the wing sweep is varied on a medium sized, single isle airliner. The Initiator determines the wing sweep by the specified cruise Mach. Thus to vary the sweep, the cruise Mach is taken from 0.72 to 0.82. Figure 4.5 presents a top view showing the effect on wing sweep and gear position.

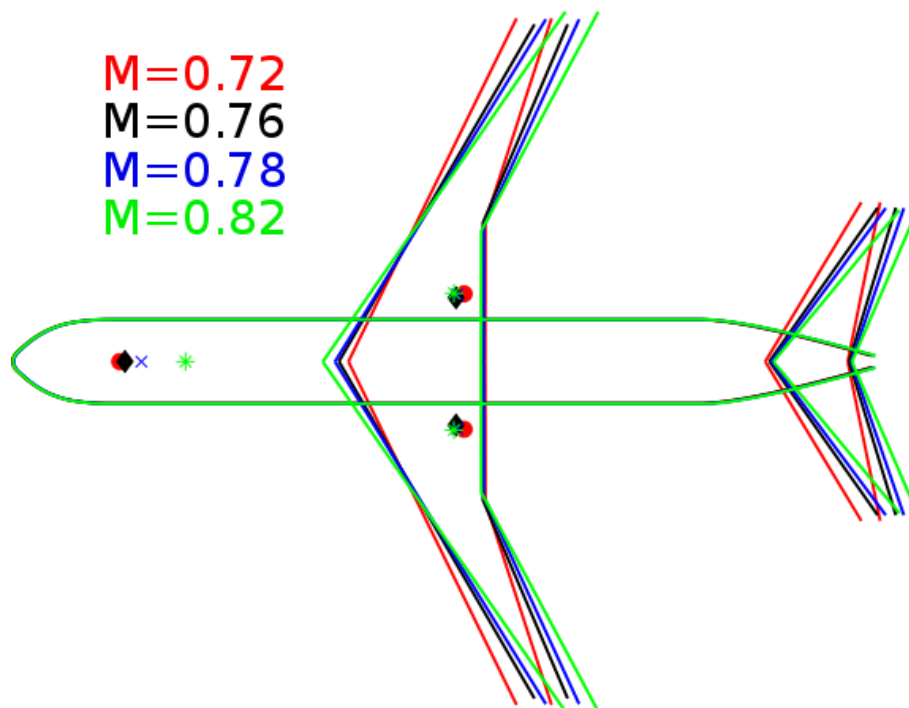


Figure 4.5: Effect of cruise Mach on aircraft concept

Figure 4.5 shows that with increasing wing sweep the main gear moves more forward, while the nose gear moves more aft. This indicates that the cg range estimated by the Initiator reduces as the wing sweep increases for this case. Table 4.4 confirms the forward shift of the cg. The minor shift of the main gear is as to be expected, as the rear spar in the main wing also moves slightly forward and the main gear has to comply with the maximum distance from the rear spar. It can also be seen in table 4.4 that for the large sweep angles the gear moves as far outboard as possible to remain as far aft as the design requirements allow. For the low sweep angles, the gear design was close to reaching the forward attachment requirement. As the sweep angle increased, this shifted to the aft attachment requirement being sizing for the design. To keep the nose gear in the front part of the fuselage, the range in which the optimizer was allowed to place the nose gear was set from 5% to 20% fuselage length. For the $M=0.82$ case, the nose gear was placed at exact that limit. This means that the wing could not be moved further aft to relieve the attachment requirements.

Table 4.4.

Table 4.4: Effect of sweep on gear design

Mach	Wing sweep [deg]	MTOM	OEM CG x [m]	MG x [m]	B [m]	T [m]
0.72	26.2	74100	19.6	21.1	16.1	6.4
0.74	28.5	73700	19.5	20.7	15.2	6.0
0.76	30.1	73000	19.5	20.7	15.6	6.0
0.78	31.7	75200	19.5	20.6	14.7	6.2
0.80	33.2	77500	19.4	20.5	12.6	6.4
0.82	34.8	79800	19.4	20.5	12.5	6.4

For this sensitivity analysis, the problem of the cg estimation becomes visible as the sweep angle of the main wing becomes large. The cg range reduces to such a small range, that the module starts having difficulties designing a valid landing gear. The user could increase the range

in which the nose gear may be placed by the optimizer, but this will result in landing gear designs with an unrealistically small wheelbase. Hence, the landing gear module behaves as to be expected with the given input but the cg estimation of the Initiator will have to be improved before the new module can be used to its full potential.

4.4 Effect of lateral tip over requirement

To evaluate the effect of the lateral tip over requirement on the gear design, a fuselage mounted landing gear is designed for a high wing turboprop aircraft. The maximum later tip over angle was varied from 40° to 70° . The results are shown in table 4.5.

Table 4.5: Effect of lateral tip over on gear design

ψ [deg]	T [m]	L_{MG}	L_{NG} [m]	M_{gear} [kg]	C_{D_0} fairing [counts]
40	8.1	1.1	1.0	660	24
45	6.7	1.1	1.0	660	20
50	5.6	1.1	1.0	660	16
55	4.6	1.1	1.0	660	13
60	3.8	1.3	1.0	660	8
65	3.7	1.3	1.0	640	6
70	3.7	1.3	1.0	640	6

Table 4.5 shows that the gear mass does not change with ψ up to an angle of 60° . However, the gear layout does change for the case with $\psi = 60^\circ$. For this case the bogie is changed from a triple type bogie to a dual type bogie. The larger wheel diameter in combination with the wheel clearance requirement increases the gear length, the resulting weight was slightly less due to a smaller number of tires. The difference between both gear layouts proved to be a couple of kilograms, which is negligible during the conceptual design phase. It is clear that for the fuselage mounted gear, the lateral tip over requirement has a large influence on the gear design. This is especially noticeable on the track width and fairing size, as the design requirement pushes the main gear further outboard. The difference in track width when comparing the 40° case with the recommended 55° shows that the track width reduces with 3.5m (43%) and the drag of the fairing by 11 counts (46%). Allowing for a slightly larger lateral tip over angle of 60° further reduces the track width and drag contribution. The track width reduces by 0.8m (17%) and the drag by 5 counts (38%). Increasing ψ more does not yield a very large gain or none at all and might prove to give tip over problems during taxi maneuvers and crosswinds on the ground. The percentile difference between the recommended[31] 55° and other cases with respect to MTOM, total C_{D_0} and total gear mass is shown in figure 4.6.

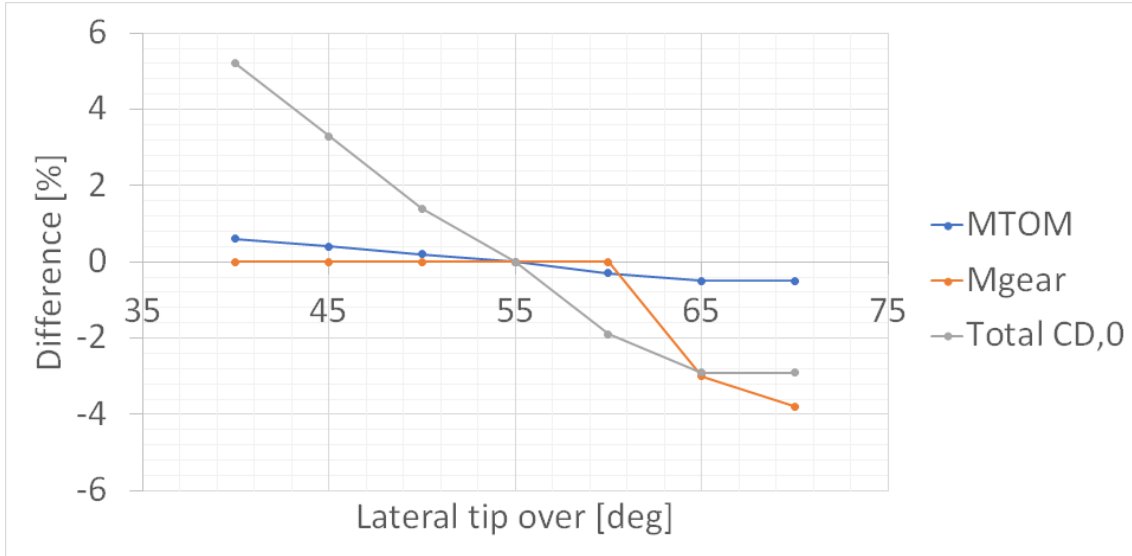


Figure 4.6: Lateral tip over effect comparison

Figure 4.6 shows that using a larger ψ reduces the MTOM, total C_{D_0} and total gear mass. Hence, it may be beneficial in terms of weight and drag reduction to use a the lateral tip over limit of 60° for fuselage mounted gear instead of the recommended 55° . The results also show that the module responds as to be expected with respect to the effect of the lateral tip over design requirement, as the track width increases as ϕ reduces and vice versa.

5 Validation

With the methodology verified, the module is used to recreate the landing gear of existing aircraft. A number of aircraft was modeled in the Initiator and compared to the original aircraft. Table 5.1 shows the gear layouts of both the actual and the resulting aircraft. The gear length of the aircraft are estimated from aircraft characteristics sheets obtained from the manufacturers. For the B727, B777, Fokker 100 and ATR 72-600 the deck angle was also estimated. The angle was estimated to be 0.9° , 1.0° , 1.0° and 1.3° respectively. The B737-800 and A320-200 seem to have no deck angle.

Table 5.1: Gear design validation

Aircraft		N_{wheels}	B [m]	T [m]	$L_{main,comp}$ [m]	L_{nose} [m]
B727-200[6]	Actual	6	19.28	5.72	2.21	1.69
	Module result	6	18.52	6.03	2.43	2.27
B737-800[7]	Actual	6	15.60	5.72	2.01	1.42
	Module result	6	14.26	6.27	2.55	2.15
B777-300[5]	Actual	14	31.22	10.97	4.65	3.05
	Module result	14	19.36	12.00	4.69	2.93
Fokker 100[15]	Actual	6	14.01	5.04	1.81	1.45
	Module result	6	12.45	4.60	1.76	1.13
ATR 72-600[3]	Actual	6	10.77	4.10	1.06	0.85
	Module result	6	11.71	4.71	1.29	0.87
A320-200[1]	Actual	6	12.64	7.59	2.93	2.43
	Module result	6	15.42	7.93	2.92	2.56

Table 5.2 shows the constraint values of each design generated by the Initiator. The driving design requirements are marked.

Table 5.2: Scaled constraint values final gear design

	B727-200	B737-800	B777-300	Fokker 100	ATR 72-600	A320-200
Long. tip over	-0.010	0.008	0.000	-0.020	-0.000	-0.023
Scrape angle	-0.328	-0.552	-0.000	-0.022	-0.142	-0.349
Nacelle/wing tip clearance	-0.035	0.000	-0.262	-0.088	-1.417	-0.000
Lat. tip over	-0.058	-0.131	-0.237	-0.078	0.000	-0.192
Minimum nose load	-0.000	-0.000	-0.000	-0.000	-0.002	-0.010
Maximum nose load	-0.000	-0.061	-0.026	-0.022	-0.034	-0.045
Nose gear stowage	-0.808	-0.702	-2.178	-1.168	-0.000	-0.173
Wheel clearance	-0.730	-0.349	-0.768	0.000	0.000	-0.597
FAA track size	-1.326	-1.317	-1.213	-1.380	-1.376	-1.254
FAA wheelbase	-1.105	-0.991	-0.983	-0.947	-0.929	-1.019
FAA 180 turn	-0.085	-0.254	-0.436	-0.377	-0.402	-0.156
Fwd attachment	-0.037	-0.048	-0.047	-0.041	N.A.	-0.040
Aft attachment	-0.000	-0.000	0.000	0.000	N.A.	-0.001
Long. stowage	-0.057	-0.020	-0.039	-0.029	N.A.	-0.057
Lat. stowage inner	-0.353	0.000	-16.143	-0.000	-20.031	0.000
Lat stowage outer	-0.000	-0.277	-0.230	-0.408	N.A.	-0.225
Engine-strut placement	N.A.	-0.053	-0.009	N.A.	N.A.	-0.100

With the data generated, a close comparison between the concepts and the actual models can be made. For all models the relative difference in gear lengths can also be due to a wrong estimation of the actual gear length, as no data of the total gear length was available. The weight of the gear was determined with equation 4.1. Table 5.3 shows the weight related differences when comparing the generated design to the actual aircraft.

Table 5.3: Relative difference in weight estimations

	B727-200	B737-800	A320-200
Difference Main gear [%]	+2.2	+40.4	-4.5
Difference Nose gear [%]	+24.2	+212.4	+46.0
Total Difference [%]	+2.1	+55.3	+2.53
$100\% \cdot \frac{MTOM_{concept}}{MTOM_{actual}}$	-21.5	-3.1	-7.7
$100\% \cdot \left[\frac{M_{gear}}{MTOM} \right]_{concept}$	3.4	3.4	3.38
$100\% \cdot \left[\frac{M_{gear}}{MTOM} \right]_{actual}$	2.5	2.1	3.0

From table 5.3 it seems that the nose gear weight has the worst overestimation. The extreme difference due of the B737 nose gear weight might be due to a mistake made in the source[9], as the nose gear weight given is only 145 kg, compared to the B727's 327 kg. The difference in total weight is a result of the difference in gear length. For example, the B737 model has a longer hence heavier gear. The ratio $\frac{M_{gear}}{MTOM}$ for the concept is slightly higher than for the actual aircraft. This is due to the fact that the MTOM of the concepts is less than the MTOM of the actual aircraft. The used Raymer equation seems to give a good estimation of the main gear weight of the A320, as the designed gear is roughly equal in length to the actual gear with an estimated weight difference of only 4.5%.

5.1 B727-200

In table 5.2 it can be seen that the driving requirements for this concept are both the minimum and maximum nose load, the maximum distance from the rear spar and the outer stowage requirement. One must note that for this case the optimization failed to fully converge, leaving a valid but not entirely optimized gear design. A minor improvement could be made by making the gear slightly shorter and moving it inboard to comply with the outer stowage requirement. However, the margin for the wing tip clearance requirement is only 3.5%, or an additional 0.28° roll with the current design. Also, as the gear moves inboard it needs to elongate to satisfy the wing tip clearance. Hence, the difference between that optimum and the current gear is negligible. To compare the designed gear with the actual aircraft, an overlay image is made of the concept and the B727 ACAP drawings[6] of the top, side and front view of the aircraft. The top view is given in figure 5.1, the front view in figure 5.2 and the side view in figure 5.3. The black outlines are the B727-200 and the red outlines the concept. The difference between the gear designs is also shown in table 5.4.

Table 5.4: B727-200 relative difference

Component	N_{wheels}	Wheelbase	Track width	L_{main}	L_{nose}
Difference [%]	0	-4.0	+5.4	+10.0	+34.3

As can be seen in table 5.4, the concept and B727 have the same amount of tires. However, the concept uses 31X13 inch nose tires and 46X18 inch main tires whereas the B727-200 uses 32X11.5 nose tires and 49X17 main tires[6]. This is due to the lower MTOM of the concept of 61.3t combined with the tire load safety factor of 1.25. This remains lower than the B727-200 of 78t. Hence, smaller tires could be used. The wheelbase is slightly smaller compared to the actual aircraft. As both the minimum and maximum nose load requirements are driving the gear design for this case, the nose wheel can only be at the resulting exact location. The shorter wheelbase is clearly visible in the top view in figure 5.1. The light blue dots indicate the B727 gear locations and the red dots the gear locations of the concept.

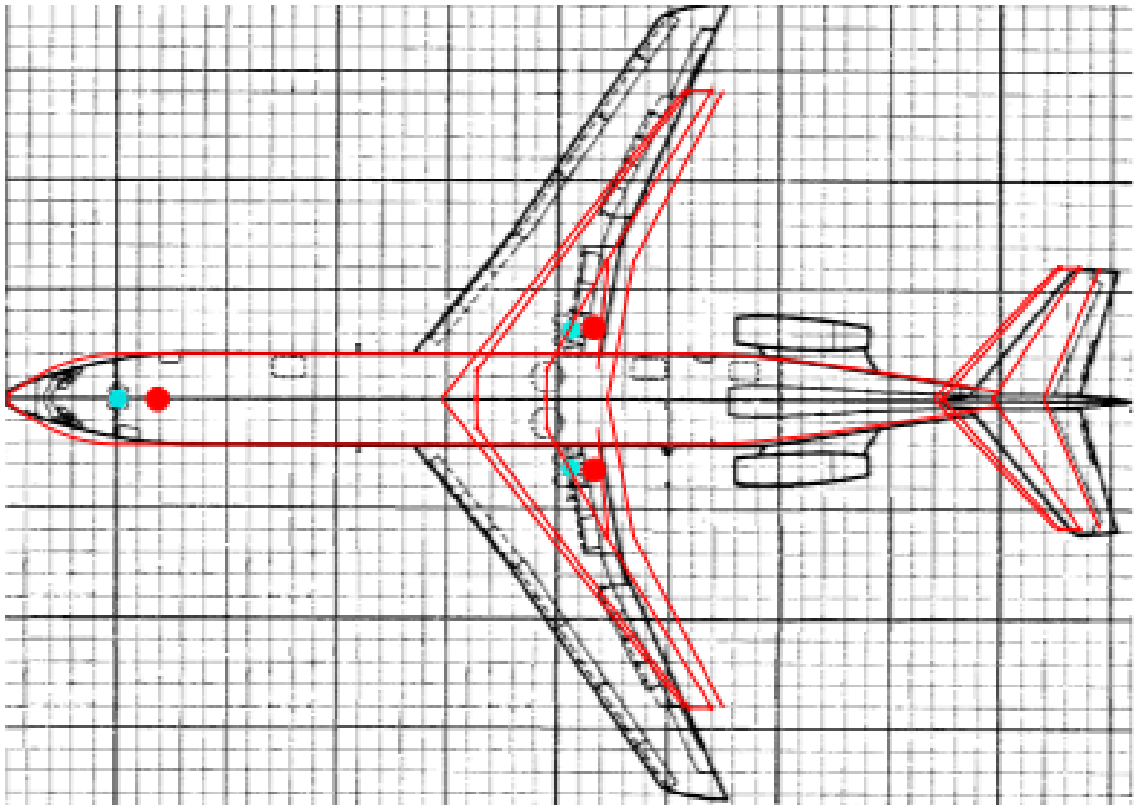


Figure 5.1: B727-200 top overlay

Another thing to notice in figure 5.1 is the much smaller span of the aircraft. This reduction in span results in a smaller wing area, which in turn increases the rotation angle at takeoff for the aircraft. As the wing is sized based on wing loading, the lower MTOM means a smaller wing area is required. The main wing and gear are also located further aft. This is again due to an error in aft cg position. The estimated aft cg is 44.6% MAC, whereas the actual aft cg is 40.8%^[6] MAC.

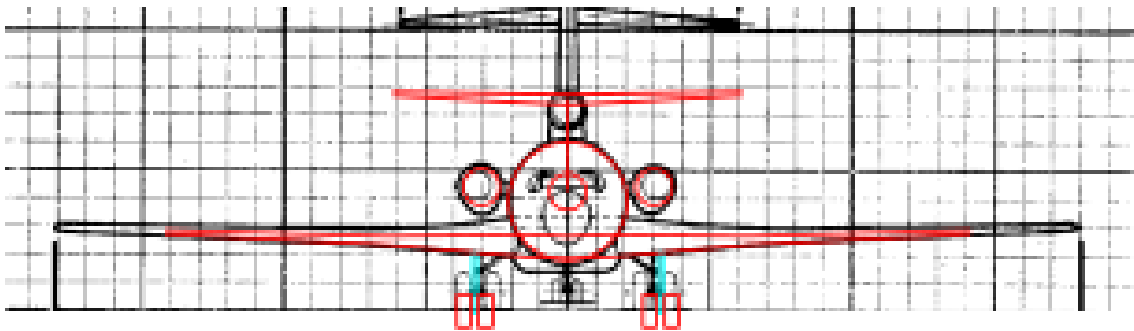


Figure 5.2: B727-200 front overlay

From figure 5.2 it becomes clear that the size of the vertical stabilizer is much smaller compared to the original aircraft. This places the horizontal stabilizer in the wake of the main wing at relatively low angles of attack, giving a large risk of deep stall. This will need to be taken into account during the sizing of the stabilizers. The size of the horizontal stabilizer of the concept is in agreement with the actual B727-200. The side view overlay in figure 5.3 shows the difference in vertical stabilizer size even more.

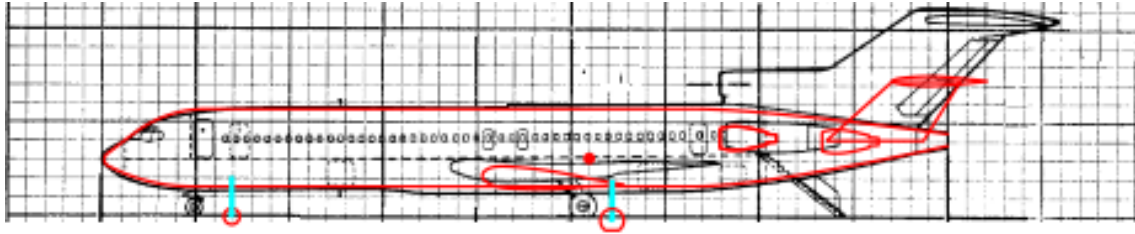


Figure 5.3: B727-200 side overlay

Another note to be made for future improvements is the modelling of the duct of the center body engine. The currently drawn engine indicates to location of the machinery, but the duct itself is not taken into account. Besides the differences between the concept and the actual aircraft, the landing gear design method produces a valid gear design with the given input and design requirements.

5.2 B737-800

Table 5.2 shows that the driving design requirements for this case are the nacelle clearance, minimum nose load, aft attachment limit and the inner lateral stowage constraint. In table 5.5 the differences with respect to the actual aircraft are shown.

Table 5.5: B737-800 relative difference

Component	N_{wheels}	Wheelbase	Track width	L_{main}	L_{nose}
Difference [%]	0	-8.6	+9.6	+26.9	+51.4

The active minimum nose load design requirement causes the wheelbase to be smaller than the wheelbase of the B737. This is clearly visible in the top view presented by figure 5.4. The blue outlines represent the B737-800, the black outlines the concept generated by the Initiator. The dots represent the locations of the undercarriage struts.

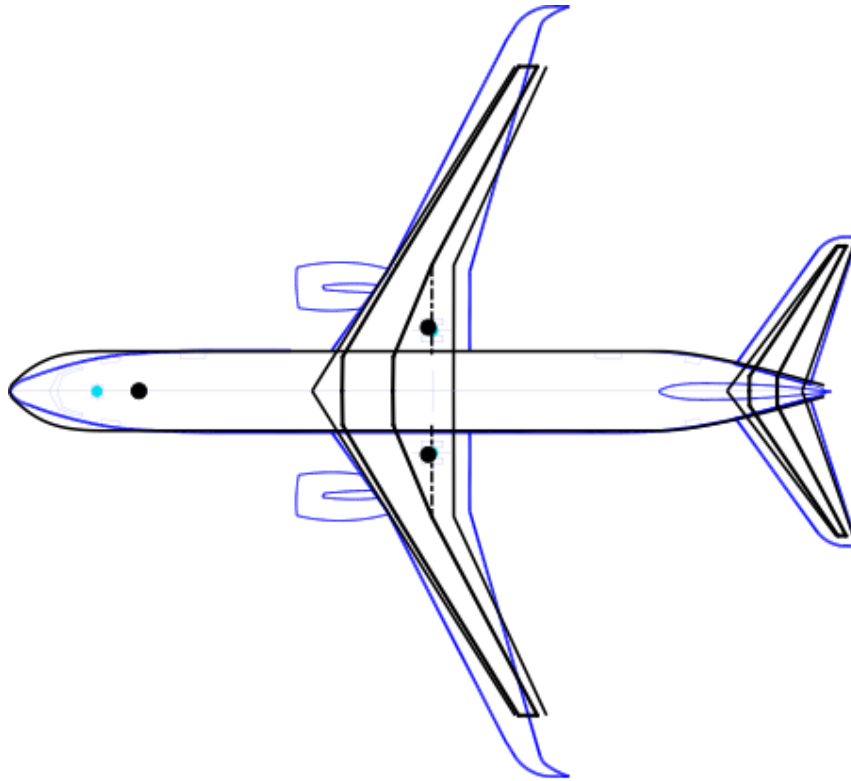


Figure 5.4: B737-800 top overlay

The specified forward and aft cg positions by Boeing are 6% MAC and 36% MAC respectively[7], while the Initiator calculated the forward and aft cg position to be 17% MAC and 35% MAC respectively. The underestimated aft cg position causes the main gear to be located slightly more forward compared to the actual aircraft. As the most forward position of the Initiator is located much more aft, the nose gear is forced to move aft as well to comply with the minimum nose load design requirement. As the aft attachment requirement is also active, the main gear cannot be placed further aft to allow the nose gear to be placed further forward. As the gear is placed on the outer most limit, the gear cannot be made shorter by increasing the track width due to conflicts with the nacelle as shown in figure 5.5.

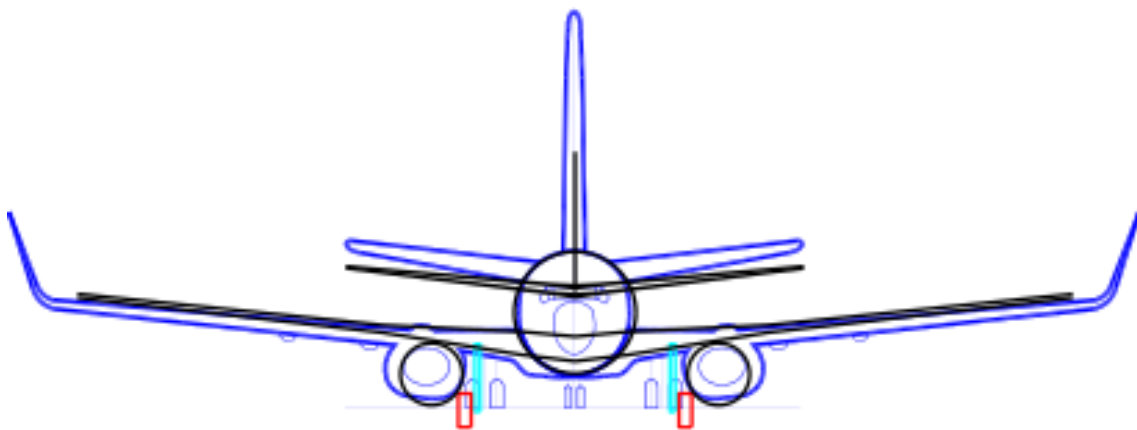


Figure 5.5: B737-800 front overlay

The gear of the concept is longer by a significant amount. This is due to nacelle clearance

constraint, in combination of the outer placement limit. A difference between the nacelle of the B737-800 and the concept is that the B737-800 uses a flattened nacelle, which is currently not modelled in the Initiator. Thus the gear of the concept can be expected to be somewhat longer due to the engine clearance requirement. The engines of the concept are also more inboard compared to the B737. This is because the Initiator uses a spanwise fraction to position the engines. The concept has a wingspan of 31.97m, while the B737-800 has a wingspan of 35.79m. As the span of the concept is smaller, the engines automatically move more inboard. This in turn lowers the engines, forcing an increase in gear length for the concept.

The main gear of the concept has a different bogie type compared to the B737, while having the same amount of tires as shown in table 5.5. The difference is due to the smaller track width of the tandem bogie compared to the dual type bogie. The larger track made it not possible to use the dual type due to the engine-strut placement requirement. As the tire dimensions are used to estimate the attachment point location, a difference in tire dimensions will affect the length of the gear. The B737-800 has a nose tire with a diameter of 0.686m and a main tire with a diameter of 1.13m[30]. The model has a nose tire diameter of 0.85m and main tire diameter of 1.168m. The slight difference will also increase the gear length difference, as the attachment location for the nose gear is based on tire diameter. The side view in figure 5.6 shows the part of the strut inside the fuselage.

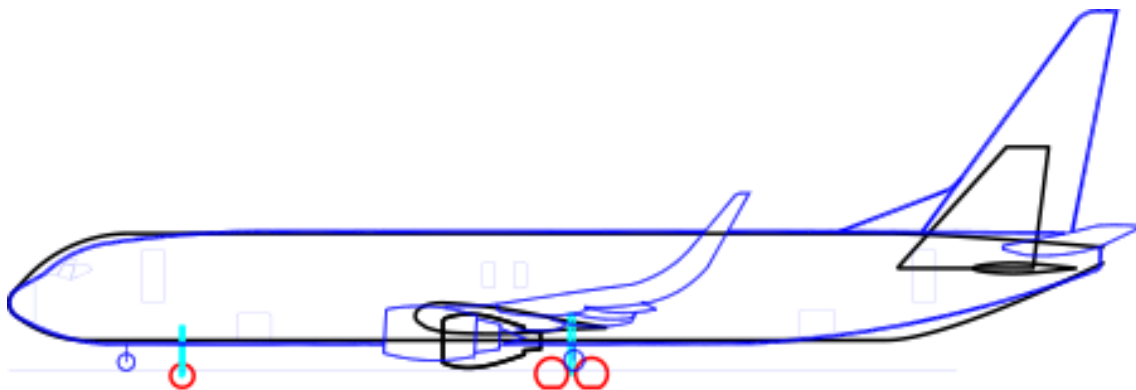


Figure 5.6: B737-800 side overlay

Figure 5.6 also shows the modeling error in the aft part of the fuselage done by the Initiator, as described in section 4. An additional note is that the estimated takeoff angle was 11.53° , whereas the actual angle is $7^\circ - 9^\circ$ [34]. The smaller wing area might be causing the required larger takeoff angle, as a smaller wing generates less lift. For the B737-800, the gear design method performs as to be expected with the given input. A closer approximation of the actual aircraft could be made by relaxing some design requirements.

5.3 B777-300

As can be seen in table 5.2, the driving design requirements for the B777 concept are the longitudinal tip over, the scrape angle, the minimum nose load and aft attachment. Table 5.6 shows the relative difference between the concept and the B777.

Table 5.6: B777-300 relative difference

Component	N_{wheels}	Wheelbase	Track width	L_{main}	L_{nose}
Difference [%]	0	-38.0	+9.3	+0.9	-3.9

The differences between the concept and the B777 are not very large, with an exception to the wheelbase. The concept has the same amount of tires as the B777, although slightly larger ones. The B777-300 uses 50X20 inch tires for the main gear and 42X17 inch tires for the nose gear[5], while the concept uses 52X20.5 inch main tires and 54X21 inch nose tires. This slight difference is due to the safety factor of 1.25 used when selecting the tires. The MTOM of the concept of 250t combined with the safety factor surpasses the B777-300 MTOM of 299t.

As both the aft attachment and longitudinal tip over design requirements are active, the main gear cannot be move further inboard or further aft. This means that the track width cannot be reduced to have a better match with the actual aircraft. The most forward cg position was estimated to be at 23.6% MAC, whereas the actual most forward cg is located at 13.88% MAC[5]. This forces the nose gear to be located further aft by a large amount to comply with the minimum nose gear load requirement, as can be seen in figure 5.7.

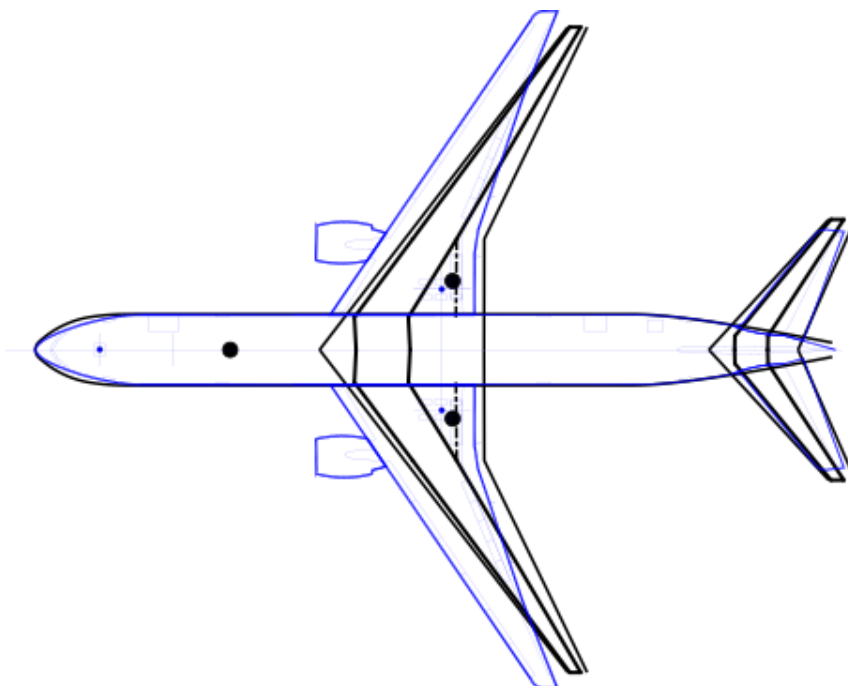


Figure 5.7: B777-300 top overlay

Figure 5.7 shows that the main gear is located slightly further aft, which is due to the longitudinal tip over requirement. The resulting main gear is slightly longer than the actual main gear. This can be seen in figure 5.8. The main wing is located slightly higher, hence the estimation of the attachment point is higher compared to the gear attachment point of the B777. It can also be seen that due to the smaller wing span, the engines of the concept are located slightly more inboard.

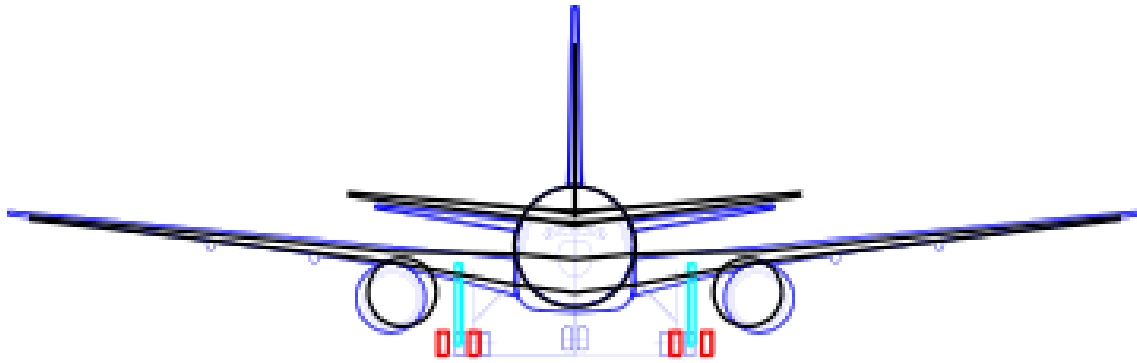


Figure 5.8: B777-300 front overlay

The nose gear was found to be slightly shorter compared to the nose gear of the B777. In the side view of figure 5.9 it seems to be actually longer. This difference is most likely due to an error made in estimating the gear length of the B777, as no actual data was available. The modelling of the rear fuselage with respect to the tail upsweep location is correctly done in this case, although the angle is slightly too large.

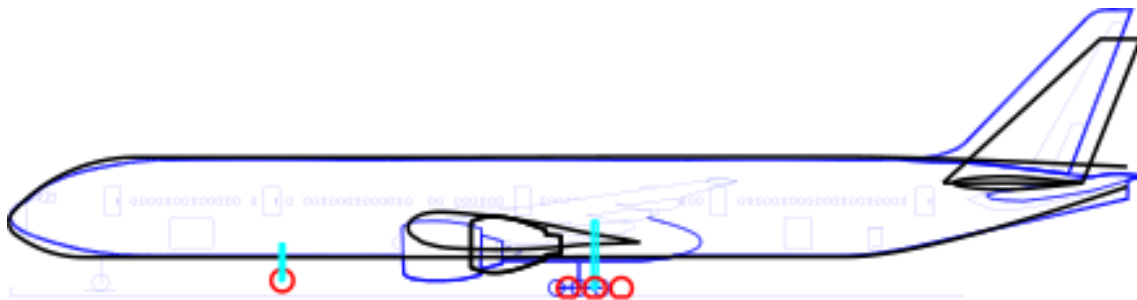


Figure 5.9: B777-300 side overlay

Besides the difference in wheelbase, which is caused by faulty input, the resulting gear of the concept matches the gear of the B777 quite well. Improving the cg estimation of the Initiator will help to improve the resulting gear design.

5.4 Fokker 100

From table 5.2 it becomes clear that the driving design requirements for the Fokker 100 model are the minimum nose load, the wheel clearance for the main gear, the aft attachment limit and the inner lateral stowage limit. In table 5.7 the differences with respect to the actual aircraft are shown.

Table 5.7: Fokker 100 relative difference

Component	N_{wheels}	Wheelbase	Track width	L_{main}	L_{nose}
Difference [%]	0	-11.1	-8.7	-2.8	-22.1

The dimensions and layout of the gear seem to be in agreement with the actual aircraft, with an exception of the nose gear. A possible cause is a wrong estimation of the actual nose gear length, as no actual data was available. As the nose gear is located such that the minimum nose loading is achieved, the nose gear cannot be placed further forward to increase the wheelbase. As the outer lateral stowage limit is not active yet, the main gear could be placed a bit further outboard to have

the track width agree with the actual aircraft. Figure 5.10 shows an overlay top view of the Fokker 100 and the generated concept. The red lines show the outline of the concept and the location of the landing gear. The blue dots indicate the gear location of the Fokker 100.

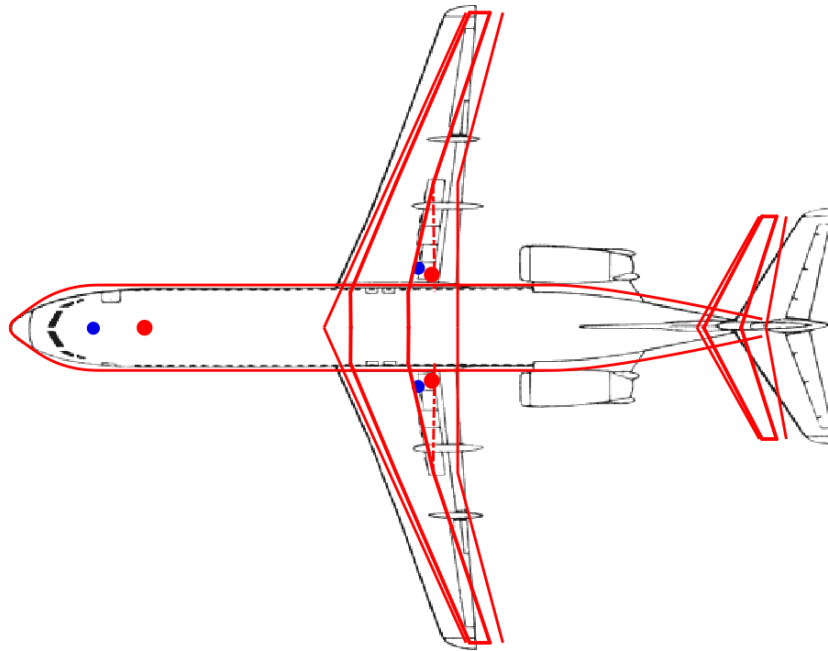


Figure 5.10: Fokker 100 top overlay

The top view shows that the nose gear is located further aft than the nose gear of the Fokker 100. The minimum nose load requirement forces the nose gear to be at the given location. Again, this is likely due to the cg estimation. The main wing of the concept is located at the same location as the wing of the Fokker 100, but has a slightly larger sweep. Another difference is the kink introduced by the landing gear design module. However, the total wing area is $4.7m^2$ smaller. The more forward location of the horizontal tail is due to the lower sweep given to the vertical tail, as seen in figure 5.12. The front view, shown in figure 5.11, shows the smaller track width and slightly larger fuselage.



Figure 5.11: Fokker 100 front overlay

As the inner lateral stowage requirement was sizing, the gear could be placed further inboard without causing problems with gear stowage. The smaller track width is again visible. The side view in figure 5.12 also shows the smaller wheelbase and gear position offset.

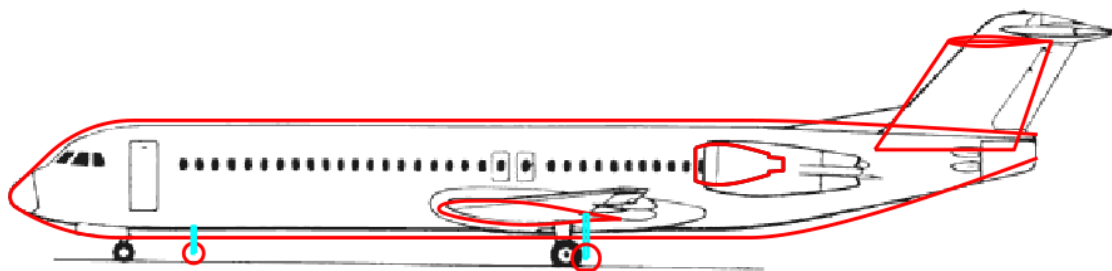


Figure 5.12: Fokker 100 side overlay

The side view also shows that the engines of the concept are slightly more forward. The difference in nacelle shape is due to a generic model being used to display them, taking only the length, diameter and location of the engine, and not the nacelle into account. The resulting gear is a close enough approximation of the actual layout when taking into account the imposed design requirements and the given input. Hence, the method produces an acceptable result.

5.5 ATR 72-600

Table 5.2 shows that the active design requirements for the ATR design are the longitudinal tip over angle, the lateral tip over limit, nose gear stowage and the wheel clearance. In table 5.8 the differences with respect to the actual aircraft are shown.

Table 5.8: ATR 72-600 relative difference

Component	N_{wheels}	Wheelbase	Track width	L_{main}	L_{nose}
Difference [%]	0	+8.7	+14.9	+21.7	+2.4

Table 5.8 shows that the largest deviations are the main gear length and the track width. The larger track size is required to comply with the lateral tip over limit, as shown by figure 3.7. The wheelbase is slightly larger compared to the actual aircraft. This is due to the track width and lateral tip over limit. Reducing the wheelbase would require a larger track to satisfy the limit. This in turn would increase the size of the fairing and thus the drag of the design. Hence, the larger wheelbase is more beneficial. As the wheel clearance requirement is also active, a shorter gear is not possible, hence a larger main gear than the ATR 72 is obtained. Figure 5.13 shows the overlay image of the concept and actual aircraft. Red indicates the generated concept, blue the gear location on the actual aircraft.

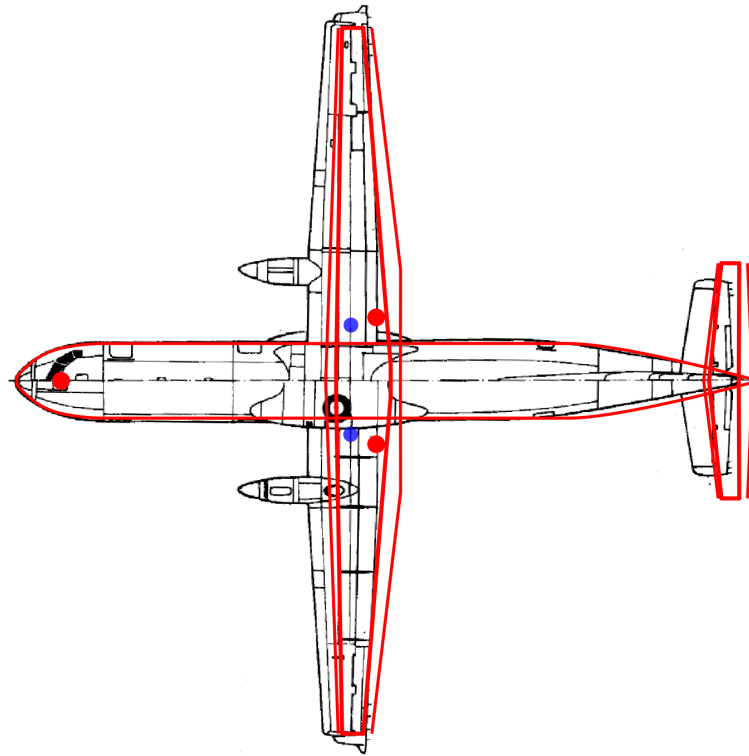


Figure 5.13: ATR 72-600 top overlay

It can be seen in the top view that the main wing and main gear are shifted further aft for the concept. The cg range of the ATR72 is 14% up to 37%[\[28\]](#). The estimated cg range for the concept is 13.7% up to 49.9%. The difference in aft cg location forced the main wing and gear to be placed further aft. If the cg was located further forward, the wheelbase could be made shorter and the main gear could be placed more inboard while still meeting the lateral tip over design requirement. This would reduce the track width and width of the fairing. The previously mentioned wider track is also shown in figure 5.14.

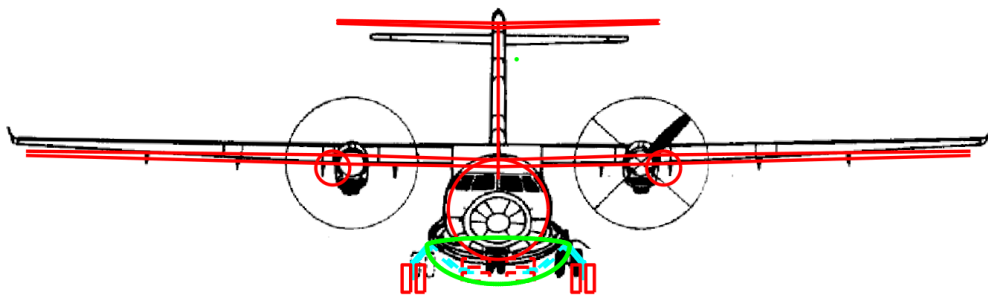


Figure 5.14: ATR 72-600 front overlay

The wider track also makes a wider fairing necessary, as can be seen in the front view. The frontal shape of the sized fairing also mimics the shape of the ATR 72 fairing well, with a slight difference in a more flattened top part. The total frontal area seems to be roughly the same, which

allows for a more accurate drag estimation. Figure 5.15 shows the side view overlay of the ATR 72 and the concept.

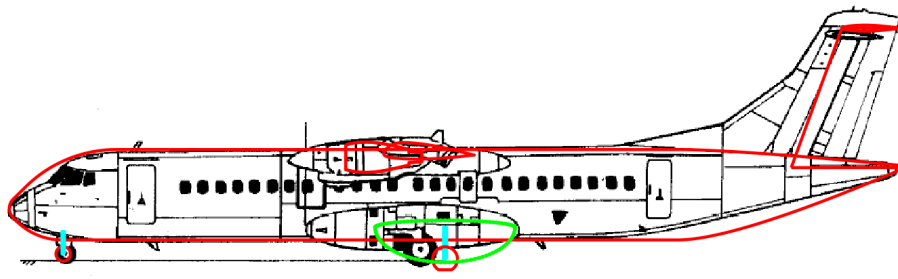


Figure 5.15: ATR 72-600 side overlay

Again, the difference in gear position and gear length can be seen. The side profile of the concept's fairing is very different from the ATR 72's fairing. The ATR 72 has a more slender fairing, which helps to reduce the zero lift drag as shown with equations 3.55 and 3.60. The fairing sizing is only based on the requirement of covering the gear when retracted. As a rough fairing estimation was required for the conceptual design phase, the resulting fairing is a good enough approximation. As stated before, the fuselage model of the ATR 72 also required a correction factor to the scrape angle.

5.6 A320-200

For the A320 concept, the active design requirements nacelle clearance and lateral inner stowage as shown in table 5.2. The relative difference between the concept and the A320 are shown in table 5.9.

Table 5.9: A320-200 relative difference

Component	N_{wheels}	Wheelbase	Track width	L_{main}	L_{nose}
Difference [%]	0	+22.0	+4.5	-0.0	+5.4

The largest difference between the concept and the A320 is again the wheelbase. However, for this design the driving requirements are not the nose load. This means that the wheelbase could be made smaller to match the wheelbase of the A320. As changing the nose gear location does not influence the length of the gear for this specific case, the optimizer chose an arbitrary location to place it. The selected bogie type matches the type used for the A320-200. The A320 uses 30X8.8 inch nose tires and 46X17 inch main tires[1]. For the concept, 42.4X15.3 inch nose tires and 46X18 inch main tires are selected. The concept has an MTOM of 71.1t which, combined with the 1.25 tire load safety factor, puts a larger load on the gear than the 78t MTOM of the A320 itself. Hence, the larger nose gear tires and wider main gear tires are used. The top view in figure 5.16 shows the clear differences in gear location.

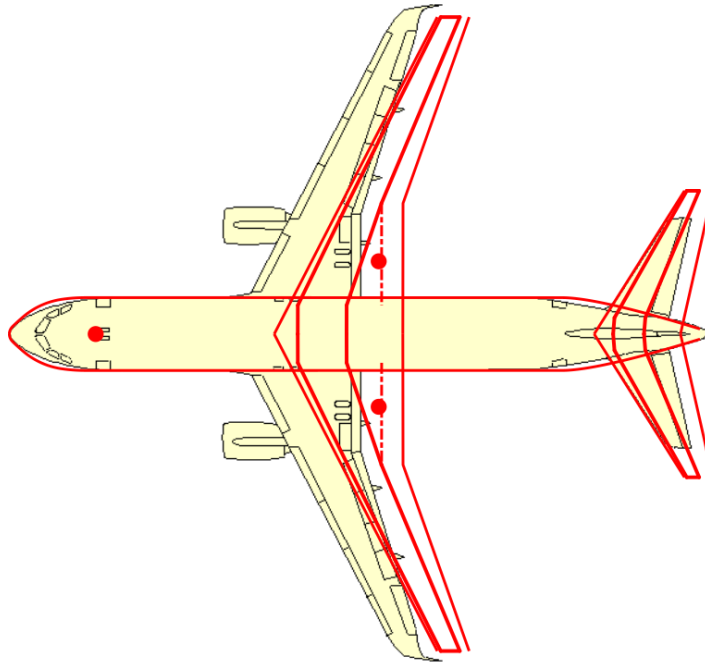


Figure 5.16: A320-200 top overlay

The increased horizontal stabilizer span is due to the further aft location of the main wing. The forward location of the cg was estimated to be 15.2% MAC, whereas the actual forward cg location of the A320 is 17% MAC[1]. This allowed the nose gear to be placed further forward. The track width was increased slightly. This is done to be able to retract and stow the main gear, as follows from the active inner lateral stowage requirement. Another difference is the main wing location. The convergence of the Initiator forced the main wing to be moved aft to be able to attach the main gear to the wing. This can also be seen in table 5.2, as the margin on the aft attachment design is minimal for the final layout of the concept. The more aft located main wing also causes the Initiator to size a larger horizontal tail, which in turn aggravates the aft shift of the cg. The wing span of the concept is 34.55m, while the A320 has a span of 35.8m. This forces the engines to be slightly more inboard, as can be seen in figure 5.17.

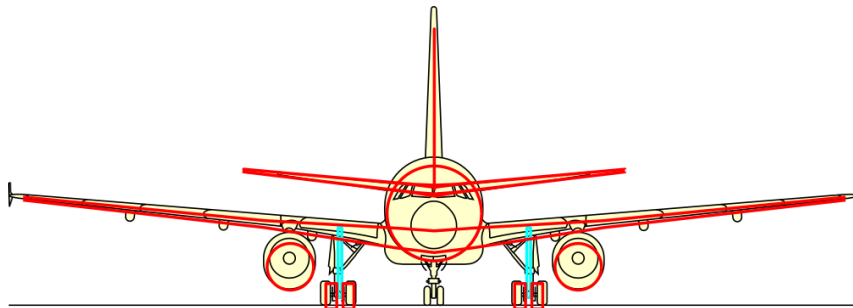


Figure 5.17: A320-200 front overlay

With the active design requirements of the inner lateral stowage and the nacelle clearance, the gear could not be made shorter. Figure 5.17 also shows the slightly smaller fuselage diameter of 3.97m of the concept, compared to the 4.14m of the A320.

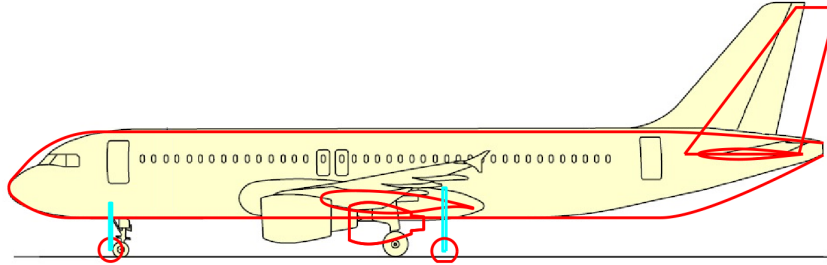


Figure 5.18: A320-200 side overlay

The side view also shows the error in the modeling of the tail upsweep location for the A320 concept. For this case, the size of the vertical tail of the concept seems to be in agreement with the A320's vertical tail. So for the A320 concept it can be said that the aft shift in cg has a large influence on the final layout. The aft shift of the cg forces the main wing to be placed further aft, which increases the wheelbase and horizontal tail size. The gear length and nose gear location of the concept are quite in agreement with the A320. Hence, it can be concluded that the landing gear design module performs as to be expected with the given input and produces a valid landing gear design.

5.7 Wrapping it up

As demonstrated by the six aircraft concepts, the new landing gear design strategy is able to reproduce the gear dimensions quite well, with the difference between the concept's track width and actual track width being less than 10%. The relative difference in gear length is larger, but this might be due to a wrong estimation of the actual gear length. The only problem the module has is the placement of the nose gear, as the cg estimation used as input often is faulty. If the cg estimation of the Initiator is improved, the resulting gear locations on the concept should be more in agreement with the actual gear locations of the aircraft. Another possible cause of differences between the resulting gear design and the actual gear of the aircraft is the possible use of different design requirements by the manufacturers. However, this can not be validated by the author.

6 Test cases

To test the hypothesis of the landing gear design method and find an answer to the research question, two test cases are investigated. The first case is based on the different gear design for two aircraft with a similar role and configuration: the B727-200 and the Tu-154. Both aircraft have a low wing configuration and use three fuselage mounted turbofan engines. However, the main difference between the two aircraft is the gear design. The B727-200 features the wing mounted, root stowed gear whereas the Tu-154 has podded gear. To investigate the influence of the gear type on the aircraft characteristics and the possible benefits of either gear type, both types of gear will be designed for a given concept.

The second case is based on the gear types often applied to high wing turboprop aircraft: the fuselage mounted gear as used on the ATR 72 and the nacelle stowed gear as seen on the

Fokker 50. Both gear types will be designed for a high wing concept and the effect on the aircraft characteristics will be evaluated.

6.1 Case 1: landing gear design for a low wing aircraft

To investigate the difference between a wing mounted gear and a podded gear, both types of gear are designed on a medium sized, fuselage mounted twin-engined jet aircraft. The aircraft is to carry 109 passengers in a two class arrangement, with a cruise Mach of 0.85. The dihedral of the wing is varied from -4 up to 4 degrees to see for what configuration which gear design would be best. For both designs, the driving constraint was the wing tip clearance constraint. Figure 6.1 shows a side-by-side comparison between both undercarriage designs, for a dihedral of -4° , 0° and 4° . The wing mounted gear is shown on the left and the podded gear on the right.

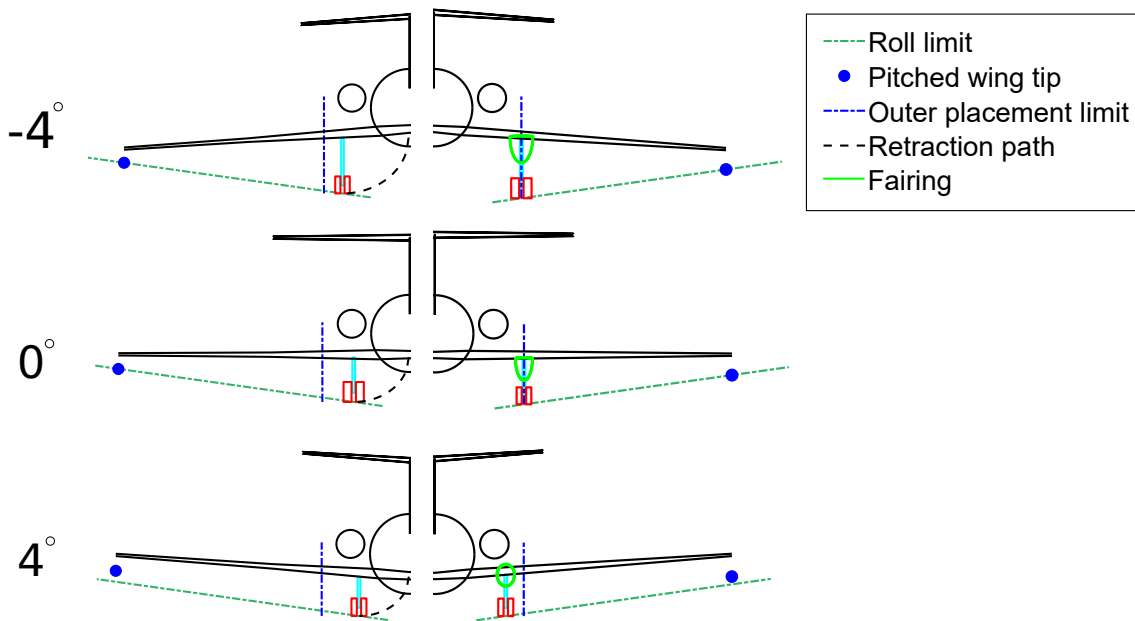


Figure 6.1: Side-by-side gear layout comparison

As can be seen in figure 6.1, the driving design requirement is the wing tip clearance in case of anhedral. For dihedral, the driving design requirement becomes the wheel clearance for both designs. As expected, the podded gear is placed at the outer limit in case when the tip clearance design requirement is active to reduce the gear length. Figure 6.2 shows the resulting gear length.

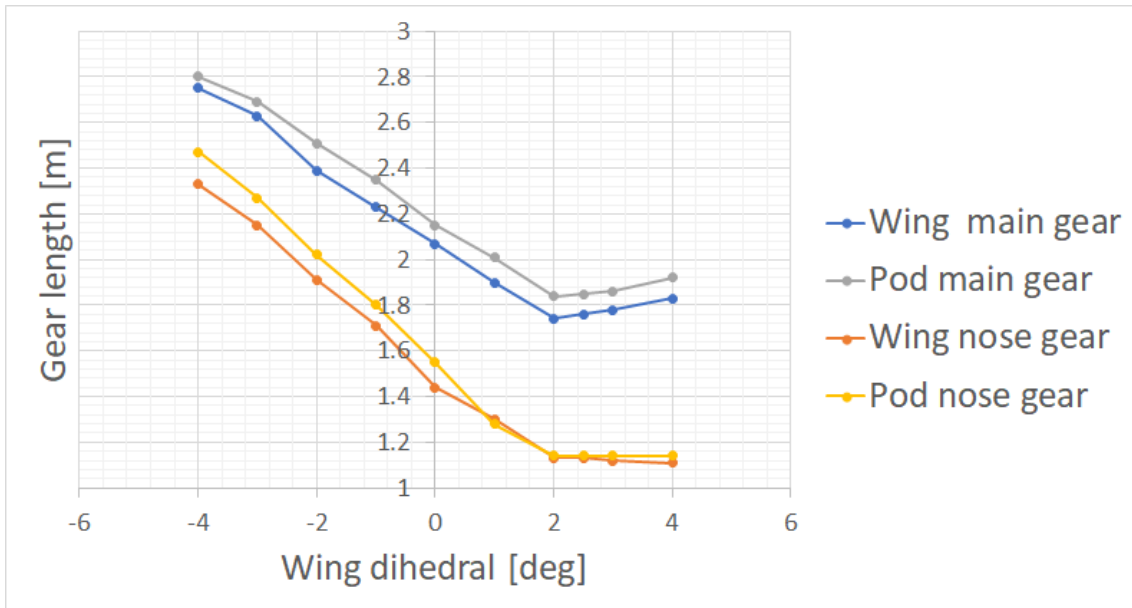


Figure 6.2: Wing dihedral vs gear length

It was expected that the gear of the podded version would be shorter than the wing mounted gear if the main wing had anhedral, as the podded gear could be placed further outboard as the lateral stowage constraints are not used for the pods. However, it was found that the takeoff AoA for the podded case was much larger than for the wing mounted case. Hence, the wing tip was rotated by a larger amount and was located lower, which can be seen in figure 6.1. This caused the podded gear to be longer than the wing mounted gear. Currently, the Initiator calculates the $C_{L_{clean,max}}$ for each iteration and overwrites the initial input value. However, $C_{L_{TO,max}}$ remains constant equal to the initial input value. For the podded gear, the value of $C_{L_{clean,max}}$ increased and as equation 3.2 is used to estimate the lift generated by flaps and slats during take-off, the estimated lift is reduced. This reduction in lift generated by the flaps caused the estimated AoA to increase. So the unexpected gear design for the podded gear is a result of invalid input from the Initiator.

For the 4° dihedral case, both gear designs use the same type of main gear tire and for both designs one of the driving requirements is the wheel clearance requirement. This means that the fuselage has the same distance to the ground for both designs. However, in figure 6.2 it can be seen that the podded gear is slightly longer. The difference in length is due to the podded gear being placed further outboard. Due to the dihedral and the increased track width, the attachment point of the gear is located higher. One can see that increasing the dihedral of the wing does reduce the required gear length while the wing tip clearance is most important, thus the module performs as expected. Another observation is that the difference in length for the designs is roughly constant. The slightly longer gear also meant that the resulted gear design was heavier. However, as the MTOM of the concept of the podded gear was higher than the MTOM of the other concept, the fraction of MTOM representing the landing gear remained close to each other, as shown in figure 6.3.

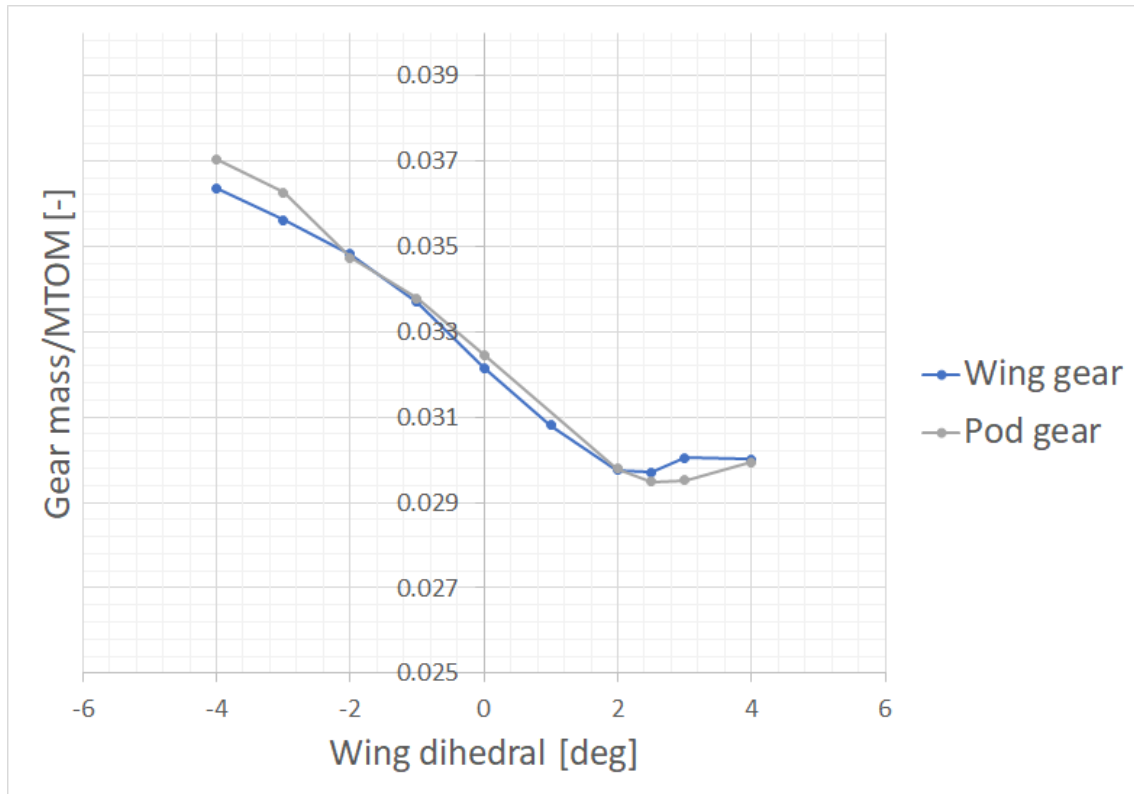


Figure 6.3: Wing dihedral vs mass ratio

As the weight equation 4.1 is a function of landing weight among other variables, this is to be expected. Using an analytical weight estimation would yield a more accurate prediction. However, this would require a more detailed landing gear design which is not available at this point. The increase in MTOM of the podded gear is a result of the increase in parasitic drag. The parasitic drag count of each aircraft design is shown in figure 6.4.

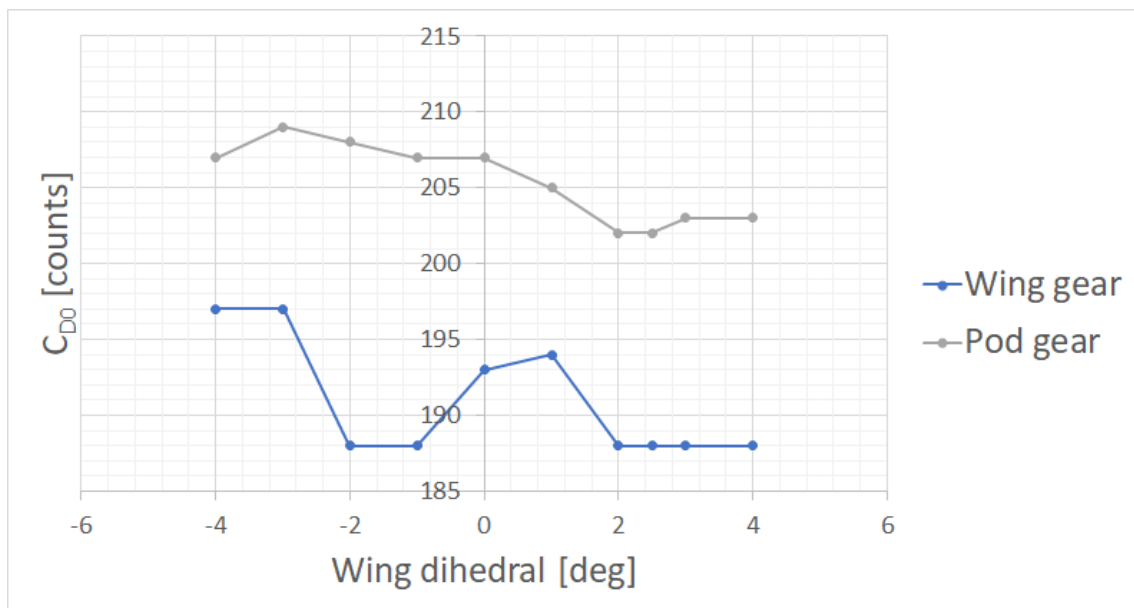


Figure 6.4: Wing dihedral vs total C_{D_0}

An additional note is that the wing/fuselage fairing is not sized at this moment. So the difference in drag between the designs may actually be smaller than presented in figure 6.4. The pods accounted for 8-12 counts of the total parasitic drag, as shown in table 6.1. The side view of three pod designs is shown in figure 6.5.

Table 6.1: Skin friction and parasitic drag coefficients of the pods

Γ [deg]	-4	-3	-2	-1	0	1	2	3	4
C_{D_0} [counts]	12	12	12	8	8	11	11	11	11
C_f [counts]	2	2	2	2	1	2	2	2	2

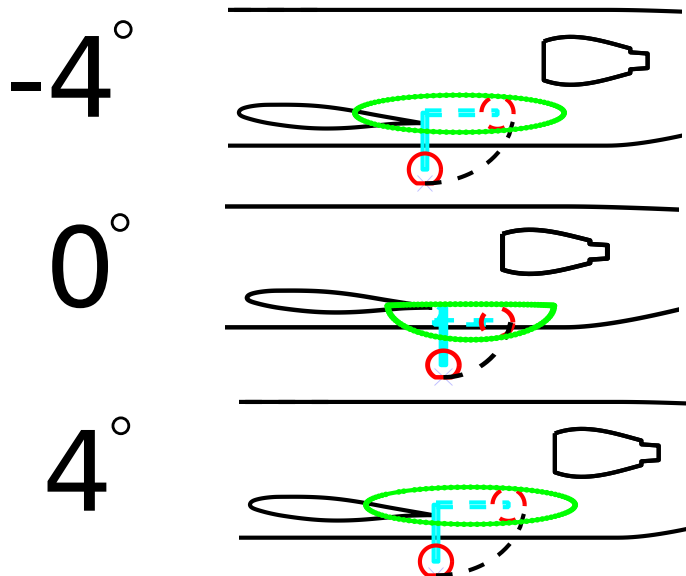


Figure 6.5: Side view pod design

Table 6.1 shows that for -1° and 0° dihedral, the pod design results in a minimum drag contribution. For this case, the concept had the smallest wheels. This resulted in a folded gear, which can be stowed in a shorter fairing. The smaller tires also made the fairing have a smaller frontal area and equivalent diameter. With the method shown in section 3.10 this resulted in a larger slenderness ratio and thus lower drag. For the other cases the difference is the fairing length, which results in a lower C_{D_0} for a shorter fairing. Due to the increase in drag, the engines get estimated heavier as they will have to produce more thrust. This increase in weight snowballs through the design and a heavier aircraft concept is the result. The increase in drag also reduced the lift-to-drag ratio of the concept, as seen in figure 6.6.

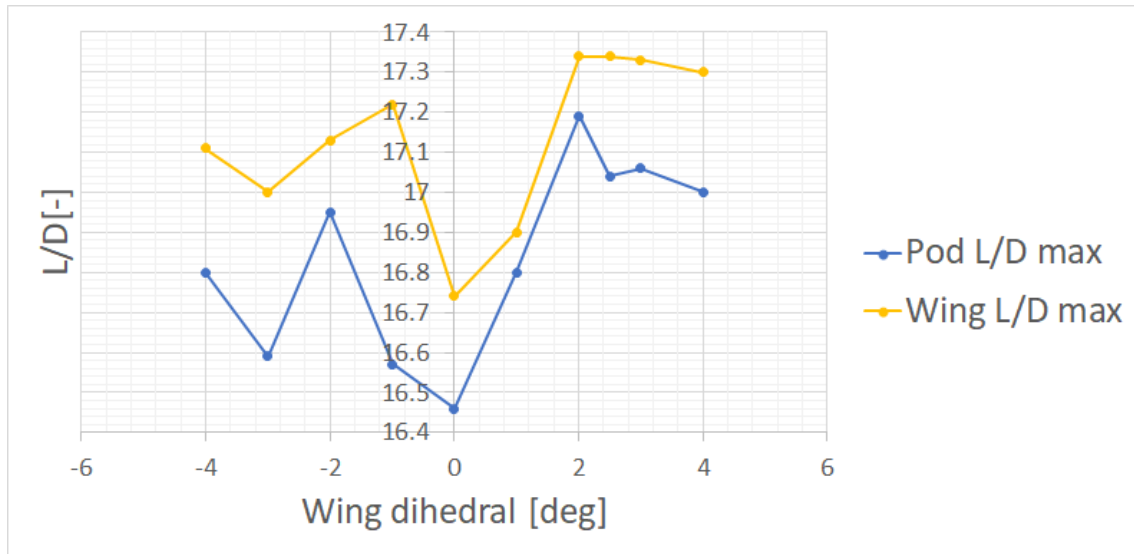


Figure 6.6: Wing dihedral vs L/D

Using a podded gear will reduce the L/D ratio of the concept, as is to be expected. As the concepts are designed to fly the same mission, the effective range of the aircraft says the same. However, the concept with the podded gear will have higher operational costs due to an increase in fuel consumption.

As answer to the research question "What is the impact of the undercarriage design on the performance parameters of a transport aircraft?", based on the given results, the benefits of podded gear are:

- A larger degree of freedom when placing the gear on the wing, as it does not have to fit into the fuselage.
- Shorter gear in case of equal α_{TO} and anhedral.
- No cutouts in fuselage required.
- More space for payload in fuselage.

For the wing mounted gear the benefits are:

- An overall lighter aircraft design.
- Less parasitic drag due to absence of fairing.
- Shorter gear in case of equal α_{TO} and dihedral.
- Lower fuel consumption

In addition, the module behaves as to be expected with varying wing dihedral and also allows to evaluate the increase in parasitic drag due the pods. This allows to make a better trade-off for this study case.

6.2 Case 2: landing gear design for a high wing turboprop

To investigate the difference between the nacelle and fuselage mounted gear, both types are designed for the same concept. The concept is a high wing, turboprop aircraft with a cruise Mach of

0.41. It is to carry 70 passengers in a single class, single isle configuration. The resulting designs are shown in figures 6.7, 6.8 and 6.9. Figure 6.7 shows a side-by-side top view, with the fuselage mounted gear on the left and the nacelle stowed gear on the right.

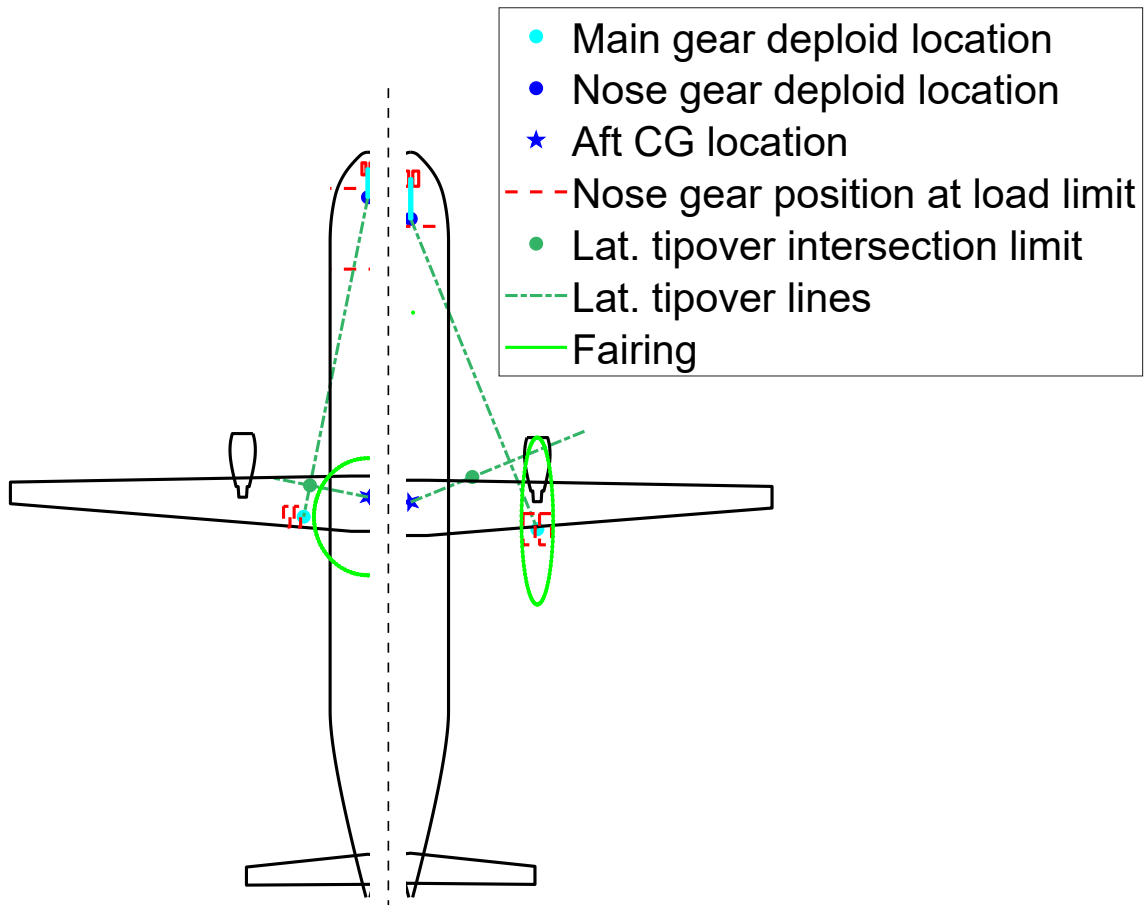


Figure 6.7: side-by-side, top comparison of gear design

From figure 6.7 it becomes clear that the wing and cg location are shifted slightly aft for the nacelle gear. This is due to the design requirement that the main gear should be located behind the rear spar. The increased distance between the main gear and the cg forces the maximum nose gear limit to move further forward, limiting the nose gear placement. For the nacelle gear, the minimum nose load limit is outside the fuselage. Another difference for the gear designs is the lateral tip over requirement. The nacelle gear has no problem meeting this design requirement, as the track width is more than required. For the fuselage mounted gear however, the lateral tip over requirement is one of the driving design requirements. The nacelle stowed design will have a more stable behavior during ground operations, such as making a turn during a taxi run. As noted in section 4.4, it may be beneficial to use different lateral tip over criteria for a fuselage mounted gear, as the driving design requirement is often this angle. The slightly longer nose gear for the nacelle gear, is the result of the larger main gear tires in combination with the tire clearance requirement. As both concepts use a 1.3° deck angle, the nose gear has to be longer to have the same angle. The side view 6.8 also shows the difference in gear length, as well as the retraction of the nacelle stowed gear.

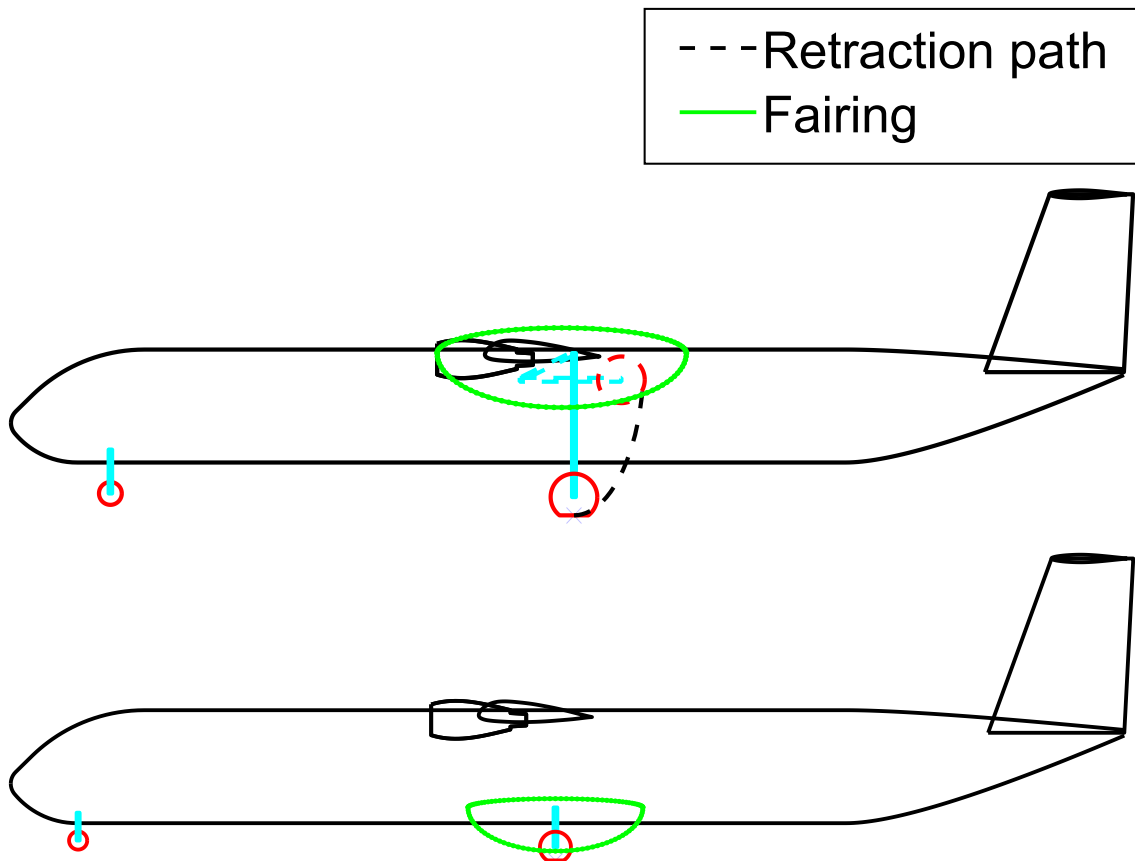


Figure 6.8: Side comparison of gear design

Figure 6.8 also shows that the side profile of the nacelle fairing is much larger than the profile of the fuselage fairing. The fuselage fairing has a length of 4.29m, while each nacelle has a length of 6.12m. The original nacelle has a length of 2.33m, with a wetted area of $9.95m^2$. To house the landing gear inside the nacelle, the new fairing was stretched to 6.12m, which increased the wetted area to $23.33m^2$ per nacelle. Hence, the total increase of wetted area for the nacelle stowed gear is $26.76m^2$. For the fuselage fairing, the increase in wetted area is $22.90m^2$. Despite the larger wetted area, the parasitic drag of the nacelles is lower due to their more slender shape, as seen in table 6.2. If the design requirement for the tire clearance is relaxed, the nacelle stowed gear can be made lower up to the nose tire clearance requirement.

	Nacelle gear	Fuselage gear
L_{MG} [m]	3.83	1.29
L_{NG} [m]	1.32	0.87
W_{gear} [kg]	940	575
T [m]	9.28	4.71
B [m]	11.41	11.71
MTOM [t]	22.3	21.9
W_{fuel} [kg]	2400	2360
L/D [-]	20.05	20.76
$C_{D_{0,total}}$ [counts]	228	231
$C_{D_{0,fairing}}$ [counts]	35	18
$C_{D_{0,engine}}$ [counts]	-	22
$C_{f_{total}}$ [-]	34	34
$C_{f_{fairing}}$ [-]	5	3
$C_{f_{engine}}$ [-]	-	3

Table 6.2: Gear design comparison

For the nacelle stowed gear, the C_{D_0} contribution equals 35 counts, of which 13 counts are due to the increased size to house the gear. The fuselage fairing adds 18 counts to the parasitic drag. So during cruise the nacelle stowed gear will be more beneficial with respect to drag reduction. However, due to the much longer gear the landing gear will cause more drag when extended during take-off and landing. The front view shown in figure 6.9 shows the difference in frontal shape of the two fairings, as well as the retraction of the fuselage gear.

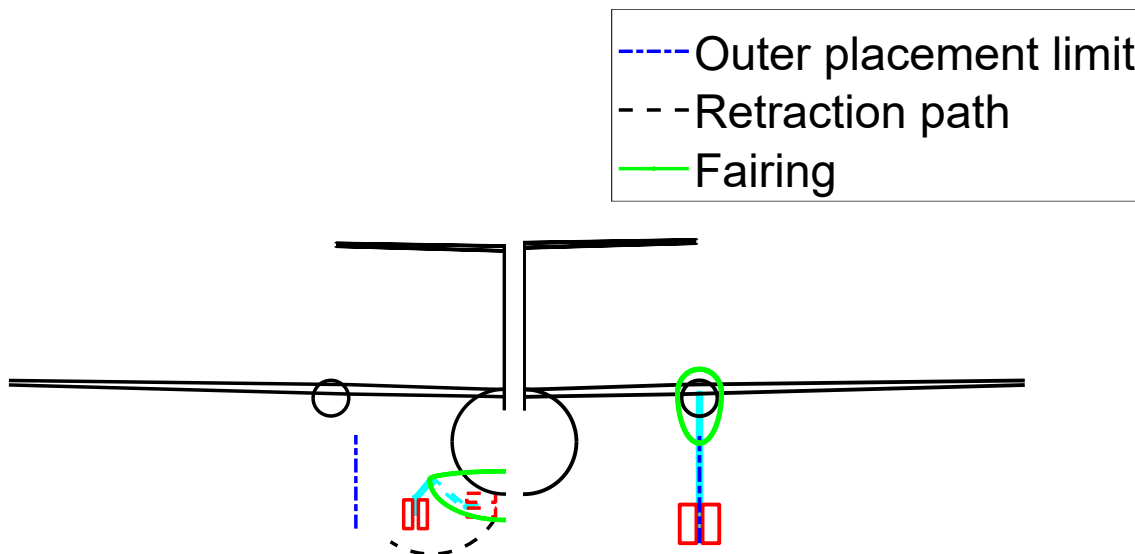


Figure 6.9: side-by-side, front comparison of gear design

Although the nacelle stowed gear results in a lower total C_{D_0} , the resulting L/D of the concept is slightly lower compared to the fuselage mounted gear as shown in table 6.2. This also results in a slightly higher fuel consumption for a 1530 km mission. The reduction in L/D is due to the larger nacelle lowering the efficiency of the wing.

So from a weight reduction perspective, the fuselage mounted gear is more attractive as the MTOM of the concept is lower. One must note that the weight equation does not take into account the larger required thickness of the nacelle stowed gear to cope with bending of the struts when,

for example, making a turn on the taxiway. The estimated gear weight will thus be larger than currently estimated, but a more accurate weight estimation would require a more detailed gear design. From a drag reduction perspective, the nacelle stowed gear is the best option. To answer the research question *"What is the impact of the undercarriage design on the performance parameters of a transport aircraft?"*, the following can be noted:

- When using a nacelle stowed gear, the main wing is shifted aft.
- Using the fuselage mounted gear, the MTOM of the concept is lower.
- The nacelle stowed gear design reduces the parasitic drag of the concept.
- The nacelle stowed gear will result in more stable behavior during ground operations.

The second case shows that the new module is capable of designing the landing gear for both nacelle stowed and fuselage mounted. Both cases also show that with the new strategy, the Initiator program can be used to investigate the influence of the landing gear design on the concept. Thus the hypotheses, *"careful integration of the design of the undercarriage into the conceptual design routine of the Initiator, results in a design method capable of assessing the impact on weight, drag and geometry of transport aircraft"*, is validated with the cases presented in this chapter.

7 Conclusion

The landing gear design module performs as expected. With an exception of the wheelbase, it is able to reproduce the designs of actual aircraft quite well. An observation made is that the deviation in wheelbase increases as the size of the aircraft increases. For smaller aircraft such as the Fokker 100 the designed gear layout represents the actual gear layout better than for larger aircraft like the B777-300. The problems of the Initiator with estimating the cg location have a large impact on the result of the landing gear design module. This issue translates in an underestimation of the wheelbase and an aft shift in nose and main gear location, as seen in section 5. Relaxing the nose load design requirements may allow for a better representation of the wheelbase, as it will allow the nose gear to be placed further forward in cases such as the B727, B737 and B777. Having a more accurate cg estimation will also solve, or at the very least lessen, the aft shift of the main wing, as seen with the A320 and ATR 72 cases. The number of tires of each concept match the number used on the actual aircraft, although due to the safety margin used the concept often uses larger tires to satisfy the flotation requirement. This larger tire also has an impact on the estimated gear length, which is larger than the gear length of the actual aircraft for most cases.

The test cases shown in section 6 show the strength of the new module, as well as the effect of a change in geometry on the gear design. The first case shows the response of the module to a change in dihedral angle, as well as a trade-off made between a conventional wing mounted gear and podded gear. It was noted that the Initiator currently caused a flaw in the trade-off, where the takeoff angle of the concept with the podded gear was much larger than the takeoff angle of the concept with the conventional gear. This was due to the Initiator updating the value of $C_{L_{clean,max}}$ and not the value of $C_{L_{TO,max}}$. With the assumption of the difference between $C_{L_{clean,max}}$ and $C_{L_{TO,max}}$ being the lift generated by the flaps, as shown with equation 3.2, it causes the flaps to become less efficient. This in turn increased the required takeoff angle, which cause the wing tip to be situated lower during a roll in combination with pitch up. The wing tip clearance requirement then forced the necessity of a longer gear, whereas it was expected that the podded gear would be shorter for a wing with anhedral. Based on the results of the Initiator, one would better chose the conventional gear in this case in terms of aircraft performance. The case did show that the module responds well to the change in dihedral angle, as gear length and spanwise position adjust correctly.

For the second case, the effect of a fuselage mounted gear and a nacelle stowed gear on a high-wing concept is investigated. The case shows the potential of the tool to investigate the influence of the gear design on the concept's weight, drag and geometry. The nacelle stowed gear caused the main wing to be slightly further aft, as well as a slight increase in vertical tail height. The MTOM of the nacelle gear concept also increased due to the increase in gear weight, but the total C_{D_0} reduced when applying this type of gear. It can also be seen that the L/D ratio reduced for the nacelle stowed gear concept, causing a slightly higher fuel consumption.

Hence, the hypothesis *"by careful integration of the design of the undercarriage into the conceptual design routine of the Initiator, results in a design method capable of assessing the impact on weight, drag and geometry of transport aircraft"* is verified. The new landing gear design module allows the user to evaluate the impact of the gear design on the aircraft. Taking into account the current state of the Initiator, the new design strategy is an improvement for the Initiator program. It allows for a fast design of a landing gear reliably, with the flexibility for the user to set the gear type. Table 7.1 shows the improvements made by implementing the new design strategy.

Table 7.1: Module features

	Old Method	New Method
Wing mounted gear	✓	✓
Fuselage mounted gear	✓	✓
Nacelle mounted gear	X	✓
Pod mounted gear	X	✓
Optimization routine	X	✓
Can adjust wing planform	X	✓
Wingbox sizing	X	✓
Fairing sizing	X	✓
Fairing drag estimation	X	✓
Landing gear drag estimation	X	✓

The addition of the fairing estimation and landing gear drag estimation also allow for more accurate results and better trade-offs.

Recommendations for future development

To improve upon the new module, one could implement an analytical weight estimation instead of the statistical method. This would require a more detailed landing gear design but would result in a more accurate weight estimation. The detailed gear design would also allow for the modelling of the kinematics of the landing gear. The model can also be adjusted to handle the gear design for unconventional aircraft designs, such as the blended wing body and boxwing. This could also need to have an increased maximum of main gear struts, as the current module only allows for a maximum of four main gear struts.

As the fairing estimation is very basic and only the dimensions are estimated, an improved version could be implemented for more accurate dimensions and a weight estimation for the fairing itself. Also the wing/fuselage fairing is currently not sized and could be added with a more accurate fairing sizing method. This would make a trade-off based on drag and/or fuel consumption more accurate.

As noise reduction is getting more important, a noise estimation method for the landing gear could also be implemented in the future. This would allow the designer the also include the noise impact in a trade-off. However, this would require a more detailed design of the landing gear than is currently available.

The results of the landing gear module depend heavily on the cg estimation of the Initiator. Updating the cg position to a more accurate method will improve the resulting gear designs. This in turn will increase the accuracy of the drag and fairing estimations.

Part II
Supportive chapters

loop is the so-called Class 2 convergence loop indicated by the orange square. In this loop, empirical methods are used to determine the geometry and characteristics of the concept. It iterates until the difference of the Class 2 weight estimation of iteration i and $i-1$ is within a predefined tolerance.

In the following loop, indicated with the blue square, the fuel fraction method is discarded and replaced by a more accurate analysis of the mission. The "Mission Analysis" module is sensitive to changes in cg and uses the trimmed drag polar. Furthermore, the off-design engine characteristics are used to estimate the effect of altitude and speed on the aircraft specific fuel consumption. The tail volume coefficient method previously used to size the horizontal tail is replaced with an X-plot method that uses requirements on stability and control. Again, the loop is iterated until the difference of the Class 2 weight estimation of iteration i and $i-1$ is within a predefined tolerance.

In the final loop, indicated with the green square, all modules from the previous loop are used. The empirical methods for the prediction of fuselage and wing weight are replaced by two more advanced methods. Both methods rely on the results of the aerodynamic analysis, as well as an estimation of the mass distribution. The computed fuselage and wing weights are added to the results of the Class 2 weight estimation for all other components, creating a Class 2.5 weight estimation. This loop is iterated until the difference of the Class 2.5 weight estimation of iteration i and $i-1$ is within a predefined tolerance. After the convergence of the third loop, the design process is completed.

A known problem with the initiator is that it currently overestimates the most forward and aft locations of the center of gravity[22]. For example, for the 707-321 the calculated cg range according to the cg is 12% to 38% MAC. According to the B707 manual, the operational range for the cg is 14% to 23% MAC. As no adjustments to the cg range are currently implemented, this will affect the result of the Initiator. One of the results was the landing gear being placed behind the wing, which resulted in an invalid design. Another problem is that the current Initiator program often cannot create a valid landing gear design. This is due to the fact that the landing gear is added as the last component and is not allowed to alter the geometry of the aircraft. Combined with the overestimation of the cg, the main gear ended up located behind the main wing with no option to attach it to the aircraft structure. Hence, the program could not be used to investigate the influence of the landing gear design on the characteristics and geometry of the aircraft concept. To address the landing gear issue, a literature study is conducted. In the study, the focus is on finding a possible solution on how to include the landing gear design in the overall design process for the Initiator.

8.2 Current design methods

The FPP department is not the only player in the field of MDO optimization programs. A lot of research has been done on how to create a knowledge based design flow using computers for the conceptual design phase of aircraft. Examples of this are DLR's Technology Integration for the Virtual Aircraft (TIVA), followup project Virtual Aircraft Multidisciplinary Analysis and Design Process (VAMP) and current project VAMPzero[10] and the Knowledge-based and Extensible Aircraft Conceptual Design Environment (KEACDE) created by F. Haocheng et al [13]. Figure 8.2[13] shows the workflow of the KEACDE program.

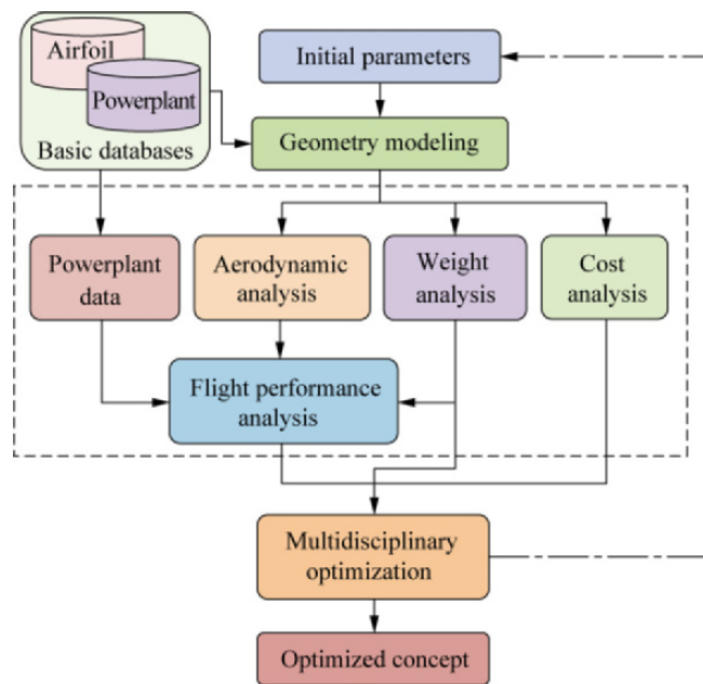


Figure 8.2: KEACDE flowchart (Hoacheng et al p. 712)

The KEACDE program allows the user to wrap the design and analysis methods of complex mathematical calculations, in-house programs and commercial CAD and CAE software into so-called "building blocks". These blocks can then be arranged in any order to allow the user to create his or her own design optimization. The extensible basic database (EBD) allows the user to create databases used during the conceptual design phase. Figure 8.2 shows that for the civil aircraft, a first geometry is modelled based on a database of aircraft after which a first analysis is done. After this is finished, the MDO optimization is started which, when finished, adjusts the initial parameters and the process is run again. The tool allows for great flexibility for creating optimization routines, but leaves the optimization methodology up to the user.

The author of this thesis had the privilege of doing his internship at DLR to help improve VAMPzero by creating a module for the design software which would design the landing gear for the conceptual design. However, this was still done "as an afterthought" when the rest of the design was more or less finished. The landing gear design had no influence on, for example, the wing design while for some designs the wing would have to be adapted in the next iteration cycle. This gives an example that there is still improvement possible by doing research on the influence of the landing gear design and create a new design strategy. The flowchart of the VAMPzero tool is shown in figure 8.3³.

³<https://www.cpacs.de/VAMPzero/Introduction/introduction.html>

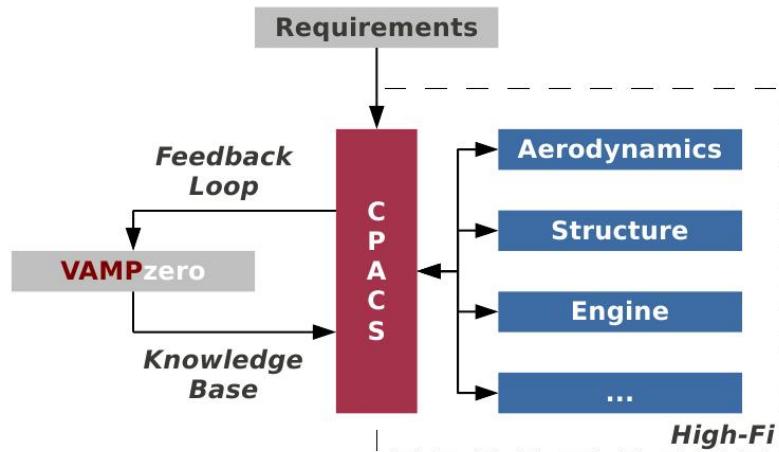


Figure 8.3: VAMPzero flowchart

The VAMPzero program focusses on easy data exchange between different disciplines by using the Common Parametric Aircraft Configuration Schema (CPACS) file. Like KEACDE, VAMPzero has the design and analysis methods in packages or blocks. The user can arrange the blocks in any order desired to create his or her own optimization routine.

So unlike the Initiator which has a fixed routine, both VAMPzero and KEACDE leave it up to the user to define the optimization routine. From these MDO methods it becomes clear that the modeling of the geometry one of the first steps that is taken. Hence starting with a good aircraft geometry will result in a better concept or less iterations. To determine the geometry some common design strategies are often used, for example the methods from Torenbeek[31], Currey[11] and Roskam[25]. The books of Torenbeek and Roskam give a more general way of sizing the gear, whereas Currey goes into more detail. In figure 8.4[25] the preliminary design process suggested by Roskam is shown.

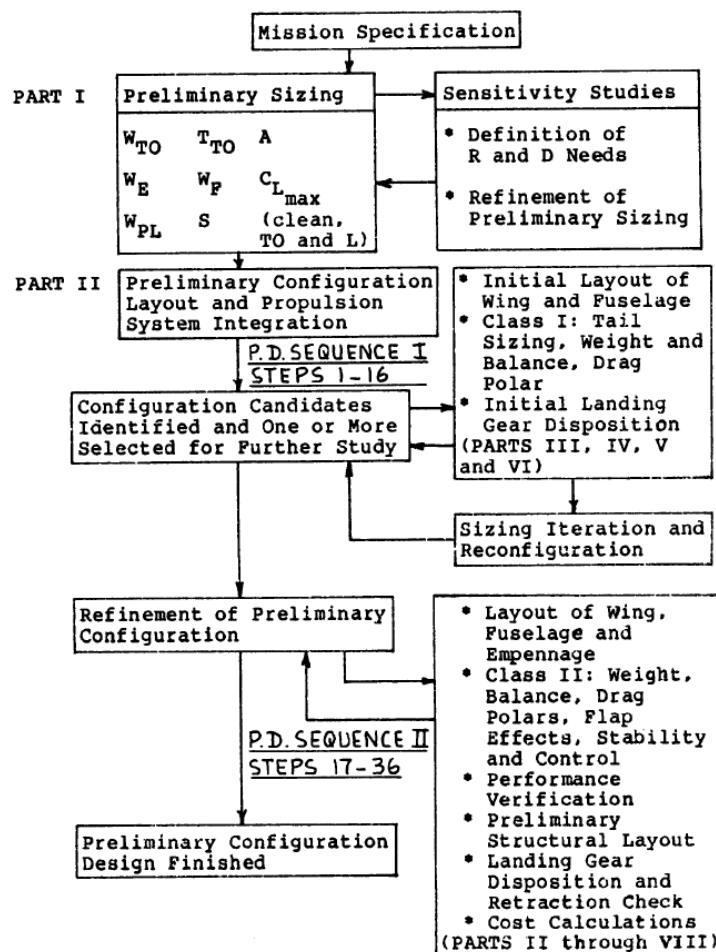


Figure 8.4: Roskam's preliminary design process (Roskam part I, p. 4)

One thing that stands out is that the landing gear retraction check is done at the later stages of the design. The retraction can have a major impact of the structural design of the aircraft, for example when the gear is retracted into the fuselage or by the additional nacelles as mentioned by Berry [27]. The design of the landing gear during the initial design and the refinement are also done with the same equations, thus a shorter loop should be possible. This is suggested by M.H. Sadraey as shown in figure 8.5[26].

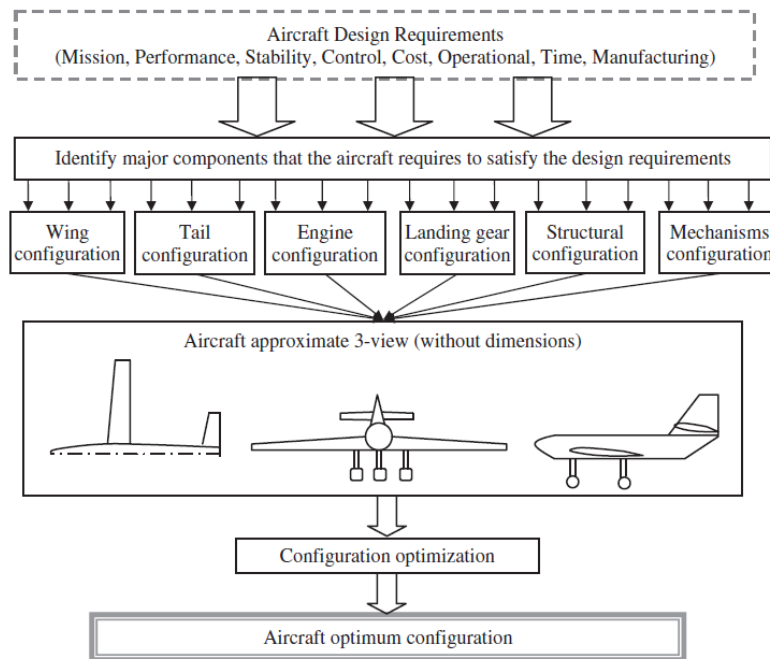


Figure 8.5: Sadraey's preliminary design process (Sadraey p. 50)

However, the influence of the landing gear is still only accounted for at the start of each next (new) iteration. Another design strategy is suggested by S. Gudmundsson. The most relevant steps of this strategy are shown in table 8.1 (Gudmundsson Chapter 1 pp.13-14) [18]. For the entire table the reader is referred to Gudmundsson's book.

Table 8.1: Gudmundsson's conceptual design strategy

Step	Task
4	Create a constraint diagram based on the requirements of Step 1 (target performance).
6	Estimate initial empty and gross weight using W-ratios and/or historical relations.
7	Using the results from the constraint diagram of Step 4 and the initial gross weight of Step 6, estimate the initial wing area.
8	Estimate initial tail surface area and special position using V_{HT} and V_{VT} methodology.
9	Propose a wing layout that suits the mission by establishing an initial AR, TR, airfoils, planform shape, dihedral, washout, etc. Note that many of these parameters are likely to change in the next iteration.
12	Using the candidate configuration, estimate empty, gross, and fuel weight
13	Determine the empty weight CG, CG loading combination cloud, gross weight CG, movement due to fuel burn, and inertia properties (I_{xx} , I_{yy} , .).
14	Determine a candidate CG envelope based on results from Step 13.
15	Determine the fuselage layout (space claims, occupant location, baggage, cargo).
17	Modify the tail surface geometry in accordance with the results from the static and dynamic stability analysis of Step 13.
18	Evaluate the following layout design modifications as needed, based on the above analyses: <ul style="list-style-type: none"> • Structural load paths (wing, HT, VT, fuselage, etc.) • Control system layout (manual, hydraulic, fly-by-wire/light) • Flight control layout (geometry, aerodynamic balancing, trim tabs) • High-lift systems and layout (flap types, LE devices) • Landing gear layout (tri-cycle, tail-dragger, fixed, retractable, etc.)

As can be seen in step 18 in table 8.1 the landing gear layout is determined after the static and dynamic stability check of step 16. However adding the landing gear can change the wing planform, making the calculations invalid and force the designer to use a large iteration loop. Changing the strategy to include the effect of the landing gear at an earlier change might result in a smaller number of iterations. The difficulty of trying to integrate the landing gear design more into the wing and tail design is in the parameters required to start with the landing gear design. To design the landing gear, the center of gravity envelope, fuselage shape, the wing and horizontal tail shape and position and engine size and position need to be known. This already puts the landing gear design on the bottom of the design list, but large iteration loops may be avoided by a more interactive way of designing. However, to determine a feasible design strategy, one needs to know the influence of the landing gear on the different aircraft components first.

8.3 Design challenges

The extended gear will cause a turbulent wake which locally deteriorates the airflow around the wing and causes noise. A study on the wake around a two-wheeled landing gear by Imamura et al[29] has been conducted to understand the flow physics of the wake. The result is shown in figure 8.6.

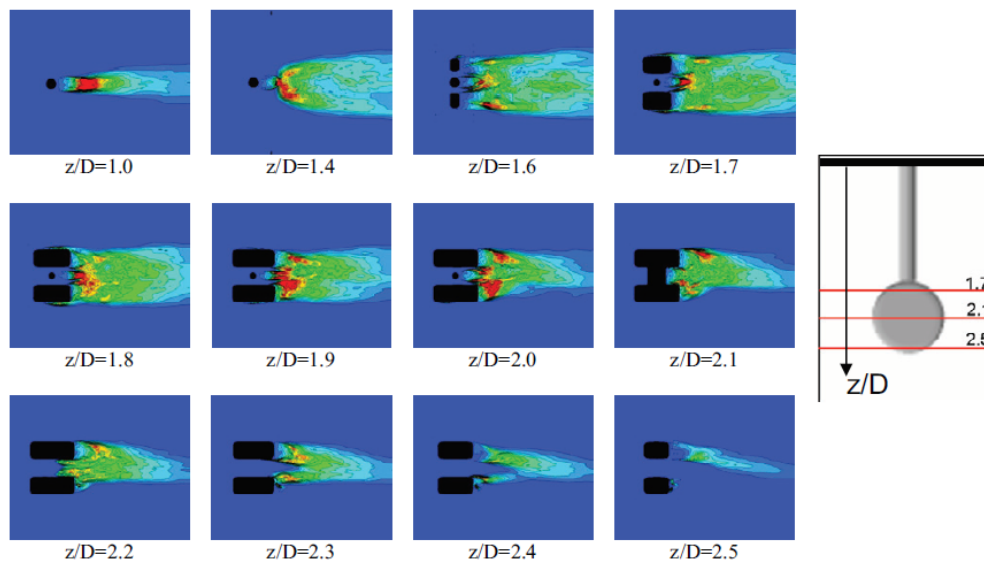


Figure 8.6: Flow around a two-wheeled landing gear(Imamura et al p. 301)

In figure 8.6 one can see that the landing gear causes a large turbulent wake, especially the wake from the wheels. This wake can have a negative influence on the wing performance and therefore should be taken into account when determining the performance of the aircraft concept. The current Initiator has no module which determines the landing gear drag and only a fixed value is used, thus a method to determine the drag of the gear will have to be implemented. Bennett et al.[8] investigated the use of CFD methods to calculate the drag caused by the landing gear. Compared to the empirical ESDU method, the CFD analysis proved more accurate but the quoted 30% error band of the ESDU method captures almost all of the CFD results. Hence, for a fast drag calculation with reasonably accuracy one should better use an empirical method as ESDU.

Noise reduction is high on the agenda as well, as aircraft fly over or near densely populated areas. Y.P. Guo et al.[35] studied the noise generated by a B737 main gear. It was found that especially the high-frequency components of the generated noise were caused by the small components of the undercarriages such as hoses, wires and cutouts. However, the effect of the small components is also noticeable in the lower frequencies as shown by figure 8.7[35].

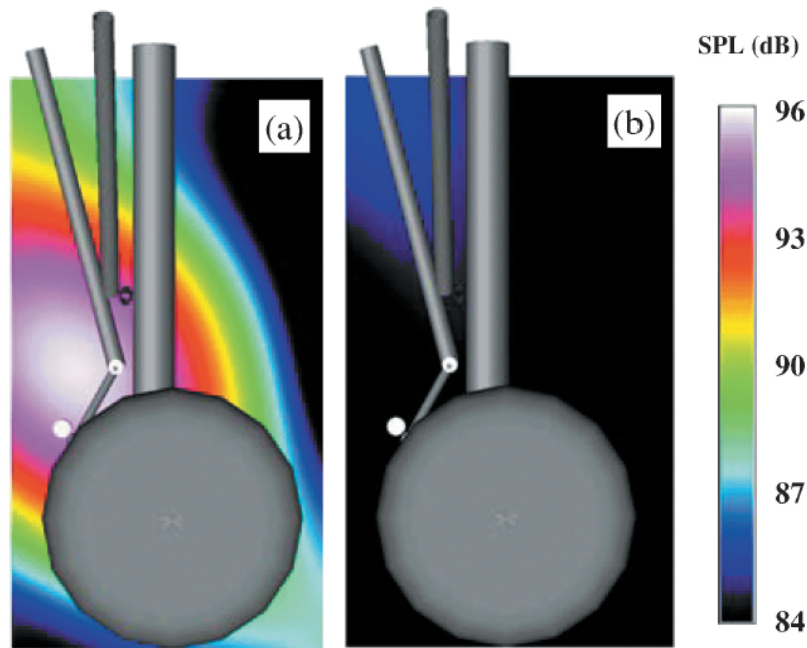


Figure 8.7: Source strength comparison at 875 Hz: a) fully configured gear and b) gear with hydraulic hoses removed (Guo et al p. 301)

Thus for a good noise estimation, a detailed gear design is required. As a detailed design is not realized during the conceptual design phase, the effect of the landing gear on the aircraft noise emissions can only be roughly estimated. It might be more efficient to include the noise estimation in the detailed design phase of the landing gear.

Another design challenge is the question of where to leave the landing gear after take off. There are multiple options for landing gear storage, each with its own positive and negative characteristics. In the book *Advances in Aircraft Landing Gear*[27] P. Berry mentions how the choice of aircraft configuration affects the landing gear design. He bases his work on the methodology of Currey[11]. When taking wing mounted main gears, the differences between a high or low wing aircraft are quite large. High wing aircraft often have longer and often heavier landing gear. However, as the gear can be retracted into the nacelle, this gives the advantage of an undisturbed wingbox. For an unswept low wing this solution is also an option. For a swept wing, the wing design often includes a yehudi, or kick spar, to avoid the side folding landing gear to disrupt the wingbox. Applying a yehudi gives the wing a thicker wingroot, which allows for more fuel storage and the option of construction of a lighter wing due to deeper root spars.

The yehudi will have a large impact on the aerodynamic performance of the aircraft, so it is important to know whether or not one is present at the early stages of the conceptual design phase. The location of the main gear dictates the size of the yehudi. This location is often driven by the longitudinal tip over angle θ_{TO} or the lateral tip over angle ψ . Figure 8.8 shows these angles. The nose gear is located at point **a** and the main gear at point **b**. The aft location of the cg is at point **d**.

needed at a later stage of the design. This may reduce the waste of precious time and resources. Also it seems there is a gap in the literature, as the design strategies do not pay attention to the consequences of adding the landing gear at the end of the design cycle. This often means that the entire design cycle will have to be reiterated losing precious time. Current MDO tools such as VAMPzero and KEACDE allow for easy use of knowledge of different disciplines and to quickly generate aircraft concepts, but the user has to set up their own optimization routine. This shows that investigating the place of the undercarriage design in the overall conceptual design routine can be of value for the future development of these MDO tools.

9 Module Integration and program structure

This section will discuss the integration of the module into the Initiator program, the interaction between the modules and the structure of the landing gear design module. As discussed in section 3.1, the landing gear module requires a set of input data before it can be run, namely:

- Wing planform
- Fuselage aft shape
- Aft and forward location center of gravity
- Engine type and location
- Landing gear attachment position
- Landing gear stowage type (Nacelle, pod, fuselage, wing root)
- Take off angle of attack

To have this data available, the module needs to be placed at a specific point inside the module execution order of the Initiator program. The N2 chart of the Initiator is shown in figure 9.1.

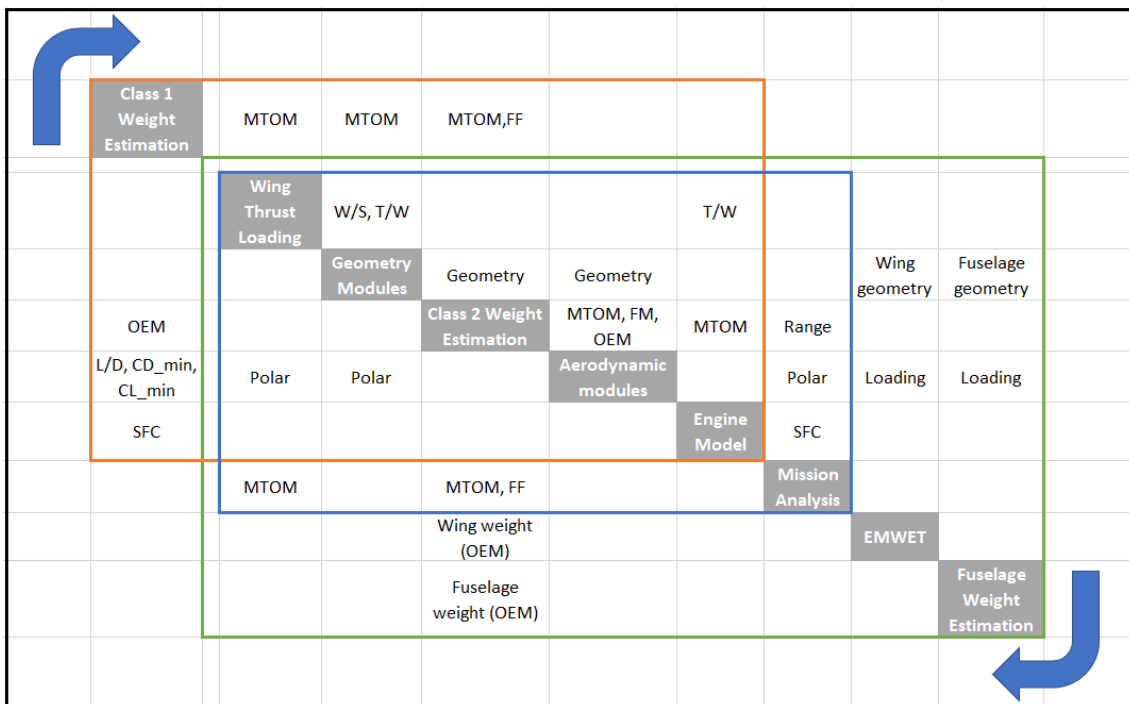


Figure 9.1: N2 chart of the Initiator

As said in section 3.1, the landing gear design module will have to be placed after the Aerodynamics module to have the required data available. Figure 9.2 shows the N2 chart of the landing gear design module integrated into the Initiator.

	Initiator	Geometry, MTOM, FM, OEM	Geometry, MTOM, OEM, cg positions	Geometry, MTOM, OEM, cg positions
		Aerodynamic modules	Takeoff performance	
	LG layout	LG layout, fairing dimensions	Position landing gear	LG layout and position, wing position limits
	Wing position, tail geometry, updated LG position			Horizontal stability estimation

Figure 9.2: N2 chart of the integrated landing gear module

The flowchart of the landing gear design module is shown in figure 9.3. It gives an overview of the different scripts used inside the landing gear design module and their interaction.

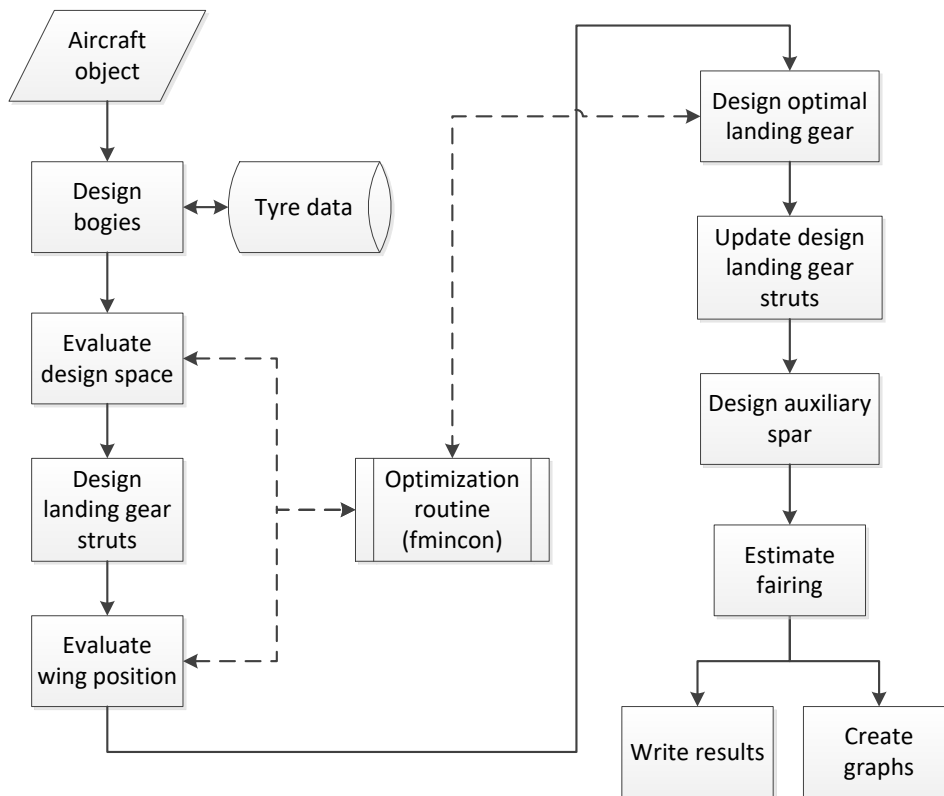


Figure 9.3: Module design steps

In the first step, the bogie designs which could be used for the aircraft concept are selected. Using the first possible bogie design, the design space is evaluated by creating a first landing gear estimation. The resulting position and length are used to calculate a first estimation of the stroke of the gear. The user is notified if a possible landing gear design exists for the given aircraft concept. The next step is to evaluate the wing positions at which a valid design is possible. This will give the forward and aft bounds used in the horizontal stability estimation module. After the main wing is set on the forward bound, a landing gear will be designed for each valid bogie type. From all these concepts the lightest option is selected. With this design the landing gear struts are redesigned. The last step is to update (or create, if not present) the kick spar in the wing planform and write the required output of the module.

9.1 Optimization routine

The module uses the `fmincon` with the Sequential Quadratic Programming (SQP) algorithm built into Matlab. The constraint tolerance, function tolerance and step tolerance of `fmincon` are set to 10^{-3} . For each iteration, SQP makes an approximation of the Hessian of the Lagrangian function using a quasi-Newton updating method. The result is then used to generate a quadratic programming subproblem. The solution of this subproblem is used to generate a search direction for the line search procedure[21].

Depending on the number of main gear struts and if the wing may be moved or not, the design vector of the routine has 4 to 6 design variables. The design vector is listed below.

Table 9.1: Design vector of the optimization routines

Vector entry	Description
1	Distance of nose gear from fuselage nose tip
2	Distance main gear gear from symmetry plane
3	Distance ground to z=0 of fuselage
4	Distance of (wing, in case of 4 struts) main gear from fuselage nose tip
5	Distance of fuselage main gear from fuselage nose tip (only for 3 or 4 struts)
last	Main wing position. This entry is only added when the main wing is allowed to be moved (for the optimization of the gear/wing combination). It is either the 5 th or 6 th entry, depending on the number of main gear struts.

The bounds of the optimization depend on the concept case. There are five possible cases at this moment: wing mounted gear, wing and fuselage mounted (3 or 4 main struts), fuselage mounted gear, engine nacelle mounted or gear stowed in a wing mounted pod. The upper and lower bounds of each case are shown in table 9.2. The flowchart of the design optimization is shown in figure 9.4 .

Table 9.2: Optimization bounds

Case	Bound	Description
Wing mounted	Nose x-coordinate	Lower: set at a percentage of fuselage length. Upper: set at a percentage of fuselage length.
	Main y-coordinate	Lower: 0. Upper: Set to 30% semispan.
	Gear height w.r.t. z=0	Lower: 0 Upper: Set by maximum height (10m by default) minus lowest point of the main wing.
	Main gear x-coordinate	Lower: Aft c.g. position Upper: Set at a percentage of fuselage length.
Fuselage mounted	Uses same bounds as wing case.	
Both	Uses same bounds as wing case, with one additional bound: Fuselage gear x-coordinate	Lower: Aft c.g. position plus 2x the tire diameter of the bogie. Upper: Set at a percentage of the fuselage length.
Engine	Uses same bounds as wing case, with one difference: Main y-coordinate	Lower: Set to inner engine y-coordinate. Upper: Set to inner engine y-coordinate.
Pod	Same bounds as wing case.	

The percentages of fuselage length mentioned in table 9.2 are set in the settings input file of

each aircraft model.

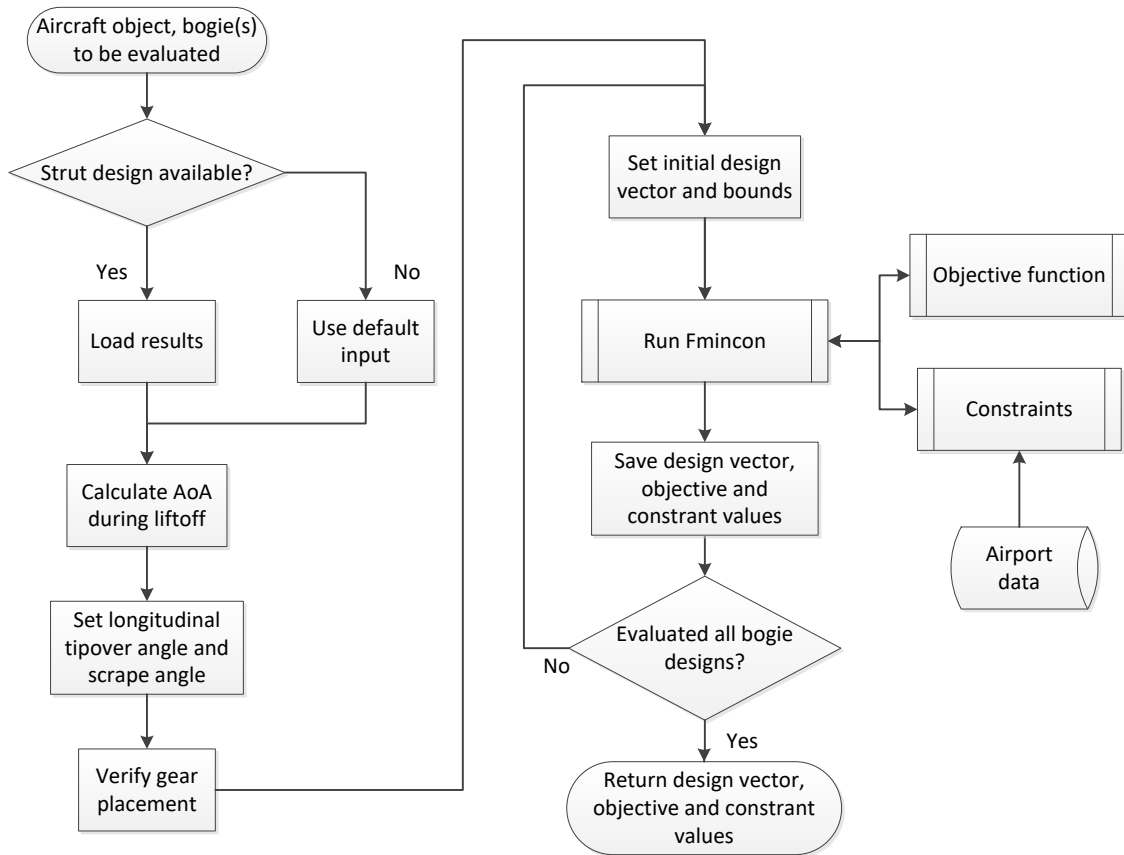


Figure 9.4: Flowchart of the optimization routine

From the aerodynamic analysis, the lift-curve slope is obtained. As stated in section 3.3, the lift curve slope is determined using the aerodynamic solver AVL⁴. The C_L at 0 AoA is determined with the DATCOM method. The objective of the optimization is to find the lowest gear length, as the landing gear weight scales with the landing gear height with equation 4.1. For the cases of a wing mounted gear, a fuselage mounted gear or a combination of the two the objective function is as shown by equation 9.1.

$$Objective = \frac{H}{H_{max}} + \frac{y_{gear}}{y_{lim}} \quad (9.1)$$

H_{max} is the maximum distance from $z=0$ down and y_{lim} the lateral placement limit of the wing mounted gear. This combination of scaled height and scaled track width force the optimization routine to go for the smallest gear while trying to keep the track as small as possible. The addition of the scaled track was done to make sure the design was optimal, as the routine would sometimes give a gear design which could be manually placed more inboard and shortened, resulting in a better design. For the cases of podded gear and nacelle mounted gear the objective function uses only the scaled gear height.

The constraints of the optimization are given in table 9.3. For the mathematical representation of the design requirements, the reader is advised to read section 3.3.

⁴<http://web.mit.edu/drela/Public/web/avl/>

Table 9.3: Constraints of the optimization

Constraint	Active during case	Description
Scrape angle	All	Scrape angle used for takeoff scrape.
Roll angle limit	All	Minimum allowed roll angle to avoid wingtip and/or engine strike.
Lateral tip over angle	All	Tip over angle to avoid tip over during a taxi turn.
Longitudinal tip over angle	All	Tip over angle to avoid auto-rotation.
Minimum nose load	All	Ensure minimum nose load to ensure good steering quality.
Maximum nose load	All	Ensure nose load to be below maximum load to ensure good steering quality.
Nose stowage	All	Ensure nose gear can be stowed.
FAA track limit	All	Ensure track is within FAA specified limit.
FAA wheelbase limit	All	Ensure wheelbase is within FAA specified limit.
180 turn limit	All	Ensure aircraft can make 180 turn on runway.
Wheel clearance	All	Ensure clearance between wheels and fuselage.
Attachment fwd limit	Wing, Both, Engine and Pod	Ensure main gear attachment is within range of rear spar.
Attachment aft limit	Wing, Both, Engine and Pod	Ensure main gear attachment is within range of rear spar.
Main gear longitudinal stowage	Wing and Both	Ensure main gear is retracted behind rear spar.
Main gear lateral stowage limits	Wing and Both	Ensure main gear bogie is within fuselage when retracted, but is not overlapping.
Strut/nacelle interference	Wing and Both, (if engine is on wing)	Ensure main gear strut is not placed within the engine nacelle.

9.2 Design bogies

The flowchart of the bogie selection is shown in figure 9.5.

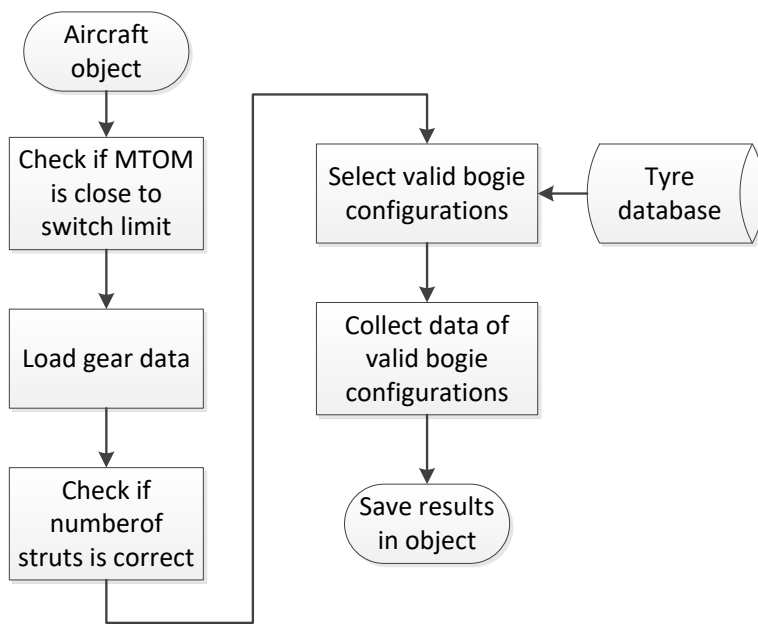


Figure 9.5: Flowchart of the bogie design script

The script checks if the MTOM of the concept is close to the so-called switch limit. It is split into four aircraft weight categories: $MTOM \leq 100t$, $MTOM \leq 200t$, $MTOM \leq 300t$ and $MTOM > 300t$. This is based on research done on the MTOM versus the number of main gear tires of 67 different transport aircraft, shown in figure 9.6.

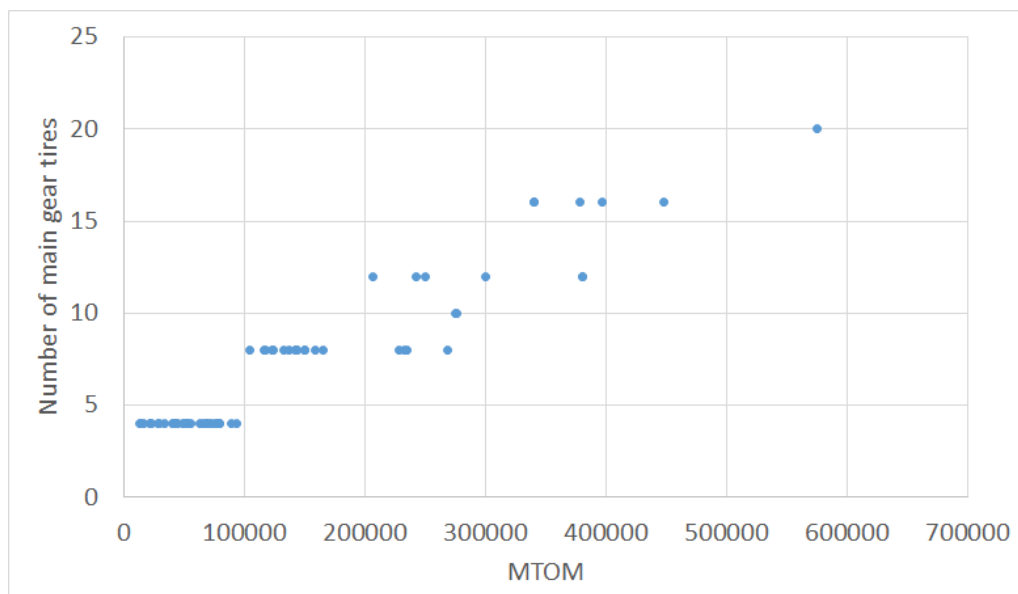


Figure 9.6: MTOM vs total number of main gear tires

For each category up to 300t, the MTOM of the concept is checked to be within 10% of the maximum MTOM of that category. If this is the case, the landing gear will be designed in such a way that it is possible to replace the bogie type with a larger one. E.g. if a dual type bogie is selected and the MTOM is within the 10% range, the gear will be placed to allow the installment

of a dual tandem bogie. This is done to allow the aircraft to operate on worse runways if required, without an entire redesign of the undercarriage.

Next, the number of struts defined by the user is compared to the resulting gear estimation of the Class 2 weight estimation module. If there is a difference, the number of struts is set to the initial gear estimation of the Class 2 weight estimation module. With the number of struts verified, all possible bogie types are evaluated. Figure 9.7 shows the implemented bogie types.

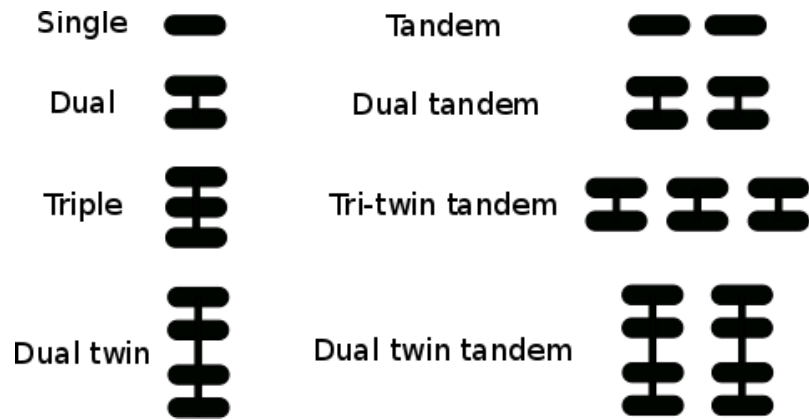


Figure 9.7: Implemented bogie types

For each bogie type, the following requirements are checked:

- Interference with floor when retracted
- Clearance between fuselage and bogie, for fuselage bogies in case of 4 main struts
- Flotation requirement
- Tire able to fit heat sink inside rim
- Tire fits inside wingbox, for low-wing aircraft with wing mounted gear

If all requirements are met, the bogie is considered a valid option for the gear design. All valid bogies are then saved in the aircraft object for further evaluation.

9.3 Design landing gear struts

To design the landing gear struts, the flowchart shown in figure 9.8 is used. For the equations used, the reader is referred to section 3.5.

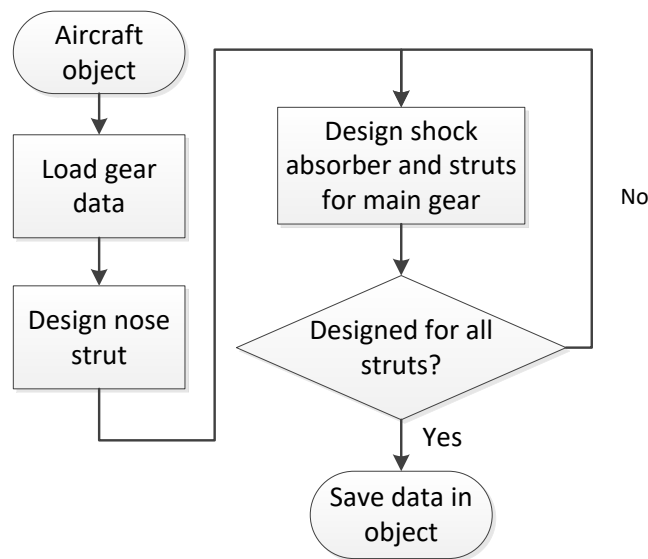


Figure 9.8: Flowchart of the strut design script

The design of the shock absorber is based on the methodology of N.S. Currey[11]. The following assumptions are used:

- The absorber is of the oleo-pneumatic type.
- The static pressure inside the strut is assumed to be 1500 psi. This is assumed to have easier maintenance of the shock absorber.
- The sink speed V_{sink} of the aircraft during landing is 10 ft/s.
- The landing load factor is 1.2. This factor should be between 0.7 and 1.5, so a slightly worse than average factor is assumed.
- The tire efficiency n_t is 0.472.
- The absorber efficiency n_s is 0.9. It is assumed that the most state of the art absorbers are used for the aircraft design.
- The pressure ratio between static and unloaded is 4/1. This ratio is typical for transport aircraft.
- The pressure ratio between fully compressed and static is 3/1. This ratio is typical for transport aircraft.

After the shock absorber is designed, the script evaluates the type of strut that will be used. For wing mounted gear and for the combined wing and fuselage mounted gear (3 or 4 main struts), a normal straight strut is assumed. For nacelle mounted gear, a folder gear is used as shown in figure 9.9a. For fuselage mounted gear, a canted gear as shown in figure 9.9 is used.

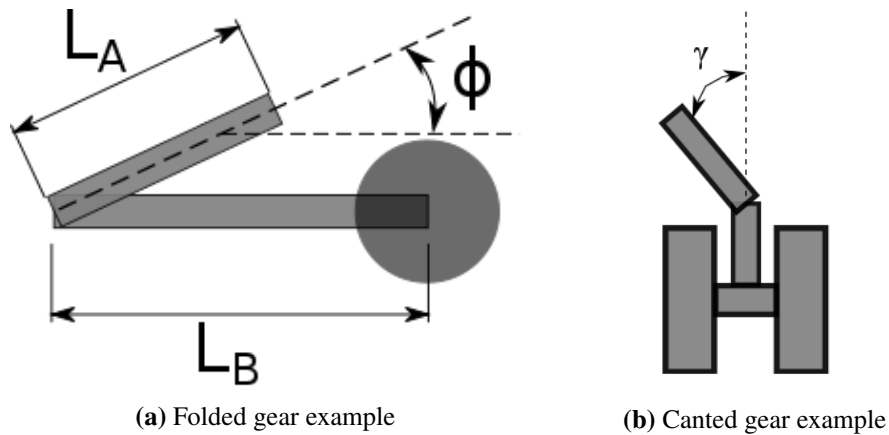


Figure 9.9: Folded and canted gear example

For the folded gear, a minimum space between the center of the tire and the attachment point of the gear of $0.55D_{tire} + 0.05$ is assumed. This is done to ensure the gear can be folded. For the canted gear, a maximum canting angle of 40° is assumed, based on the gear design of the ATR 72-600. The resulting shock stroke, piston diameter, strut diameter and strut length are saved into the object.

9.4 Evaluate wing position

To find the range of the main wing position for which a valid gear can be designed, the flowchart shown in figure 9.10 is used.

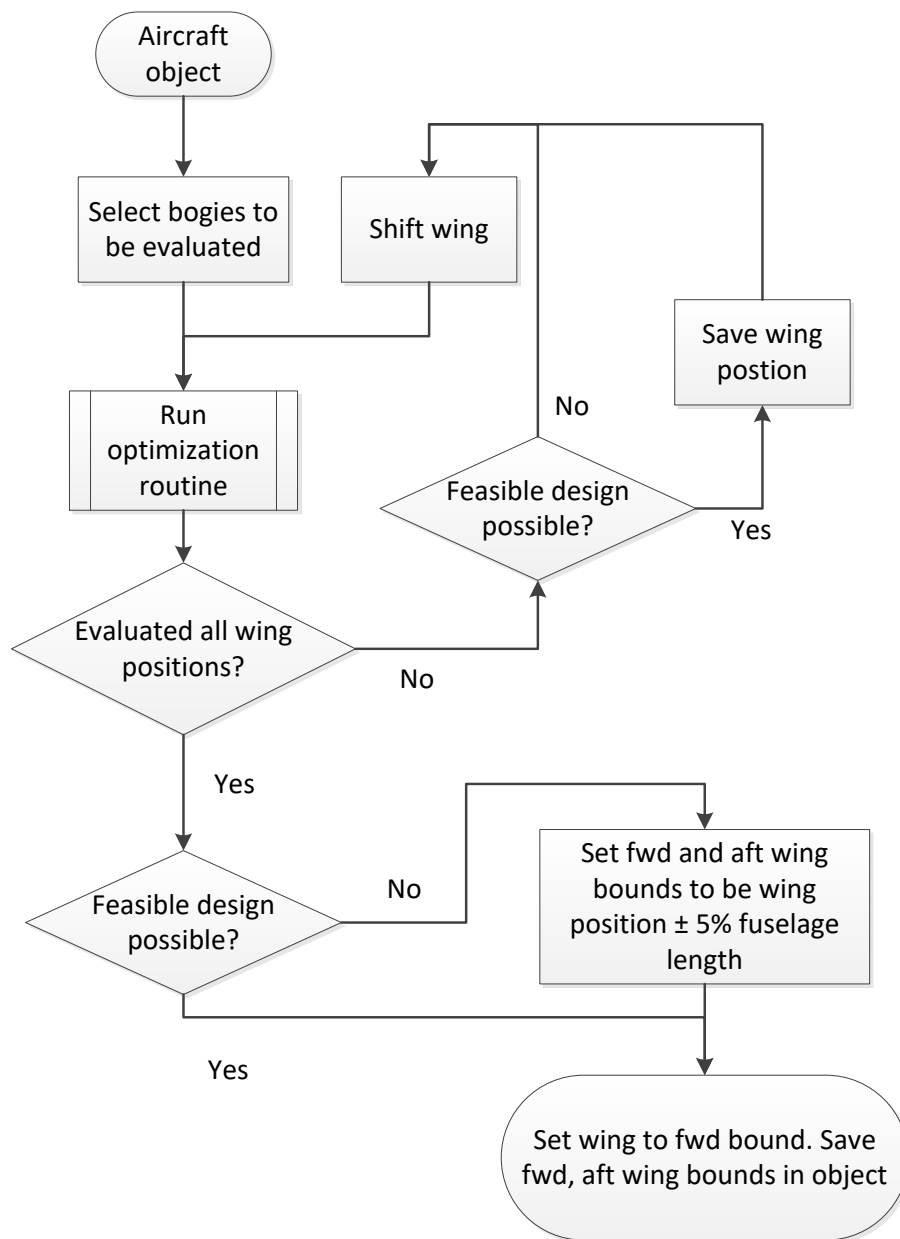


Figure 9.10: Flowchart of the wing position evaluation script

If the main gear is attached to the wing, the script selects the bogie which should be used for the evaluation based on the smallest wheelbase. If multiple bogie design fit the description, the first one is used. The wing is set at 90% of its initial value and moved aft up to the aft c.g. position with a step size of 10cm. For each position, the optimization routine is run to see if a landing gear design is possible. The change in c.g. is estimated using a Class I estimation[33]. For details on the Class I estimation, the reader is referred to section 3.6. If a valid design is possible for a given wing position, the position is saved. If no wing position with a valid gear design can be found, the default forward and aft bounds for the wing position are used. Else, the wing is placed on the forward bound to evaluate all possible gear designs.

9.5 Design optimal landing gear

To find the optimal landing gear for the given concept, a landing gear is designed for each selected bogie type. The flowchart of the script is shown in figure 9.11.

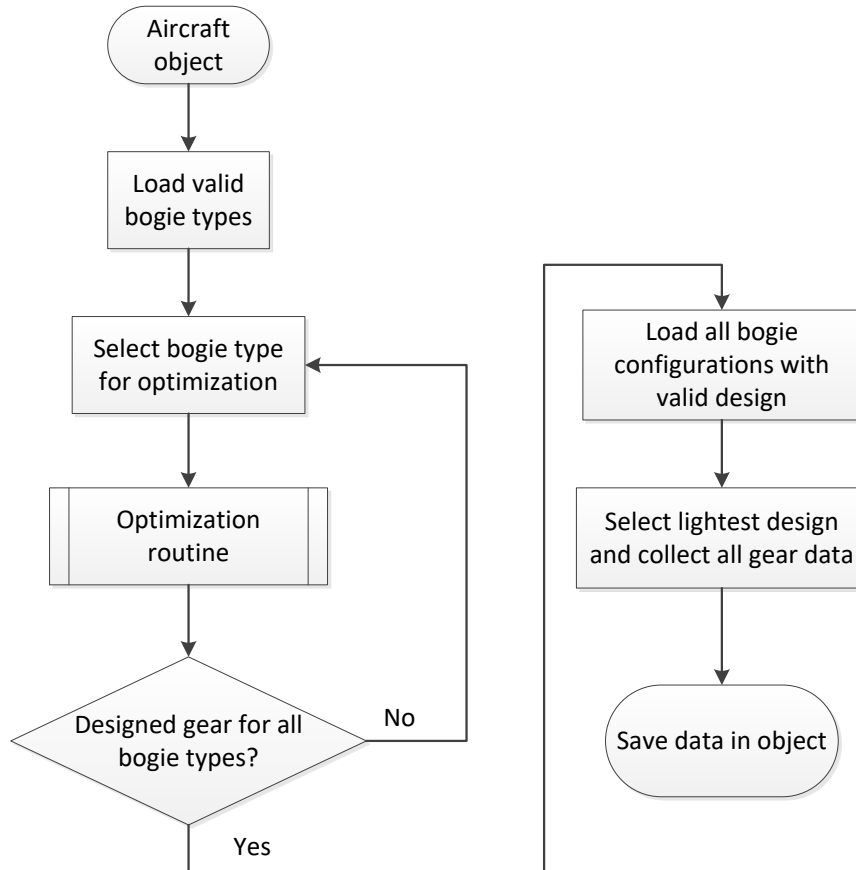


Figure 9.11: Flowchart of the optimal design script

To select the lightest gear, the weight equation shown in equation 9.2 is used.

$$W_{mlg} = 0.0106 \cdot k_{mp} \cdot k_x \cdot W_l^{0.888} \cdot N_l^{0.25} \cdot L_m^{0.4} \cdot N_{mw}^{0.321} \cdot N_{mss}^{-0.5} \cdot V_{st}^{0.1} \quad (9.2)$$

in which k_{mp} is 1.126 for kneeling main gears and 1.0 otherwise, k_x is 0.536 for XC-142 type (experimental VTOL aircraft) and 1.0 otherwise. In case of a landing gear with a tandem bogie, the weight is increased by 10%. This is based on the assumption that the additional moment due to the wheel layout will result in a heavier bogie. This helps to decide which design to use in case of two gear designs of equal length, but one with a dual type of bogie and one with the tandem type. If no valid design is found, the user is notified and the design with the best fit to the design requirements is selected to continue the convergence of the Initiator.

9.6 Design auxiliary spar

After the landing gear is designed, the auxiliary spar can be (re)designed if required. Figure 9.12 shows the flowchart used to design the auxiliary spar.

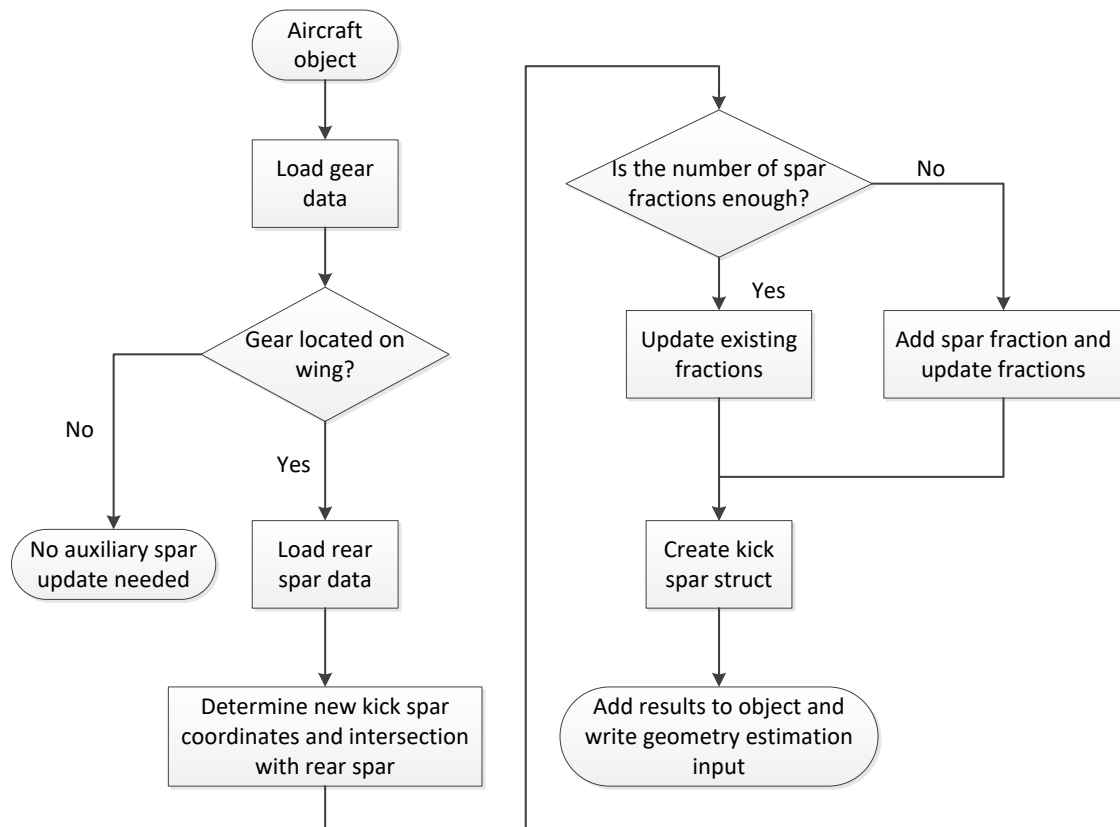


Figure 9.12: Flowchart of the auxiliary spar design script

The auxiliary spar is only sized if the gear is of the wing mounted, root stowed type or in case of 3 or 4 main struts. To create the wing planform, the Initiator uses wing sections. These wing sections contain the information of the airfoil at the location, as well as the location of the section. For the spars, the so-called spar sections are used. The definition of the wing and spar sections is shown in figure 9.13. The wing sections are indicated with the green lines. The spar sections use the same sections, with the additional blue section to create the wingbox. The wing contour is shown with the black lines, the spars with the red lines.

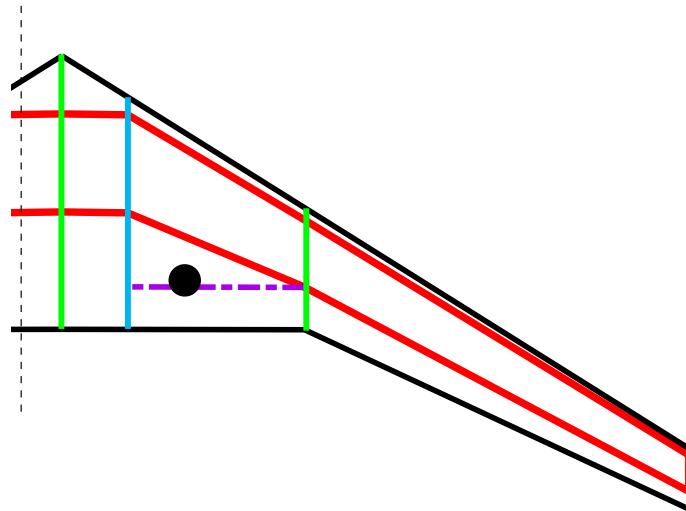


Figure 9.13: Wing planform definition

The location of the spars is indicated with a chord fraction of the sections. The auxiliary spar, indicated by the purple dashed line in figure 9.13, is assumed to run perpendicular to the fuselage. It runs from the wingbox to the kink location, which is the intersection of the auxiliary spar with the rear spar. The auxiliary spar is placed one strut diameter behind the main gear, to allow enough space for the attachment. As the number of spar sections is based on the number of wing sections, there may not be enough spar sections in case of a wing without a kink. If this is the case, an additional spar section is created. If no auxiliary spar was present, a new set of location fractions is added to the spar sections for the auxiliary spar. Next the location fractions for each section are updated to match the spar locations. The new spar location fractions and kink location are passed on to the Geometry Estimation module.

9.7 Estimation of the gear fairing and drag calculation

For the gear fairing dimensions a rough estimation of the fairing was made. It was decided that the fairing would consist of elliptical shapes, as they are easy to implement and give a fairly good approximation. The fairing is not created when the undercarriage is of the wing mounted type. There are three types of fairing which can be created: a fuselage fairing, an extended engine fairing and a wing mounted pod. An example of the fairing is shown in figure 9.14.

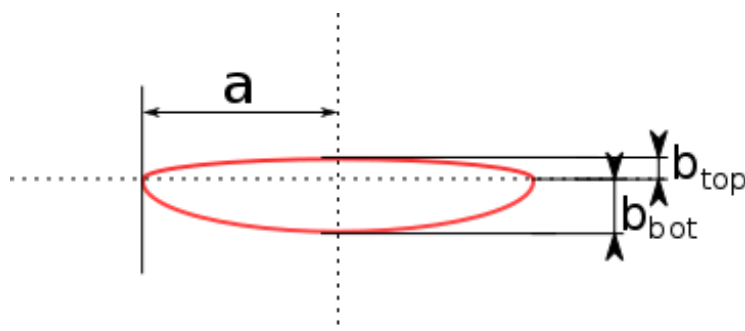


Figure 9.14: Fairing shape example

a indicates the major axis and **b** the minor axis. The flowchart of the script is shown in figure 9.15.

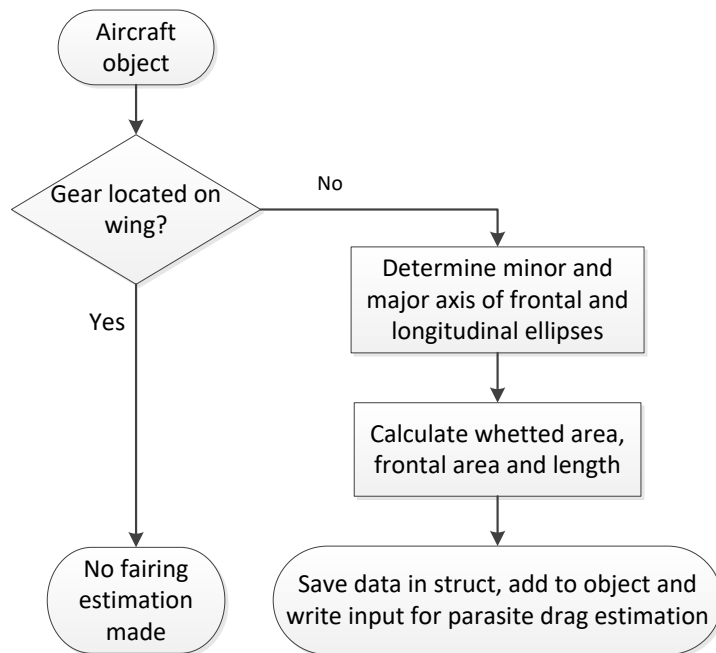


Figure 9.15: Flowchart of the fairing estimation script

For the equations used to estimate the fairing, the reader is referred to section 3.8. The resulting fairing dimensions are passed on to the parasitic drag module, which calculates the contribution to C_{D_0} of the fairing and the landing gear. Both the landing gear drag and fairing drag are estimated based on the methods of Raymer[24]. For further details on the landing gear drag, the reader is referred to section 3.9. For the fairing drag, the type of gear determines the calculations done. For the podded gear and fuselage mounted gear, the drag is calculated separately and added to the total C_{D_0} . For nacelle stowed gear, the engine nacelle is replaced by the larger fairing and the drag is included in the engine drag. For the equations used for the fairing drag estimation, the reader is referred to section 3.10.

10 Conclusion

The landing gear design module performs as expected. With an exception of the wheelbase, it is able to reproduce the designs of actual aircraft quite well. An observation made is that the deviation in wheelbase increases as the size of the aircraft increases. For smaller aircraft such as the Fokker 100 the designed gear layout represents the actual gear layout better than for larger aircraft like the B777-300. The problems of the Initiator with estimating the cg location have a large impact on the result of the landing gear design module. This issue translates in an underestimation of the wheelbase and an aft shift in nose and main gear location, as seen in section 5. Relaxing the nose load design requirements may allow for a better representation of the wheelbase, as it will allow the nose gear to be placed further forward in cases such as the B727, B737 and B777. Having a more accurate cg estimation will also solve, or at the very least lessen, the aft shift of the main wing, as seen with the A320 and ATR 72 cases. The number of tires of each concept match the number used on the actual aircraft, although due to the safety margin used the concept often uses larger tires to satisfy the flotation requirement. This larger tire also has an impact on the estimated gear length, which is larger than the gear length of the actual aircraft for most cases.

The test cases shown in section 6 show the strength of the new module, as well as the effect of a change in geometry on the gear design. The first case shows the response of the module to a change in dihedral angle, as well as a trade-off made between a conventional wing mounted gear and podded gear. It was noted that the Initiator currently caused a flaw in the trade-off, where the takeoff angle of the concept with the podded gear was much larger than the takeoff angle of the concept with the conventional gear. This was due to the Initiator updating the value of $C_{L_{clean,max}}$ and not the value of $C_{L_{TO,max}}$. With the assumption of the difference between $C_{L_{clean,max}}$ and $C_{L_{TO,max}}$ being the lift generated by the flaps, as shown with equation 3.2, it causes the flaps to become less efficient. This in turn increased the required takeoff angle, which cause the wing tip to be situated lower during a roll in combination with pitch up. The wing tip clearance requirement then forced the necessity of a longer gear, whereas it was expected that the podded gear would be shorter for a wing with anhedral. Based on the results of the Initiator, one would better chose the conventional gear in this case in terms of aircraft performance. The case did show that the module responds well to the change in dihedral angle, as gear length and spanwise position adjust correctly.

For the second case, the effect of a fuselage mounted gear and a nacelle stowed gear on a high-wing concept is investigated. The case shows the potential of the tool to investigate the influence of the gear design on the concept's weight, drag and geometry. The nacelle stowed gear caused the main wing to be slightly further aft, as well as a slight increase in vertical tail height. The MTOM of the nacelle gear concept also increased due to the increase in gear weight, but the total C_{D_0} reduced when applying this type of gear. It can also be seen that the L/D ratio reduced for the nacelle stowed gear concept, causing a slightly higher fuel consumption.

Hence, the hypothesis *"by careful integration of the design of the undercarriage into the conceptual design routine of the Initiator, results in a design method capable of assessing the impact on weight, drag and geometry of transport aircraft"* is verified. The new landing gear design module allows the user to evaluate the impact of the gear design on the aircraft. Taking into account the current state of the Initiator, the new design strategy is an improvement for the Initiator program. It allows for a fast design of a landing gear reliably, with the flexibility for the user to set the gear type. Table 10.1 shows the improvements made by implementing the new design strategy.

Table 10.1: Module features

	Old Method	New Method
Wing mounted gear	✓	✓
Fuselage mounted gear	✓	✓
Nacelle mounted gear	X	✓
Pod mounted gear	X	✓
Optimization routine	X	✓
Can adjust wing planform	X	✓
Wingbox sizing	X	✓
Fairing sizing	X	✓
Fairing drag estimation	X	✓
Landing gear drag estimation	X	✓

The addition of the fairing estimation and landing gear drag estimation also allow for more accurate results and better trade-offs.

Recommendations for future development

To improve upon the new module, one could implement an analytical weight estimation instead of the statistical method. This would require a more detailed landing gear design but would result in a more accurate weight estimation. The detailed gear design would also allow for the modelling of the kinematics of the landing gear. The model can also be adjusted to handle the gear design for unconventional aircraft designs, such as the blended wing body and boxwing. This could also need to have an increased maximum of main gear struts, as the current module only allows for a maximum of four main gear struts.

As the fairing estimation is very basic and only the dimensions are estimated, an improved version could be implemented for more accurate dimensions and a weight estimation for the fairing itself. Also the wing/fuselage fairing is currently not sized and could be added with a more accurate fairing sizing method. This would make a trade-off based on drag and/or fuel consumption more accurate.

As noise reduction is getting more important, a noise estimation method for the landing gear could also be implemented in the future. This would allow the designer the also include the noise impact in a trade-off. However, as stated in section 8, this would require a more detailed design of the landing gear than is currently available.

The results of the landing gear module depend heavily on the cg estimation of the Initiator. Updating the cg position to a more accurate method will improve the resulting gear designs. This in turn will increase the accuracy of the drag and fairing estimations.

The drag estimation for the landing gear currently uses the statistical method described by Raymer. A future improvement may be to change to the ESDU drag estimation method. As said in section 8, the ESDU method gives fairly good results when compared to a more computational demanding CFD analysis.

References

- [1] Airbus S.A.S., 1 Rond Point Maurice Bellonte, 31707 Blagnac Cedex, France. *A320 Aircraft Characteristics, Airport and Maintenance Planning, Rev.34*, 01 2018.
- [2] J.D. Anderson. *Fundamentals of Aerodynamics, 4th edition*. McGraw-Hill, 1221 Avenue of the Americas, New York, NY 10020, USA, 2007.
- [3] Avions de Transport Régional, allée Pierre Nadot, 31712 Blagnac Cedex, France. *ATR 72-600*, 06 2014.
- [4] I.J.M. Besselink. *Shimmy of Aircraft Main Landing Gear*. PhD thesis, Delft University of Technology, PO Box 5, 2600AA Delft, 2000.
- [5] The Boeing Company, P.O. Box 3707, Seattle, Washington 98124. *B777 Airplane Characteristics, Airport Planning*, 07 1998.
- [6] The Boeing Company, P.O. Box 3707, Seattle, Washington 98124. *B727 Airplane Characteristics, Airport Planning*, 05 2011.
- [7] The Boeing Company, P.O. Box 3707, Seattle, Washington 98124. *B737 Airplane Characteristics, Airport Planning*, 09 2013.
- [8] *Undercarriage drag predictions for a Scottish Aviation Bulldog 120 light aircraft*, volume 1, Denver, Colorado, 2017. AIAA.
- [9] S.T. Chai and W.H. Mason. Landing gear integration in aircraft conceptual design. Technical Report MAD 96-09-01, NASA Ames Research Center, 09 1996.
- [10] M. Hepperle C.M. Liersch. A distributed toolbox for multidisciplinary preliminary aircraft design. *CEAS Aeronautical Journal*, 2(1):57–68, 2011.
- [11] N.S. Currey. *Aircraft Landing Gear Design: Principles and Practices*. American Institute of Aeronautics and Astronautics, Inc., 370 L'Enfant Promenade, S.W., Washington, D.C. 20024, 1988.
- [12] Vough Aeronautics Division. Cargo/transport statistical weight estimation equations. Technical report, Vough Aeronautics Division, 1968.
- [13] L. Hu W. Zhe F. Haocheng, L. Mingqiang. A knowledge-based and extensible aircraft conceptual design environment. *Chinese Journal of Aeronautics*, 24(6):709–719, 2011.
- [14] FAA, 800 Independence Avenue SW, Washington DC 20591, USA. *FAA Advisory Circular No. 150/5300-13A - Change 1*, 09 2012.
- [15] Fokker Services, Hoeksteen 40, 2132 MS Hoofddorp. *Fokker 100 Basics*.
- [16] A.G. Gonzalbo and J.M.D. Parrila. Aircraft with a nacelle-housed main landing gear, 2014.
- [17] The Goodyear Tire & Rubber Company, 200 Innovation Way, Akron, Ohio 44316. *Global Aviation Tires*, 07 2016.
- [18] S. Gudmundsson. *General Aviation Aircraft Design*. Butterworth-Heinemann, Oxford, United Kingdom, 2013.

- [19] N.C. Heerens. Landing gear design in an automated design environment. Master's thesis, Delft University of Technology, PO Box 5, 2600AA Delft, 2014.
- [20] R.B. Heslehurst. Undercarriage lateral tip-over criteria: A parametric study. *Journal of Aircraft*, 48(6):1825–1828, 2011.
- [21] MathWorks. *Matlab Product Documentation*.
- [22] Delft University of Technology. Initiator wiki page. <http://fppwiki.lr.tudelft.nl/index.php/Synthesis/Initiator>, 2019. Accessed: 12-11-2018.
- [23] J.I. Pritchard. An overview of landing gear dynamics. Technical Report NASA/TM-1999-209143, NASA Center for Aerospace Information, 05 1999.
- [24] D.P. Raymer. *Aircraft Design: A Conceptual Approach*. American Institute of Aeronautics and Astronautics, Inc., 370 L'Enfant Promenade, S.W., Washington, D.C. 20024, 1992.
- [25] Dr. J. Roskam. *Airplane Design. Part IV: Layout Design of Landing Gear and Systems*. DARcorporation, 1989.
- [26] M.H. Sadraey. *Aircraft design: a systems engineering approach*. John Wiley & Sons, Ltd, The Atrium, Southern Gate, Chichester, West Sussex, PO19 8SQ, United Kingdom, 2013.
- [27] R.K. Schmidt. *Advances in Aircraft Landing Gear*. SAE International, 2015.
- [28] At76, dublin ireland, 2015. https://www.skybrary.aero/index.php/AT76,_Dublin_Ireland,_2015. Accessed: 28-01-2019.
- [29] K. Amemiya Y. Yokokawa S. Enomoto T. Imamura, T. Hirai and K. Yamamoto. Aerodynamic and aeroacoustic simulations of a two-wheel landing gear. *Procedia Engineering*, 6:293–302, 2010.
- [30] Goodyear Aviation Tires. Tire line details. <https://www.goodyearaviation.com/tires/tire-line-details> 2018. Accessed 17-12-2018.
- [31] E. Torenbeek. *Synthesis of Subsonic Airplane Design*. Kluwer Academic Publishers, Dordrecht, 1982.
- [32] E. Torenbeek. *Advanced Aircraft Design: Conceptual Design, Technology and Optimization of Subsonic Civil Airplanes*. John Wiley & Sons, Inc, 111 River Street, Hoboken, NJ 07030-5774, United States of America, 2013.
- [33] R. Vos and J.A. Melkert. Empennage and gear design. TU Delft Course: Aerospace Design & Systems Engineering, 2017.
- [34] I. Wakefield and C. Dubuque. Exceeding tire speed rating during takeoff. *AERO*, 02:107–125, 2009.
- [35] K.J. Yamamoto Y.P. Guo and R.W. Stoker. Experimental study on aircraft landing gear noise. *Journal of Aircraft*, 43(2):306–317, 2006.